NAVAL POSTGRADUATE SCHOOL
Monterey, California

THESIS

SPECTRAL DOMAIN ANALYSIS OF FIN-LINE

by

Paul Mark Shayda

December 1979

Thesis Advisor: J.B. Knorr

ADA083836

80   5   6 025

REPORT DOCUMENTATION PAGE		READ INSTRUCTIONS BEFORE COMPLETING FORM
1. REPORT NUMBER	2. GOVT ACCESSION NO. AD-AC83 856	3. RECIPIENT'S CATALOG NUMBER
4. TITLE (and Subtitle) Spectral Domain Analysis of Fin-Line		5. TYPE OF REPORT & PERIOD COVERED Master's Thesis; December 1979
		6. PERFORMING ORG. REPORT NUMBER
7. AUTHOR(s) Paul Mark Shayda		8. CONTRACT OR GRANT NUMBER(s)
9. PERFORMING ORGANIZATION NAME AND ADDRESS Naval Postgraduate School Monterey, California 93940		10. PROGRAM ELEMENT, PROJECT, TASK AREA & WORK UNIT NUMBERS
11. CONTROLLING OFFICE NAME AND ADDRESS Naval Postgraduate School Monterey, California 93940		12. REPORT DATE December 1979
		13. NUMBER OF PAGES 128
14. MONITORING AGENCY NAME & ADDRESS(if different from Controlling Office)		15. SECURITY CLASS. (of this report) Unclassified
		15a. DECLASSIFICATION/DOWNGRADING SCHEDULE

16. DISTRIBUTION STATEMENT (of this Report)

Approved for public release; distribution unlimited.

17. DISTRIBUTION STATEMENT (of the abstract entered in Block 20, if different from Report)

18. SUPPLEMENTARY NOTES

19. KEY WORDS (Continue on reverse side if necessary and identify by block number)

Fin-line
Shielded Slotline
Integrated Fin-line

20. ABSTRACT (Continue on reverse side if necessary and identify by block number)

An analysis of fin-line characteristics is presented. The dispersion characteristic and characteristic impedance of the structure are determined by the application of the spectral domain technique. Numerical results are presented and compared

#20 - ABSTRACT - CONTINUED

with known data for ridged waveguide, dielectric slab loaded
waveguide and slotline. Excellent agreement has been obtained.
Design curves are also presented for practical millimeter
wave fin-line structures covering the 26.5 - 140 GHz frequency
range.

Spectral Domain Analysis of Fin-Line

by

Paul Mark Shayda
Lieutenant, United States Navy
B.S.E.E., Marquette University, 1973

Submitted in partial fulfillment of the
requirements for the degree of

MASTER OF SCIENCE IN ELECTRICAL ENGINEERING

from the

NAVAL POSTGRADUATE SCHOOL

December 1979

Author _____

Approved by: _____
                                    Thesis Advisor

_____
                                    Second Reader

_____
Chairman, Department of Electrical Engineering

_____
            Dean of Science and Engineering

3

ABSTRACT

An analysis of fin-line characteristics is presented.
The dispersion characteristic and characteristic impedance
of the structure are determined by the application of the
spectral domain technique. Numerical results are presented
and compared with known data for ridged waveguide, dielectric
slab loaded waveguide and slotline. Excellent agreement has
been obtained. Design curves are also presented for practi-
cal millimeter wave fin-line structures covering the 26.5 -
140 GHz frequency range.

TABLE OF CONTENTS

LIST OF TABLES

LIST OF FIGURES

ACKNOWLEDGMENT

The author gratefully expresses his gratitude to
Professor Jeffrey B. Knorr for his considerable help and
guidance during this study and his patience in editing this
thesis.

To my wife, Martha, I would like to offer my special
thanks and love for her patience, understanding and encourage-
ment during the development of this work.

I. INTRODUCTION

A. BACKGROUND

A variety of waveguiding structures have been proposed for use at microwave and millimeter wave frequencies [Ref. 1]. In recent years, one of these structures, fin-line, has gained in importance as a transmission medium in millimeter wave circuit construction [Refs. 2-7]. Fin-line has been found superior to microstrip at millimeter wavelengths as the former provides eased production tolerances, better compatibility with hybrid devices, greater freedom from radiation and higher mode propagation, combined with the ability to construct simple transitions to conventional rectangular waveguide.

Figure 1 shows a 3-dimensional view of fin-line. This structure is interesting in that it may be viewed in various ways depending upon the value of W/b, the ratio of slot width to waveguide height. For small values of W/b, the structure may be appropriately viewed as a slotline with a rectangular shield. For large values of W/b, the structure is more easily seen as a ridged waveguide loaded with dielectric. When W/b = 1, a dielectric slab loaded waveguide exists and finally for W/b = 1 and ϵ_r = 1, the structure takes on the configuration of empty rectangular waveguide.

The most commonly used transmission line to date in microwave integrated circuits is the microstrip line. This

11
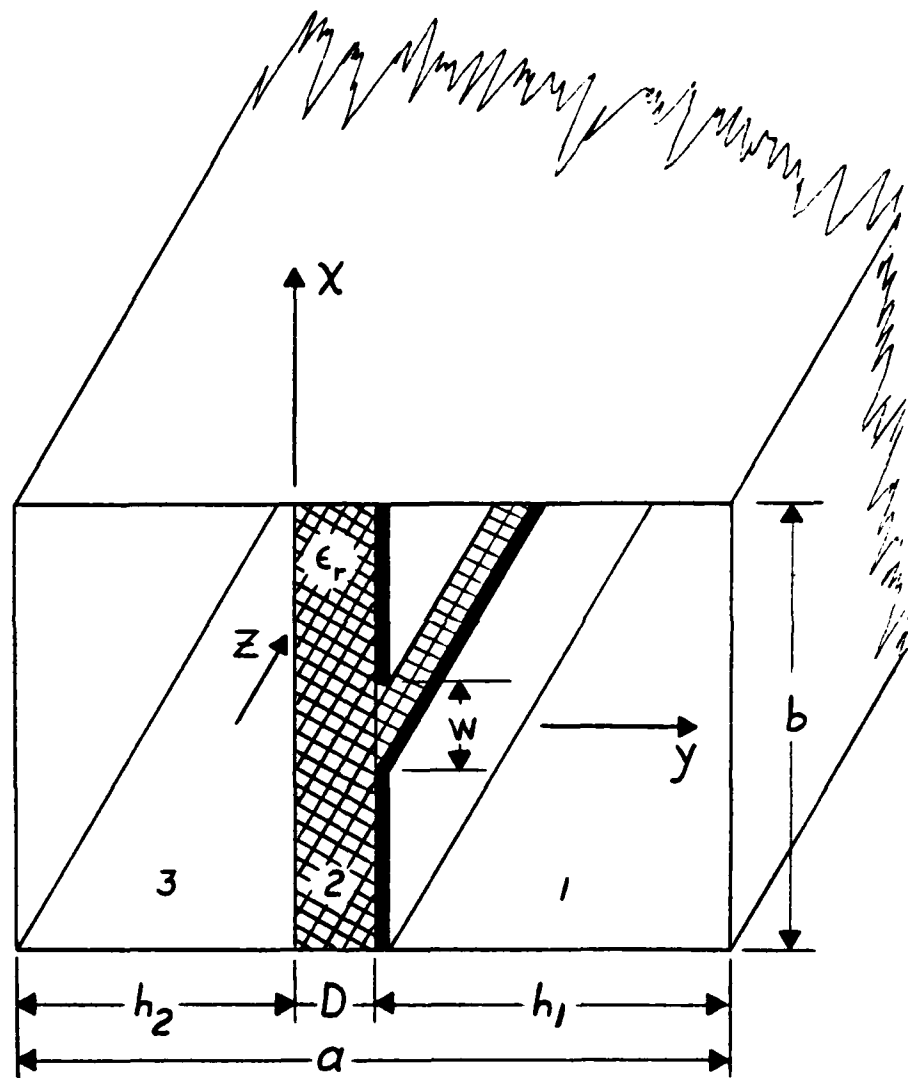
Figure 1.   3-Dimensional View of Fin-line Structure

structure when used at high frequencies (millimeter wave range) results in problems which include radiation loss, spurious coupling, dispersion and higher mode propagation.

In fin-line structures, metal fins are printed on a dielectric substrate which bridges the broad walls of a rectangular waveguide. In effect, the line is a printed ridged waveguide and can be designed to have a wider useful bandwidth than conventional line and can provide bandwidths in excess of an octave with less attenuation than microstrip. This adaption of ridged waveguide permits circuit elements to be fabricated by photo-etching at low cost and is compatible with thin-film hybrid techniques.

In passive circuits, such as filters, the fins as illustrated in Figure 1 may be directly grounded to the metal walls of the waveguide, and lumped elements, such as beam-lead capacitors, may be added. The gap between the fins can be varied along the longitudinal axis to provide low-cost circuit elements. When fin-lines are constructed as illustrated by Figure 2, the waveguide is parted along a plane where the current flow is parallel to the break, as in a common slotted line and the dielectric material extends through the separation in the broad wall of the shield. The upper fin is insulated from the housing at dc by a dielectric gasket. By making the thickness of the broad walls a quarter wavelength, a short circuit will appear between the fin and the inner wall of the shield at RF. Thus a practical fin-line will have the same electrical characteristic as the idealized structure of
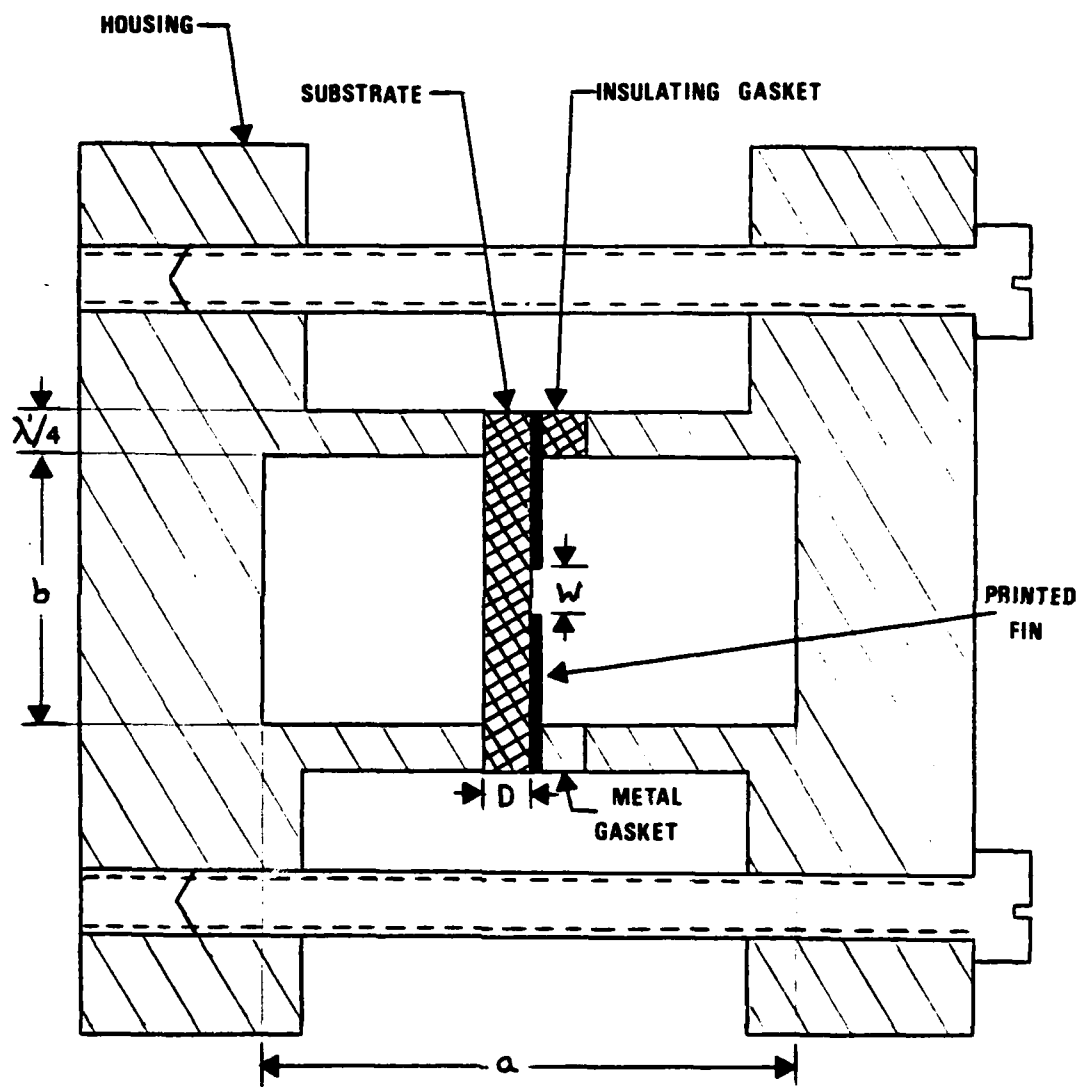
Figure 2.   Integrated Fin-line Semiconductor Mount

Figure 1. The lower fin is grounded directly by a metal
gasket to provide a dc return when solid state devices are
mounted on the fins.

B. RELATED WORK

Fin-line was first proposed in 1972 by Meier [Refs. 2
and 3] and has since received considerable attention by a
number of other investigators. Meier's work was primarily
experimental in nature and the wavelength and impedance
calculations were approximated. Previous analytical work on
fin-line has been based on various methods [Refs. 8-11].
In this study, dispersion of different fin-line geometries
was obtained by applying Galerkin's method to the electric
fields in the slot interface [Ref. 8]. Another approach used
the Transmission Line Matrix (TLM) technique yielding the
dispersion characteristic of the fundamental and higher order
modes of propagation [Ref. 9].

C. STATEMENT OF OBJECTIVES

The Spectral Domain technique is used here in the analy-
sis of the fin-line structure shown in Figure 1. This tech-
nicue was first suggested by Itoh and Mittra [Ref. 12] and
has since been applied to the analysis of other structures
[Refs. 13-15].

One of the advantages of this approach is that it is
numerically more efficient than the conventional methods that
work directly in the space domain. This is due primarily to
the fact that the process of Fourier transformation of the

coupled integral equations in the space domain yields a pair of algebraic equations in the transform domain that are relatively easier to handle. Another important advantage is that the Green's function takes a much simpler form in the transform domain, as compared to the space domain where no convenient form of the Green's function is known to exist.

The Spectral Domain Transform method is first applied here in the formulation of the dispersion characteristic of the fin-line structure of Figure 1. During the application, a new matrix approach to the implementation of this method is presented. The characteristic impedance is next formulated using this technique in terms of the dispersion characteristic. Following the theroetical analysis, an explanation of the computer program used in determination of the wavelength and characteristic impedance is presented. Numerical results are then compared with known data for ridged waveguide, slab loaded waveguide and slotline. These comparisons establish the accuracy of the numerical results and illustrate the applicability of this method for the full range of structure parameters. Finally, several families of design curves are presented for a practical choice of fin-line parameters.

II. THEORETICAL ANALYSIS OF FIN-LINE

A. FIELD AND BOUNDARY CONDITIONS

Fin-line supports a hybrid field and it is known that all hybrid field components can be obtained from the superposition of TE and TM modes which are related to the two scalar potential functions $\phi^e(x,y)$ and $\phi^h(x,y)$, where the superscripts e and h denote electric and magnetic, respectively [Ref. 16]. The axial components of TM and TE are then

$$E_z = k_c^2 \, \phi^e(x,y) \, e^{\Gamma z} \tag{1}$$

$$H_z = k_c^2 \, \phi^h(x,y) \, e^{\Gamma z} \tag{2}$$

where $k_{ci}^2 = k_i^2 + \Gamma^2$ and $k_i = \omega^2 \mu_i \epsilon_i$, $i = 1, 2, 3$ for each of the three regions defined in Figure (1).

Through Maxwell's curl equations the transverse field components are then determined by these axial components and can be given as

$$E_x = (\Gamma \, \frac{\partial \phi^e}{\partial x} - j \, \omega \, \mu \, \frac{\partial \phi^h}{\partial y}) \, e^{\Gamma z} \tag{3}$$

$$E_y = (\Gamma \, \frac{\partial \phi^e}{\partial y} + j \, \omega \, \mu \, \frac{\partial \phi^h}{\partial x}) \, e^{\Gamma z} \tag{4}$$

$$H_x = (\Gamma \, \frac{\partial \phi^h}{\partial x} + j \, \omega \, \epsilon \, \frac{\partial \phi^e}{\partial y}) \, e^{\Gamma z} \tag{5}$$

$$H_y = (\Gamma \frac{\partial \phi^h}{\partial y} - j \omega \epsilon \frac{\partial \phi^e}{\partial x}) e^{\Gamma z}. \qquad (6)$$

Since the lossless case is assumed, the propagation constant is $\Gamma = \pm j\beta$ and $k_{ci}^2 = k_i^2 - \beta^2$. We will also assume that $\epsilon_1 = \epsilon_3 = \epsilon_o$ and $\epsilon_2 = \epsilon_o \epsilon_r$.

Applying boundary conditions at the walls in region 1, tangential field components must be zero, so it follows that at $y = h_1 + D$

$$E_{z1}(x,h_1+D,z) = 0 \qquad \frac{\partial H_{z1}}{\partial y}(x,h_1+D,z) = 0 \qquad (7)$$

$$E_{x1}(x,h_1+D,z) = 0 \qquad \frac{\partial H_{x1}}{\partial y}(x,h_1+D,z) = 0. \qquad (8)$$

At the interface between region 1 and 2, tangential field components must be continuous.

At $y = D$

$$E_{z1}(x,D,z) = E_{z2}(x,D,z) \qquad (9)$$

$$E_{x1}(c,D,z) = E_{x2}(x,D,z). \qquad (10)$$

Also the electric fields at $y = D$ will exist only in the slot and can be expressed as,

$$E_{z1}(x,D,z) = \begin{cases} 0 & |x| \geq W/2 \\ \\ e_z(x)\,e^{\Gamma z} & |x| < W/2 \end{cases} \quad (11)$$

$$E_{x1}(x,D,z) = \begin{cases} 0 & |x| \geq W/2 \\ \\ e_x(x)\,e^{\Gamma z} & |x| < W/2 \;. \end{cases} \quad (12)$$

Similarly, tangential magnetic fields must be discontinuous by corresponding surface current densities.

$$H_{z1}(x,D,z) - H_{z2}(x,D,z) = \begin{cases} j_x(x)\,e^{\Gamma z} & |x| \geq W/2 \\ \\ 0 & |x| < W/2 \end{cases} \quad (13)$$

$$H_{x1}(x,D,z) - H_{x2}(x,D,z) = \begin{cases} j_z(x)\,e^{\Gamma z} & |x| \geq W/2 \\ \\ 0 & |x| < W/2 \end{cases} \quad (14)$$

The tangential field components at the interface between region 2 and 3 must also be continuous. At $y = 0$

$$E_{z2}(x,0,z) = E_{z3}(x,0,z) \quad (15)$$

$$E_{x2}(x,0,z) = E_{x3}(x,0,z) \quad (16)$$

$$H_{z2}(x,0,z) = H_{z3}(x,0,z) \tag{17}$$

$$H_{x2}(x,0,z) = H_{x3}(x,0,z) . \tag{18}$$

Once again at the shield wall in region 3, the tangential field components must be zero, therefore at $y = -h_2$

$$E_{z3}(x,-h_2,z) = 0 \qquad \frac{\partial H_{z3}}{\partial y}(x,-h_2,z) = 0 \tag{19}$$

$$E_{x3}(x,-h_2,z) = 0 \qquad \frac{\partial H_{x3}}{\partial y}(x,-h_2,z) = 0 . \tag{20}$$

The final boundary conditions occur at $x = \pm b/2$ where the tangential components must be zero in all regions. At $x = \pm b/2$

$$E_{zi}(\pm b/2,y,z) = 0 \tag{21}$$

$$E_{xi}(\pm b/2,y,z) = 0 . \tag{22}$$

B. SPECTRAL DOMAIN APPROACH TO DISPERSION CHARACTERISTIC

The approach used in the analysis of the dispersion characteristic is basically a modification of Galerkin's approach adapted for application in the Fourier transform or spectral domain.

The scalar potential functions ϕ^e and ϕ^h satisfy the Helmholtz equations in the three spatial regions, thus

$$\nabla_t^2 \phi_i + k_{ci} \phi_i = 0 \qquad (23)$$

where ∇_t^2 denotes the two-dimensional Laplacian operator in the transverse direction. These equations are second-order differential equations for the unknown potential functions which may be Fourier transformed with respect to x to obtain ordinary differential equations via the transformation defined as

$$F\{\phi(x,y)\} = \phi(\alpha_n, y) = \int_{-\infty}^{\infty} \phi(x,y) \, e^{j\alpha_n x} \, dx . \qquad (24)$$

The Helmholtz equations of (23) are transformed into

$$\frac{\partial^2 \phi_i(\alpha_n, y)}{\partial y^2} = (\alpha_n^2 - k_{ci}^2) \, \phi_i(\alpha_n, y) \qquad (25)$$

for the electric field, ϕ^e, and the magnetic field, ϕ^h.

The solutions to these ordinary differential equations for the three regions after applying the boundary conditions at $y = h_1 + D$ and $y = -h_2$ (equations (7), (8), (19) and (20)) can be written as

$$\phi_1^e(\alpha_n, y) = A^e(\alpha_n) \, \sinh \gamma_1(D+h_1-y) \qquad (26a)$$

$$\phi_2^e(\alpha_n, y) = B^e(\alpha_n) \, \sinh \gamma_2 y + C^e(\alpha_n) \, \cosh \gamma_2 y \qquad (26b)$$

$$\phi_3^e(\alpha_n, y) = D^e(\alpha_n) \sinh \gamma_3(h_2+y) \qquad (26c)$$

$$\phi_1^h(\alpha_n, y) = A^h(\alpha_n) \cosh \gamma_1(D+h_1-y) \qquad (26d)$$

$$\phi_2^h(\alpha_n, y) = B^h(\alpha_n) \sinh \gamma_2 y + C^h(\alpha_n) \cosh \gamma_2 y \qquad (26e)$$

$$\phi_3^h(\alpha_n, y) = D^h(\alpha_n) \cosh \gamma_3(h_2+y) \qquad (26f)$$

where

$$\gamma_i^2 = \alpha_n^2 - k_{ci}^2 = \alpha_n^2 + \beta^2 - k_i^2 \qquad (27)$$

and

$$\alpha_n = \begin{cases} n2\pi/b & \phi^h \text{ even} \qquad (28a) \\ \\ (2n-1)\pi/b & \phi^h \text{ odd} \qquad (28b) \end{cases}$$

It is important to observe at this point that γ_i^2 may be less than zero in any of the three regions of the structure under certain conditions. Therefore three sets of solutions can exist for equations (26a) to (26f). When $\alpha_n = 0$ and k_i approaches k_o (where k_o is the wave number for free space) β is less than k_i and so $\gamma_i^2 < 0$. Under this condition the hyperbolic functions in all three regions are replaced by trigonometric functions. If $k_o < \beta < k_2$, then γ_1^2 and γ_3^2

are greater than zero and $\gamma_2^2 < 0$ for some values of α_n and the trigonometric functions replace the hyperbolic functions in the spatial region 2 only. This suggests that the nature of the field is dependent upon the values of the transform variable, α_n. The last solution occurs when $\gamma_i^2 > 0$ for which the solutions are given above. For conditions when $\gamma_i^2 < 0$, γ_i'' replaces γ_i such that $(\gamma_i'')^2 = -\gamma_i^2$ and $\cosh \gamma_i y$ is replaced by $\cos \gamma_i'' y$ and $\sinh \gamma_i y$ is replaced by $j \sin \gamma_i'' y$.

The next step in obtaining a solution to the differential equations is the application of the continuity or boundary conditions at the interfaces between the three spatial regions, namely at $y = 0$ and $y = D$. These conditions are given in equations (9) through (18). Through their application, the eight coefficients A^e through D^h may be related to each other, to the fin surface current $\bar{j}(x)$ and the slot field $\bar{e}(x)$. The resulting set of linear equations (really a set of transformed boundary equations) may be written in a matrix form as follows:

$$[M_E] \begin{bmatrix} A^e \\ B^e \\ \cdot \\ \cdot \\ \cdot \\ \cdot \\ D^h \end{bmatrix} = \begin{bmatrix} 0 \\ 0 \\ \cdot \\ \cdot \\ \cdot \\ Ex \\ Ez \end{bmatrix} \tag{29a}$$

23

$$[M_J] \begin{bmatrix} A^e \\ B^e \\ \cdot \\ \cdot \\ \cdot \\ \cdot \\ D^n \end{bmatrix} = \begin{bmatrix} 0 \\ 0 \\ \cdot \\ \cdot \\ \cdot \\ J_x \\ J_z \end{bmatrix} \qquad (29b)$$

where $E_i(\alpha_n)$ is the transform of the slot field and $J_i(\alpha_n)$ is the transform of the surface current. The matrices $[M_E]$ and $[M_J]$ are square 8×8 matrices and differ only in the last two rows. Details of the application of the continuity conditions and the formation of the $[M_E]$ and $[M_J]$ matrices are shown in Appendix A, with a listing of the matrix elements under the conditions $\gamma_i^2 > 0$ and $\gamma_i^2 < 0$ and normalized with respect to D.

To solve the matrix equations (29), the unknown coefficients A^e through D^h are determined by

$$\begin{bmatrix} A^e \\ B^e \\ \cdot \\ \cdot \\ \cdot \\ \cdot \\ D^h \end{bmatrix} = [M_E]^{-1} \begin{bmatrix} 0 \\ 0 \\ \cdot \\ \cdot \\ \cdot \\ E_x \\ E_z \end{bmatrix} \qquad (30)$$

where $[M_E]^{-1}$ is the inverse matrix of $[M_E]$. Now substituting

equation (30) into (29b) results in the single matrix equation

$$[M_J][M_E]^{-1} \begin{bmatrix} 0 \\ 0 \\ . \\ . \\ . \\ E_x \\ E_z \end{bmatrix} = \begin{bmatrix} 0 \\ 0 \\ . \\ . \\ . \\ J_x \\ J_z \end{bmatrix} . \qquad (31)$$

Using the four lower right hand corner elements of the matrix $[M_J][M_E]^{-1}$, (31) is converted to

$$\begin{bmatrix} G_1(\alpha_n, \beta) & G_2(\alpha_n, \beta) \\ \\ G_3(\alpha_n, \beta) & G_4(\alpha_n, \beta) \end{bmatrix} \begin{bmatrix} E_x(\alpha_n) \\ \\ E_z(\alpha_n) \end{bmatrix} = \begin{bmatrix} J_x(\alpha_n) \\ \\ J_z(\alpha_n) \end{bmatrix}$$

$$(32)$$

where the elements of the matrix [G] are the Fourier transforms of the components of the dyadic Green's function for this structure.

A solution to equation (32) is obtained by using the Method of Moments [Ref. 17]. The inner product is defined as

$$\langle f(\alpha_n), g(\alpha_n) \rangle = \sum_{n=-\infty}^{\infty} f(\alpha_n) g^*(\alpha_n) . \qquad (33)$$

Galerkin's method is used here and thus the Fourier transforms for the electric field components, E_x and E_z will be used for the weighting functions, $W(\alpha_n)$. Taking the inner product of equations (32) with $W_1(\alpha_n) = E_x(\alpha_n)$ and $W_2(\alpha_n) = E_z(\alpha_n)$ yields

$$\langle G_1 E_x, E_x \rangle + \langle G_2 E_z, E_x \rangle = 0$$

$$(34)$$

$$\langle G_3 E_x, E_z \rangle + \langle G_4 E_x, E_z \rangle = 0 \ .$$

Following from Parseval's theorem, the right-hand side of these equations are zero because of the orthogonality of the electric field and surface current at $y = D$.

Up to this point, the formulation of the problem is exact since no approximations have been made. The electric field components and their transforms although unknown can be expanded in a set of basis functions. An investigation of various one-term approximations made by Knorr and Kuchler [Ref. 18] suggests good accuracy can be achieved if the electric field distribution between the fins is approximated by

$$e_x(x) = \begin{cases} 1 & |x| \le W/2 \\ \\ 0 & \text{elsewhere} \end{cases}$$

$$(35)$$

$$e_z(x) = 0$$

26

for the dominant mode. This choice (shown in Figure 3 for A = 1) has been shown to give accurate results for slotlines with W/D $\leq$ 2 [Ref. 18] and it is exact for dielectric slab-loaded waveguide (W/b = 1). Assuming that $e_z(x) = 0$ reduces equation (34) to

$$<G_1 E_x, E_x> = \sum_{n=-\infty}^{\infty} G_1(\alpha_n, \beta) |E_x(\alpha_n)|^2 = 0 \quad (36)$$

where $E_x(\alpha_n)$ is the transform of the electric field distribution

$$E_x(\alpha_n) = \int_{-W/2}^{W/2} e_x(x) \, e^{j\alpha_n x} \, dx = AW \, \frac{\sin(\alpha_n W/2)}{\alpha_n W/2} .$$
$$(37)$$

So, one can see that (36) is dependent on the ratio of λ/λ' or effective dielectric constant, $\varepsilon_{r_{eff}}$, defined by

$$\varepsilon_{r_{eff}} = (\lambda/\lambda')^2 = \beta^2/k^2 .$$

The dispersion characteristic of the dominant fin-line mode can now be found by varying β, the propagation constant, such that equation (36) is satisfied for a given set of physical parameters at a desired frequency of operation.

27
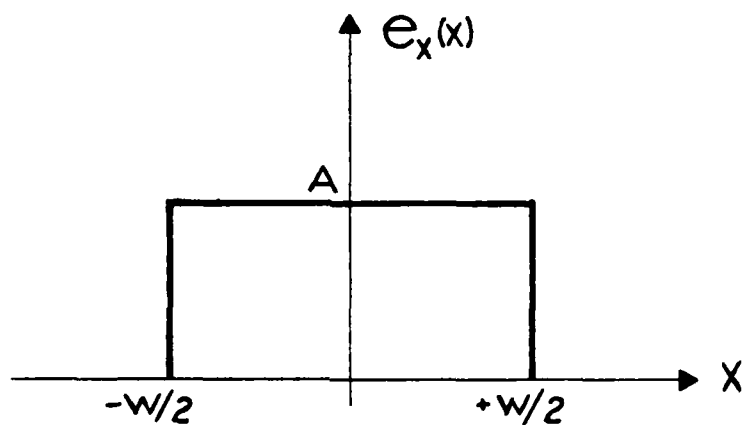
Figure 3. Assumed Electric Field Component in Slot
in x-direction Versus x for Fin-line

C. CHARACTERISTIC IMPEDANCE IN TERMS OF DISPERSION CHARACTERISTICS

The definition of the characteristic impedance for an ideal TEM transmission line is uniquely given by static quantities. Since fin-line is not a TEM transmission line nor does it support a pure TE or TM waveguide mode but rather supports hybrid modes, no unique definition of the characteristic impedance can be found.

One possible choice is to define it as

$$z_0 = \frac{V_0^2}{2 P_{avg}} \qquad (38)$$

where V_0 is the slot voltage defined as

$$V_0 = - \int_{slot} \overline{E} \cdot d\overline{\ell} .$$

Assuming the electric field shown in Figure 3 and (35),

$$V_0 = \int_{-W/2}^{W/2} A \, dx = 1$$

where A was arbitrarily selected as $1/W$ so that $AW = 1$. P_{avg} is the time-averaged power flow in the fin-line structure which is given by

$$P_{avg} = \frac{1}{2} \text{Re} \int\int_s \bar{E} \times \bar{H}^* \cdot \bar{a}_z \, da$$

$$= \frac{1}{2} \text{Re} \int\int_s (E_x H_y^* - E_y H_x^*) \, dx \, dy \, . \qquad (39)$$

Substituting equations (3), (4), (5) and (6) into (39) results in

$$P_{avg} = \frac{1}{2} \text{Re} \int_{-b/2}^{b/2} \int_{-h_2}^{D+h_1} [(j\beta\frac{\partial \phi^e}{\partial x} - j\omega\mu\frac{\partial \phi^h}{\partial y})(-j\beta\frac{\partial \phi^h}{\partial y} + j\omega\epsilon\frac{\partial \phi^e}{\partial x})$$

$$- (j\beta\frac{\partial \phi^e}{\partial y} + j\omega\mu\frac{\partial \phi^h}{\partial x})(-j\beta\frac{\partial \phi^h}{\partial x} - j\omega\epsilon\frac{\partial \phi^e}{\partial y})] dxdy. \qquad (40)$$

This formulation applies to the time-averaged power flow in the spatial domain. Through the use of Parseval's theorem, it is possible to transform this expression into the spectral domain where the scalar potential functions are known. The integration with respect to x is transformed via Parseval's relation into an infinite summation. Applying this theorem where $\phi^e(x,y)$ and $\phi^h(x,y)$ are real yields

$$\int_{-b/2}^{b/2} \int_{-h_2}^{D+h_1} \phi^e(x,y) \phi^h(x,y) dxdy$$

$$= \frac{1}{b} \sum \int_{-h_2}^{D+h_1} \phi^e(\alpha_n,y) \phi^{h*}(\alpha_n,y) \, dy \, .$$

Therefore, equation (40) is transformed into

$$P_{avg} = \frac{1}{2b} \text{Re} \sum_{n=-\infty}^{\infty} \int_{-h_2}^{D+h_1} \{ -\beta\omega\varepsilon\alpha_n^2 |\phi^e|^2 - \beta\omega\mu\alpha_n^2 |\phi^h|^2 - \beta\omega\varepsilon \left|\frac{\partial\phi^e}{\partial y}\right|^2$$

$$- \beta\omega\mu \left|\frac{\partial\phi^h}{\partial y}\right|^2 - j\beta^2\alpha_n [\phi^e \frac{\partial(\phi^h)^*}{\partial y} + \frac{\partial\phi^e}{\partial y}(\phi^h)^*]$$

$$+ jk^2\alpha_n [\phi^h \frac{\partial(\phi^e)^*}{\partial y} + \frac{\partial\phi^h}{\partial y}(\phi^e)^*] \} \, dy. \qquad (41)$$

This expression must be evaluated in each of the three regions of the fin-line shown in Figure 1. Therefore the power flow may be expressed by

$$P_{avg} = P_1 + P_2 + P_3$$

where P_1, P_2 and P_3 are defined as

$$P_1 = \frac{1}{2b} \text{Re} \sum_{n=-\infty}^{\infty} \int_{D}^{D+h_1} \{ f(\phi_1^e, \phi_1^h) \} \, dy \qquad (42a)$$

$$P_2 = \frac{1}{2b} \text{Re} \sum_{n=-\infty}^{\infty} \int_{0}^{D} \{ f(\phi_2^e, \phi_2^h) \} \, dy \qquad (42b)$$

$$P_3 = \frac{1}{2b} \text{Re} \sum_{n=-\infty}^{\infty} \int_{-h_2}^{0} \{ f(\phi_3^e, \phi_3^h) \} \, dy . \qquad (42c)$$

31

The simple functional dependence on the variable y allows one to perform the integration in equations (42a)-(42c) analytically (see Appendix B). This leaves P_{avg} as the summation of the power flow in each region.

$$P_{avg} = \frac{1}{2b} \sum_{n=-\infty}^{\infty} (P_1 + P_2 + P_3) \, . \qquad (43)$$

Now that P_{avg} can be determined by the application of the dispersion characteristic or propagation constant determined earlier and that the slot voltage V_o is known, the characteristic impedance can be computed. The details of these lengthy but straightforward algebraic manipulations are shown in Appendix B.

III. COMPUTER PROGRAMMING

In Section II the theoretical background of the analysis
was provided. This section concerns itself with the computer
programming technique used for fin-line analysis. The program
was designed for the determination of the wavelength and the
characteristic impedance of a particular fin-line structure
over a range of frequencies but due to the nature of the
structure various other configurations may be considered by
the proper selection of input parameters. Dielectric slab
loaded and ridged waveguide along with rectangular waveguide
may also be analyzed. Before the program is described some
general considerations which lead to its development are
necessary for understanding of the numerical methods used.

A. REMARKS ON NUMERICAL ANALYSIS

The computation of the characteristic impedance is based
upon the solution to the dispersion characteristic problem
for the transmission line under consideration. In other
words, the wavelength ratio, λ'/λ, or the wave propagation
constant, β, must be known before any other investigations can
be started since only in this case are the scalar potential
functions in the transform domain known. Hence, in the analy-
sis of the various structures, the starting point is a solu-
tion for β, the propagation constant of equation (36).

33

In general a β is sought such that

$$\sum_{n=-\infty}^{\infty} G_1(\alpha_n,\beta)\,|E(\alpha_n)|^2 \;=\; 0 \qquad\qquad (44)$$

where $G_1(\alpha_n,\beta)$ is a component of the transformed dyadic
Green's function and $E(\alpha_n)$ is the approximation to the
Fourier transform of the electric field in the slot in the
plane $y = D$. A first order approximation is assumed here
which eliminated the other terms of equation (34).

It is obvious that an analytic solution for β cannot be
obtained due to the algebraic complexity leading to the quan-
tity $G_1(\alpha_n,\beta)$ as shown in Appendix A. Thus a numerical
solution is mandatory and must be obtained by computer
programming.

It is shown in Section II that the transforms of the dyadic
Green's function components were obtained by mathematical
manipulation of matrices. The matrix elements are either
real or imaginary so that in general a complex computation on
the computer is necessary. Furthermore, it is shown that the
elements change from hyperbolic to trigonometric functions.
For examaple $\sinh\gamma_2 D$ becomes $j\sin\gamma_2'' D$. It was found that
these quantities are not only pure real or pure imaginary
but change from real to imaginary or vice versa for the
cases $\gamma_i^2 > 0$ and $\gamma_i^2 < 0$.

Previously, equation (32) was obtained by lengthy alge-
braic manipulation of the boundary equations. In the approach

34

described here the matrices (29a) and (29b) are defined directly from the boundary equations and equation (32) is arrived at by numerical computation. There is some sacrifice in numerical efficiency in this approach but the formulation of the problem is straightforward.

Since in equation (44) the absolute value squared of the assumed electric field is taken, this part of the series will be in general a real and even function of α_n. Preliminary numerical investigations by Kuchler [Ref. 19] of the coefficients of these series indicated an even distribution with respect to the variable α_n, also exists. Therefore, all terms of the series (44) are even functions which allows the saving of computation time by summing over only half the interval.

A desired solution for equation (44) can now be found by assigning an arbitrary numerical value for the wavelength ratio and then iteratively changing this until the series converges to zero or more precisely a small enough value so that a prescribed accuracy for the wavelength ratio is realized.

The next task is the determination of the time average power flow. Here again complex arithmetic expressions are involved as seen in Appendix B.

Dielectric substrates are commercially available for various thicknesses D so that in general the line parameters should be computed for each thickness and frequency. A more generalized method of analysis is simply to scale the various geometric quantities involved with respect to this thickness

to obtain more versatile parameters for a varying normalized frequency D/λ. The resulting design curves may then be applied to the structures scaled to different operating frequencies.

B. COMPUTER PROGRAM DESCRIPTION FOR FIN-LINE CONFIGURED TRANSMISSION LINE

A computer program which provides a numerical analysis of fin-line is shown in Appendix C with the main program called 'FIN-LINE' and its accompanying subroutines 'CALC' and "CMTRIN,' all written in the FORTRAN IV programming language.

The program 'FIN-LINE' starts by reading the input data which includes the structure dimensions, the dielectric constant, the initial values of the slot width and frequency and the iteration steps. After the input data is read, initialization of computation loops occur for varying slot widths and normalized frequencies. Next, the program determines the type of structure that exists and whether or not the configuration is operating in the dominant mode. Operation at higher order empty waveguide modes are allowed but program termination occurs at the onset of surface waves.

The program proceeds with preliminary computations used in the determination of the dispersion characteristic. The first major computation of the program that takes place is the finding of the wavelength ratio λ'/λ which satisfies equation (36). The necessary coefficients for determining the series are provided by the subroutine 'CALC'. An initial

36

value of $\lambda'/\lambda = 1/\sqrt{\varepsilon_r}$ is selected where $1/\sqrt{\varepsilon_r}$ is the lower limit of λ'/λ, that is when $\lambda' = \lambda_d$, this wavelength of the dielectric material. The results from the initial computation are used to select a new value for λ'/λ through a bisectional zero finding method to improve the results and the procedure starts over again. The computation is terminated when the correct value for λ'/λ is determined which satisfies equation (36) or when the absolute value of the difference between the old and the new value for λ'/λ is less than $5 \cdot 10^{-4}$ and thus produces a three digit accuracy after the decimal point.

Using the determined value of the wavelength ratio, the program continues with the computation of the characteristic impedance. The coefficients for this computation (equation 40) are provided again by the subroutine 'CALC'.

After completion of the dispersion and impedance computations, the program prints these values and restarts with new values for the normalized frequency and/or slot width.

Figure 4 presents a flow diagram for the main program 'FIN-LINE'. All the variable names have been chosen such that the statements can be readily compared with the respective equations of the appropriate appendices.

The subroutine 'CALC' provides the coefficients and matrix elements as well as an extensive amount of the computation used in the determination of both the dispersion and impedance. The entry variable is λ/λ' for both characteristics. A flow diagram for the function 'CALC' is shown in Figure 5.
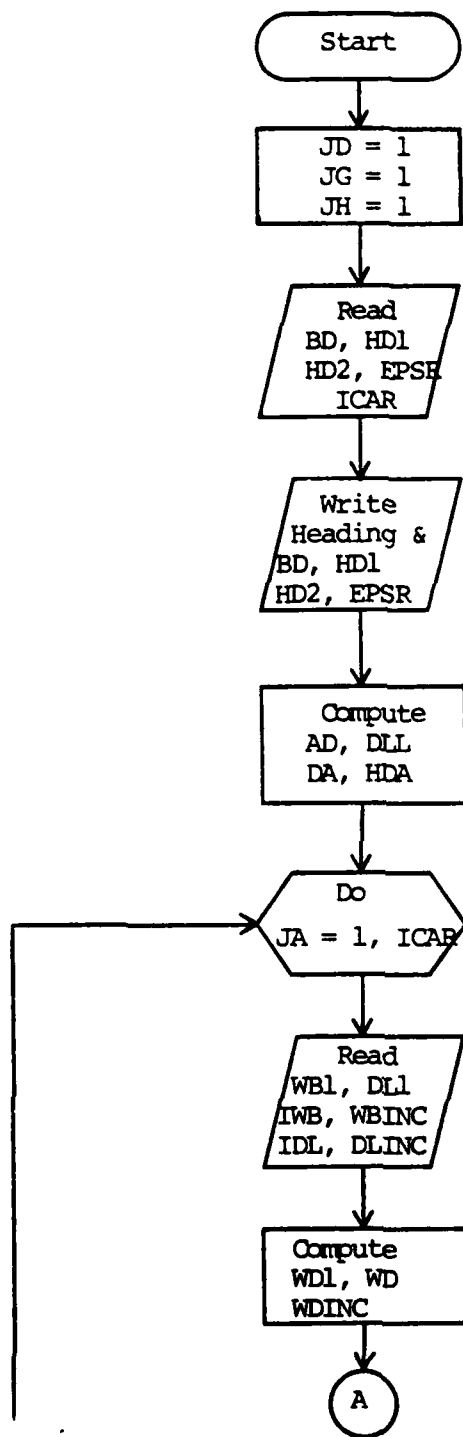
Figure 4a.   Flow Diagram for Main Program 'FIN-LINE'

38
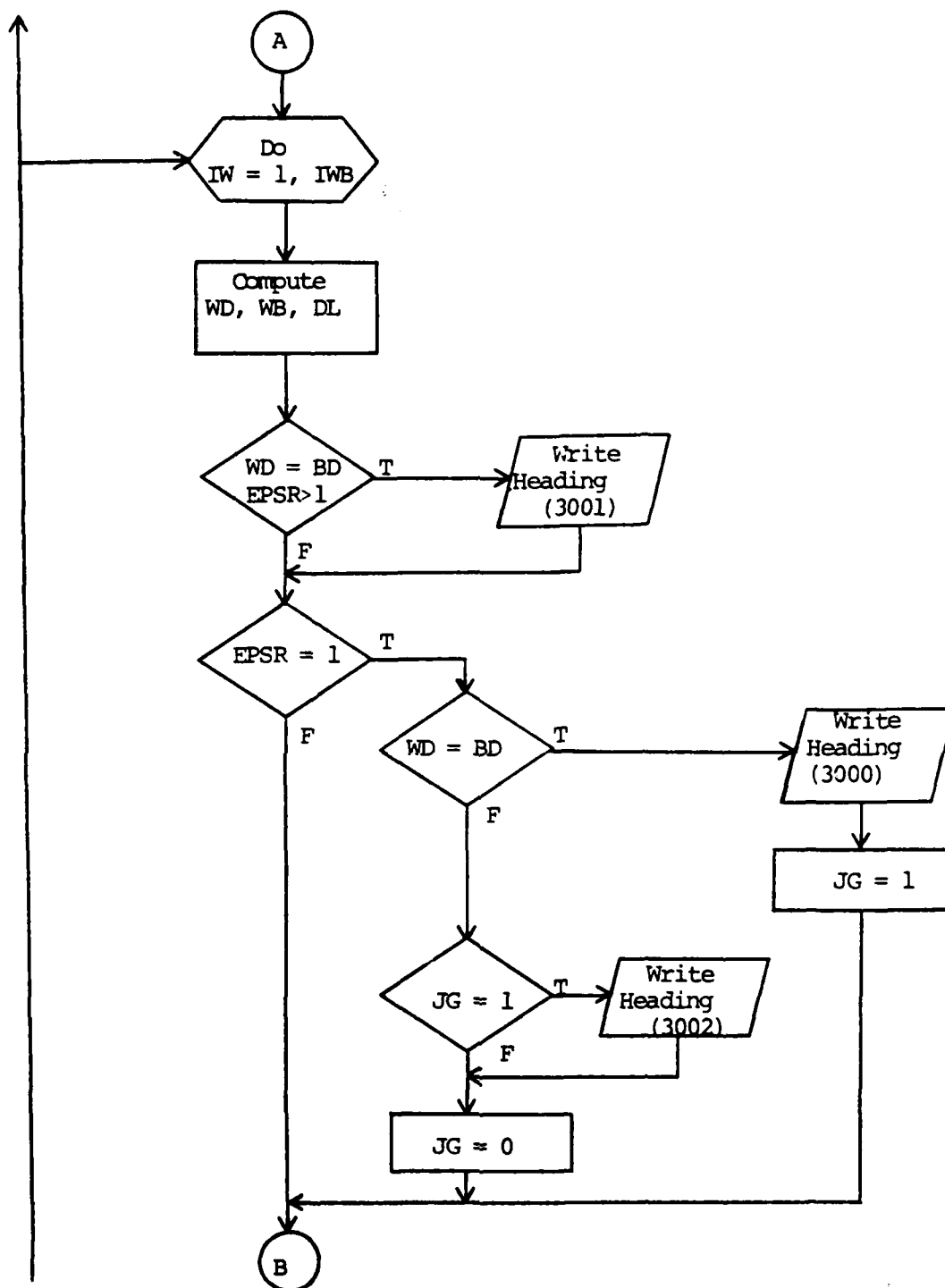
Figure 4b. Flow Diagram for Main Program 'FIN-LINE'
(Continued)
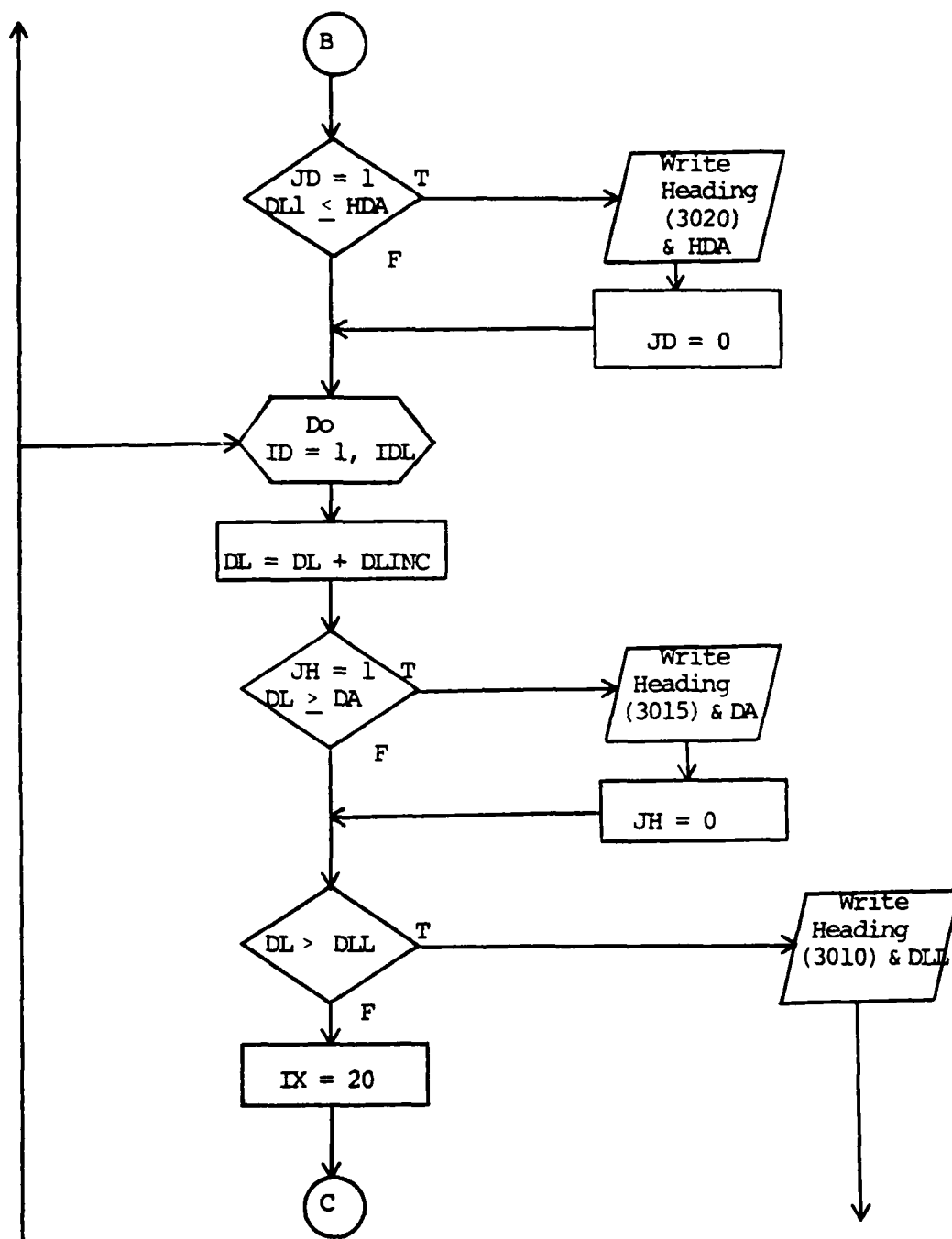
Figure 4c.   Flow Diagram for Main Program 'FIN-LINE'
             (Continued)
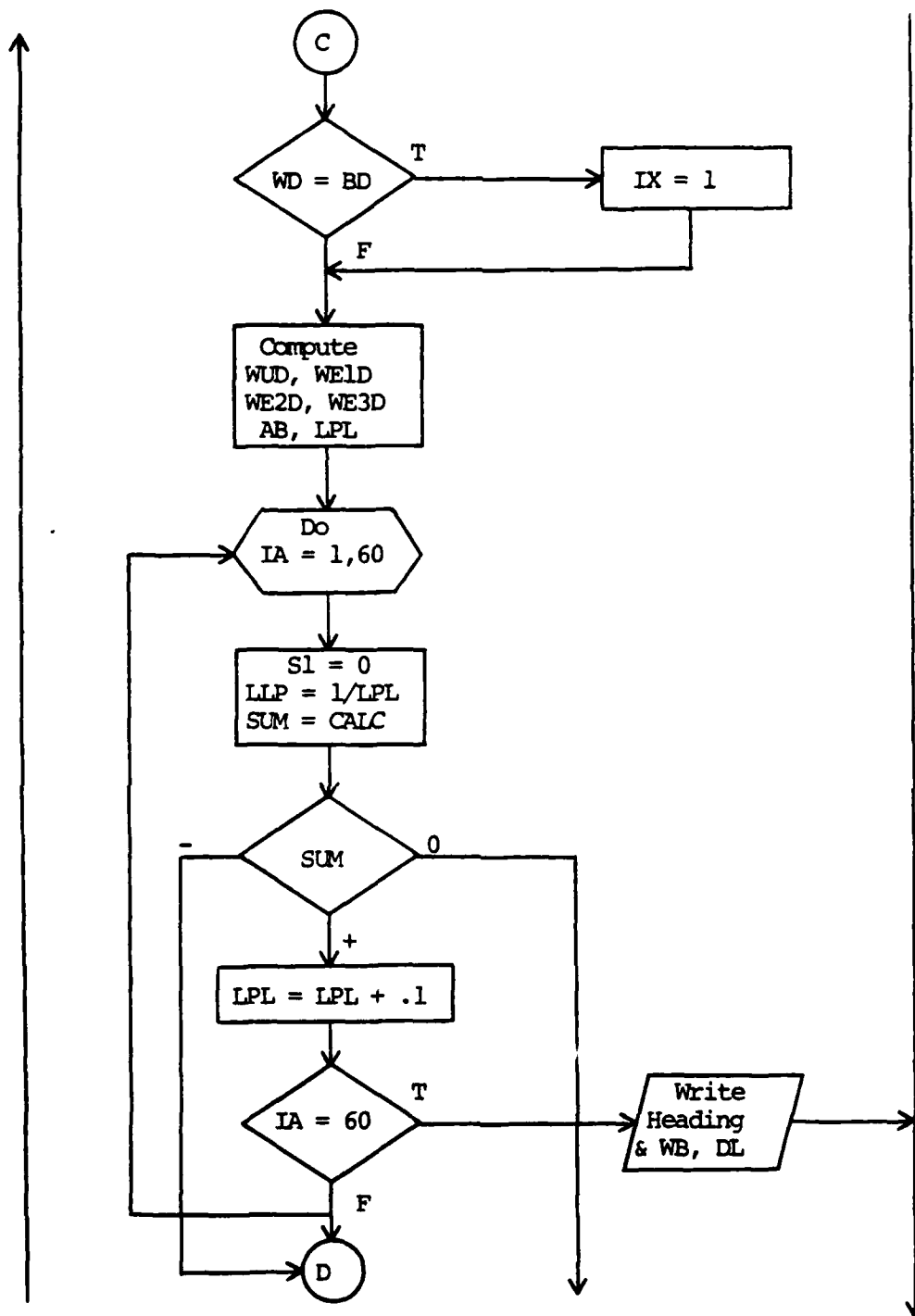
Figure 4d.   Flow Diagram for Main Program 'FIN-LINE'
(Continued)
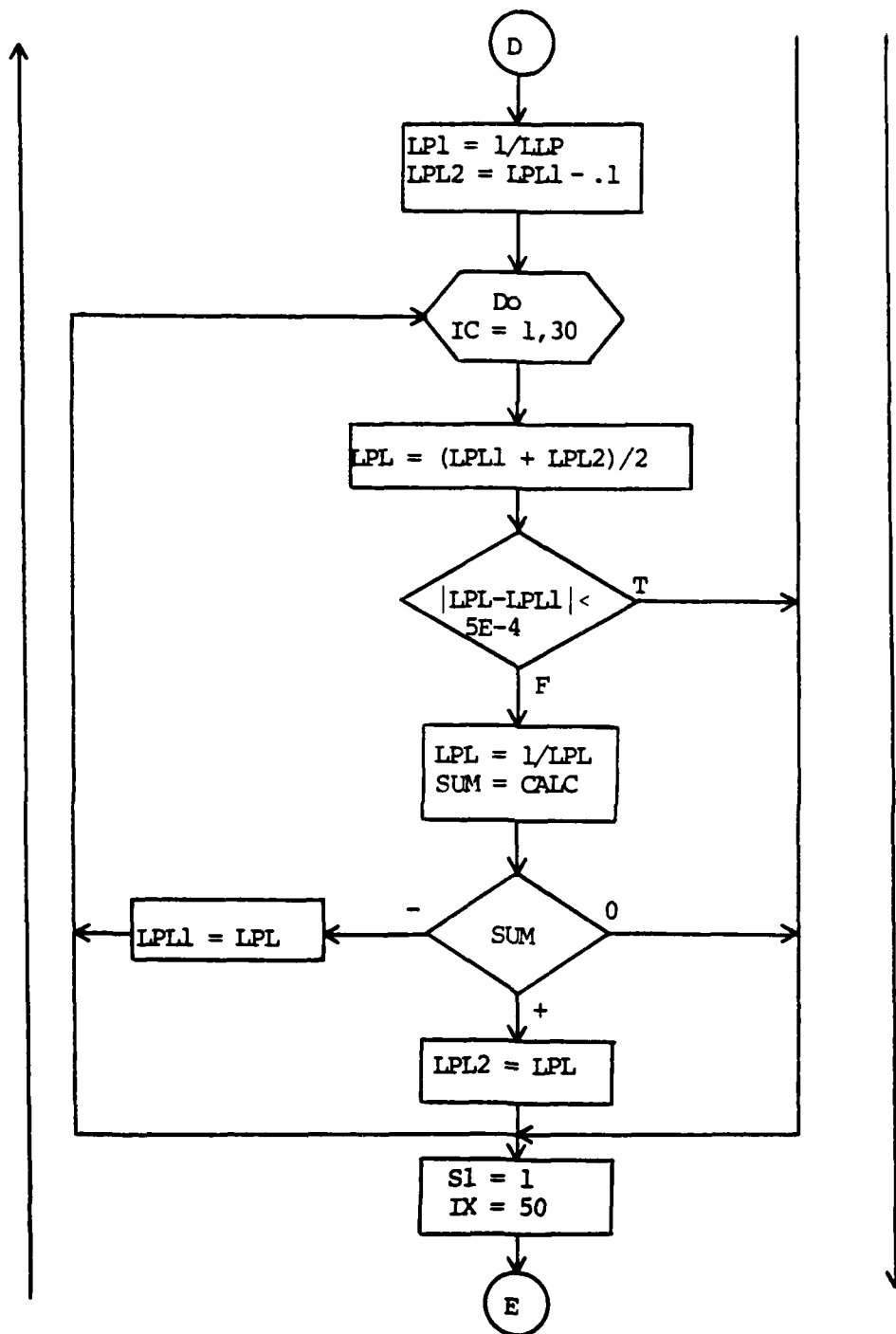
Figure 4e. Flow Diagram for Main Program 'FIN-LINE'
(Continued

42
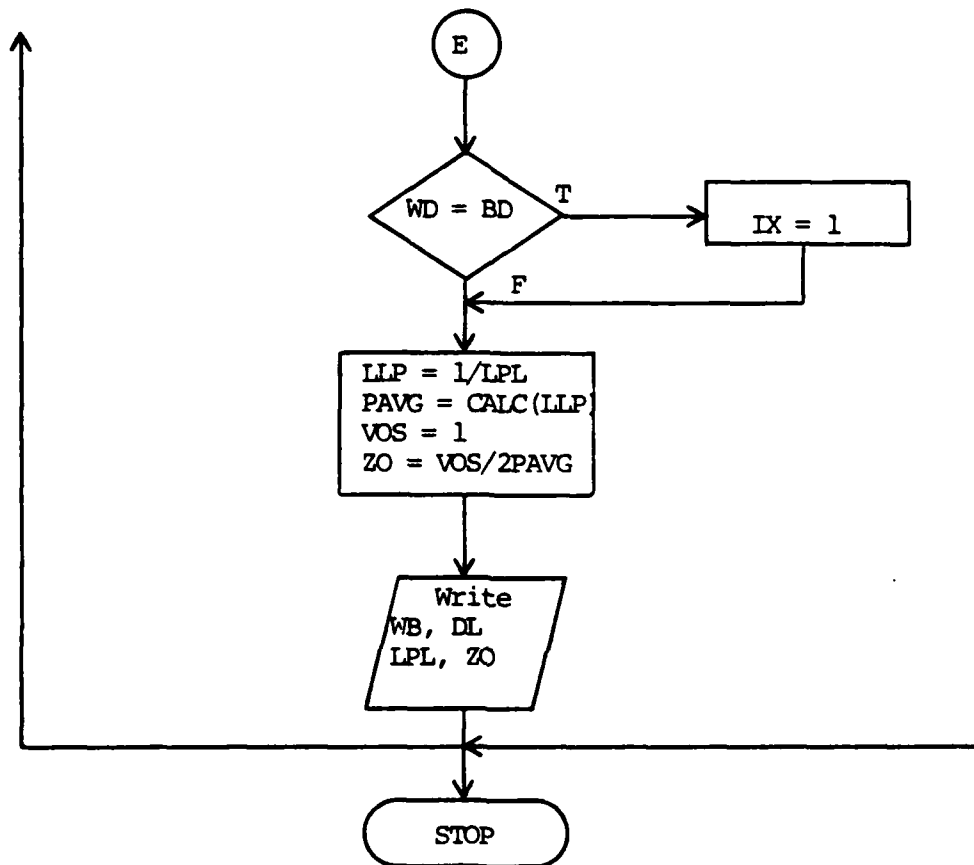
Figure 4f. Flow Diagram for Main Program 'FIN-LINE'
(Continued)
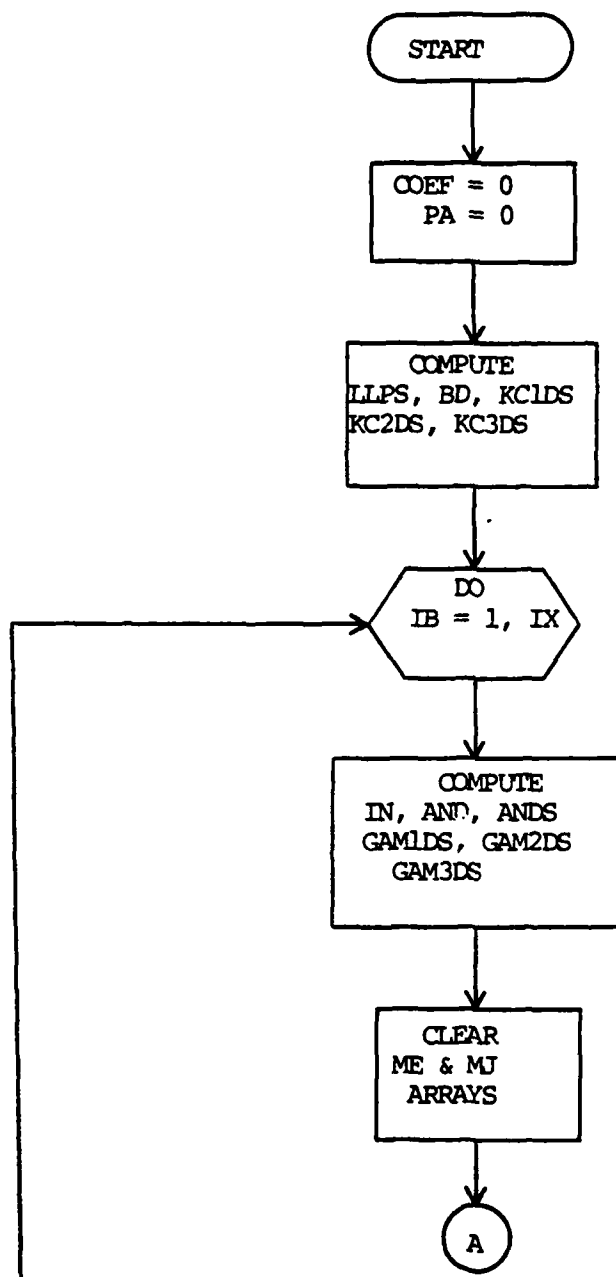
Figure 5a.   Flow Diagram of Subroutine 'CALC'
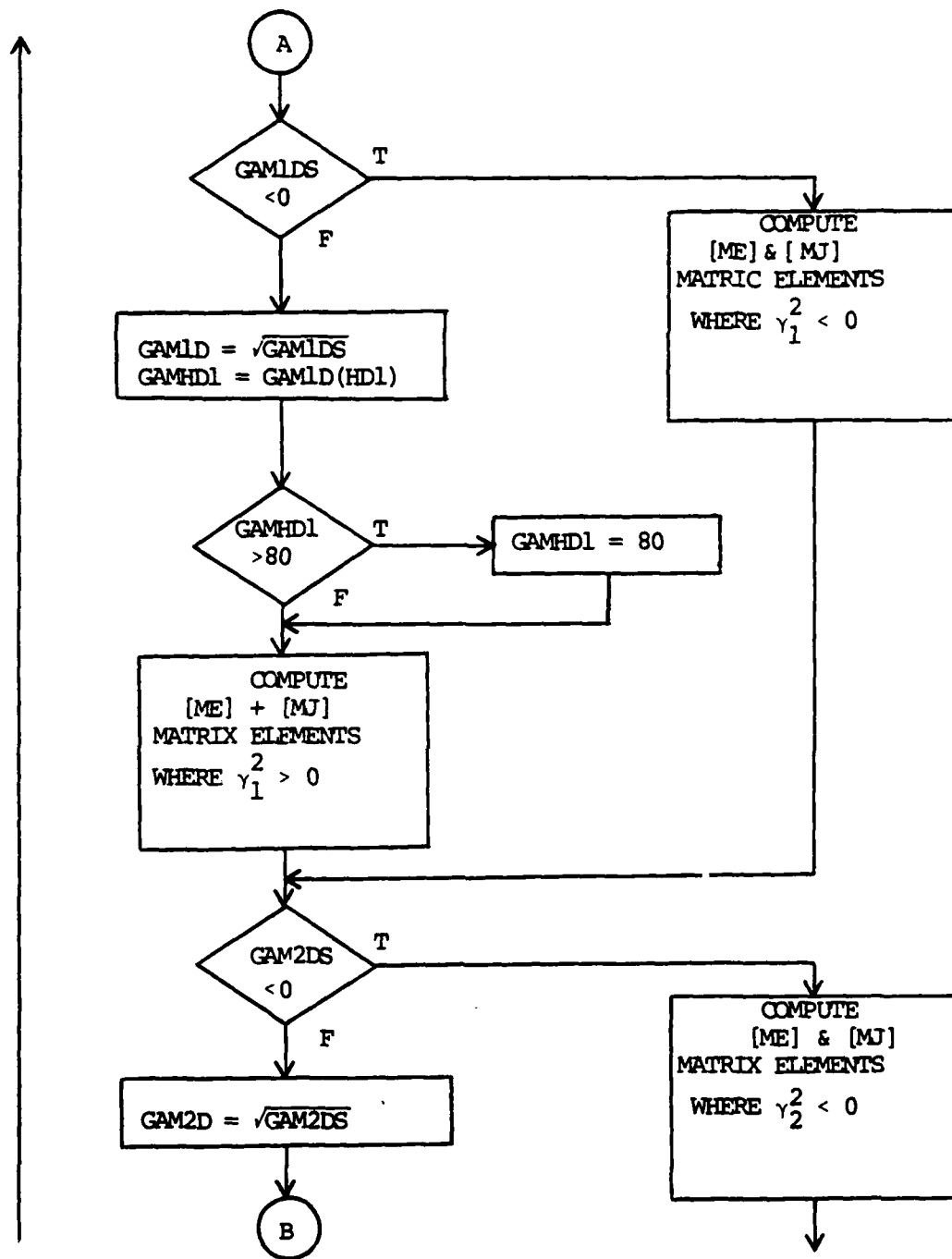
Figure 5b.   Flow Diagram of Subroutine 'CALC'
             (Continued)
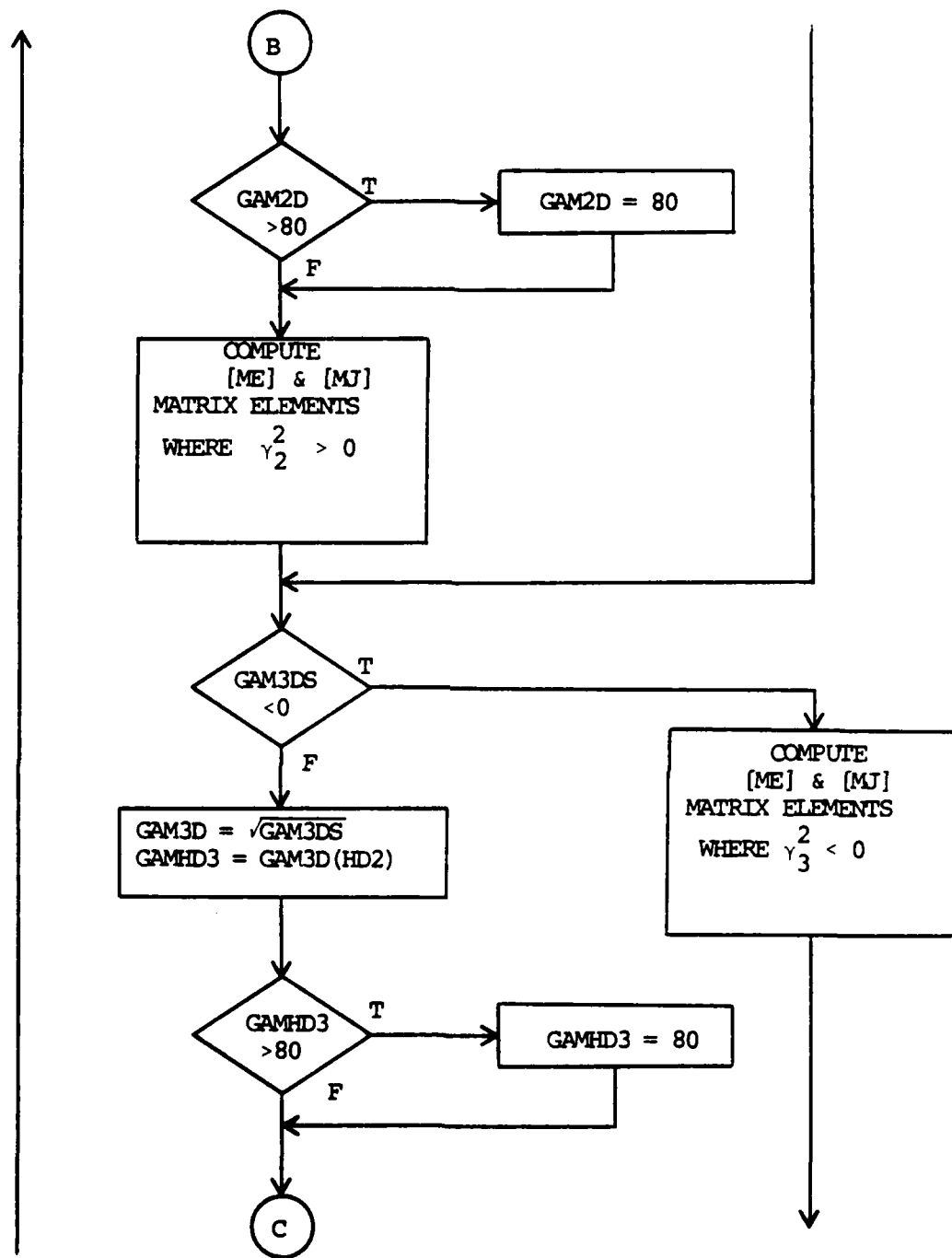
Figure 5c. Flow Diagram of Subroutine 'CALC'
(Continued)
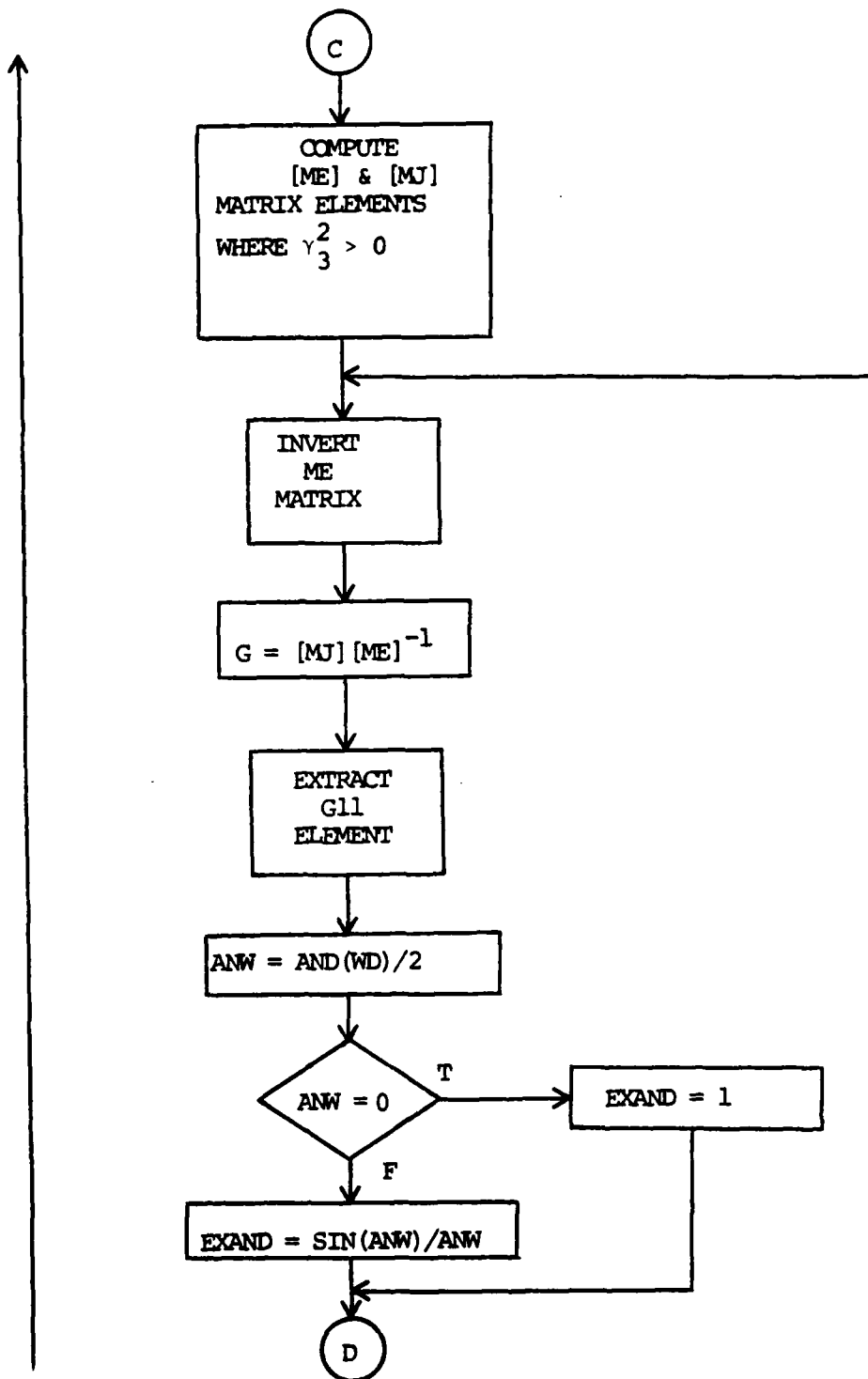
Figure 5d. Flow Diagram of a Subroutine 'CALC'
(Continued)
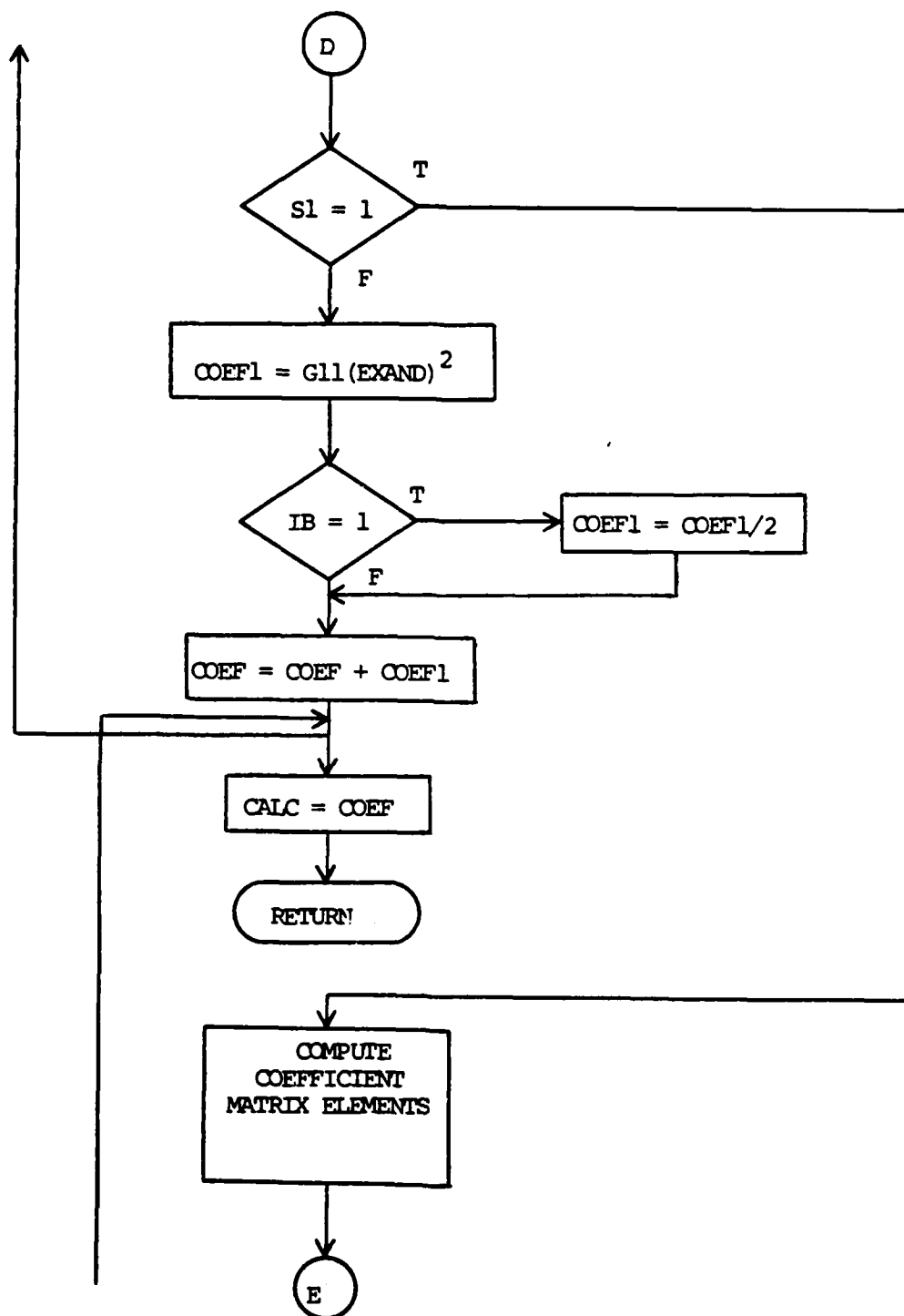
Figure 5e.   Flow Diagram of Subroutine 'CALC' (Continued)
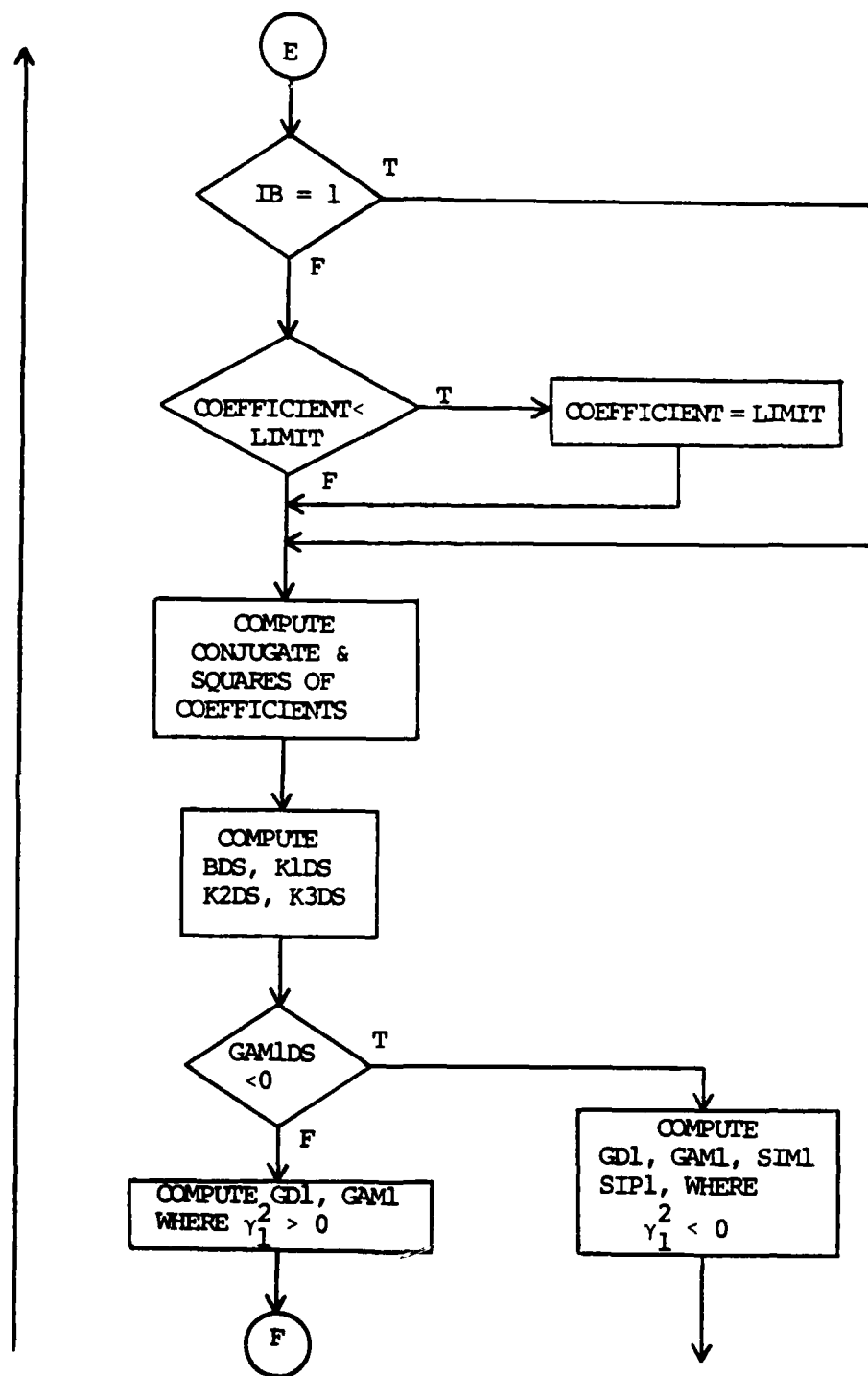
Figure 5f. Flow Diagram of Subroutine 'CALC'
(Continued)
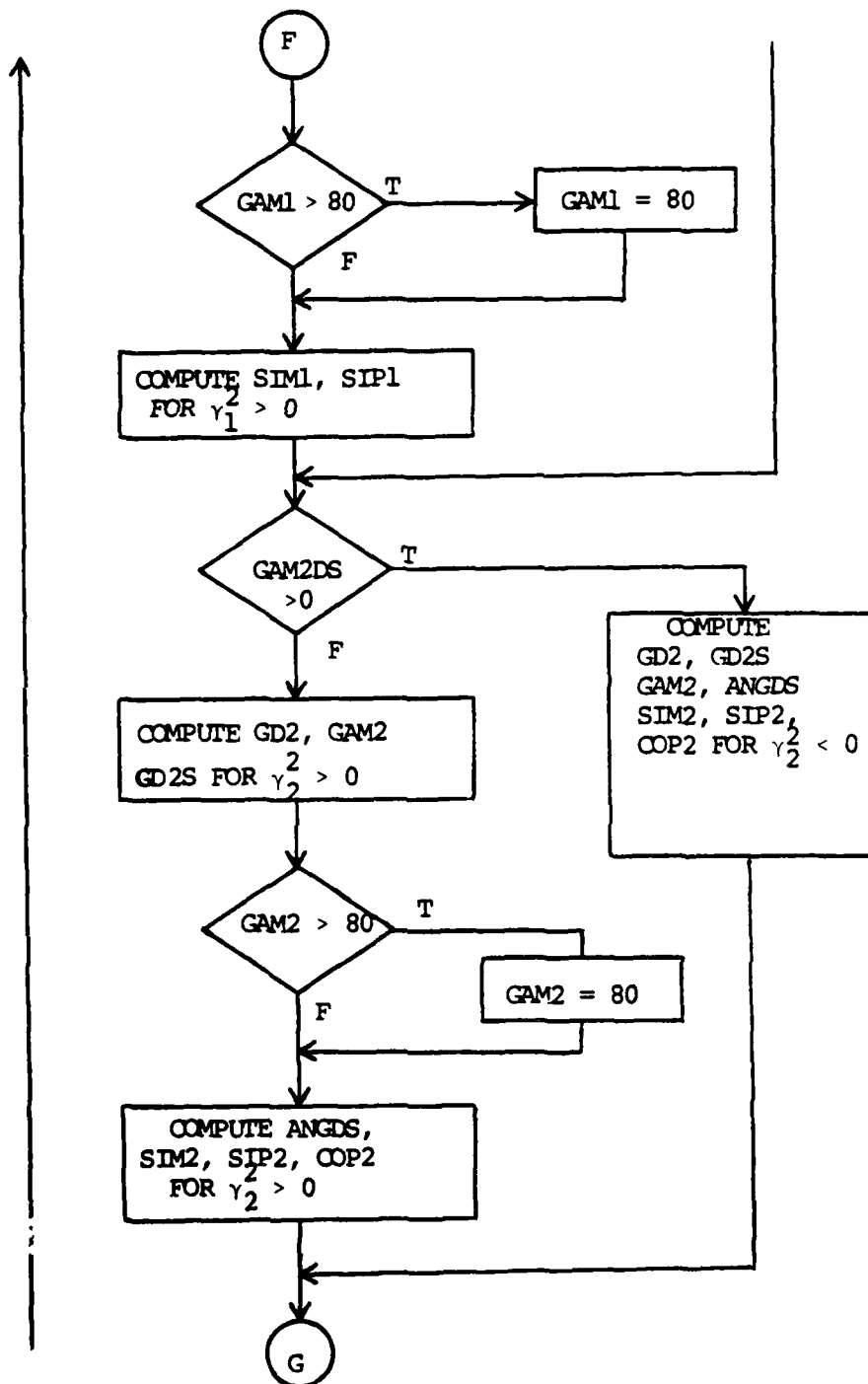
Figure 5g. Flow Diagram of Subroutine 'CALC'
(Continued)
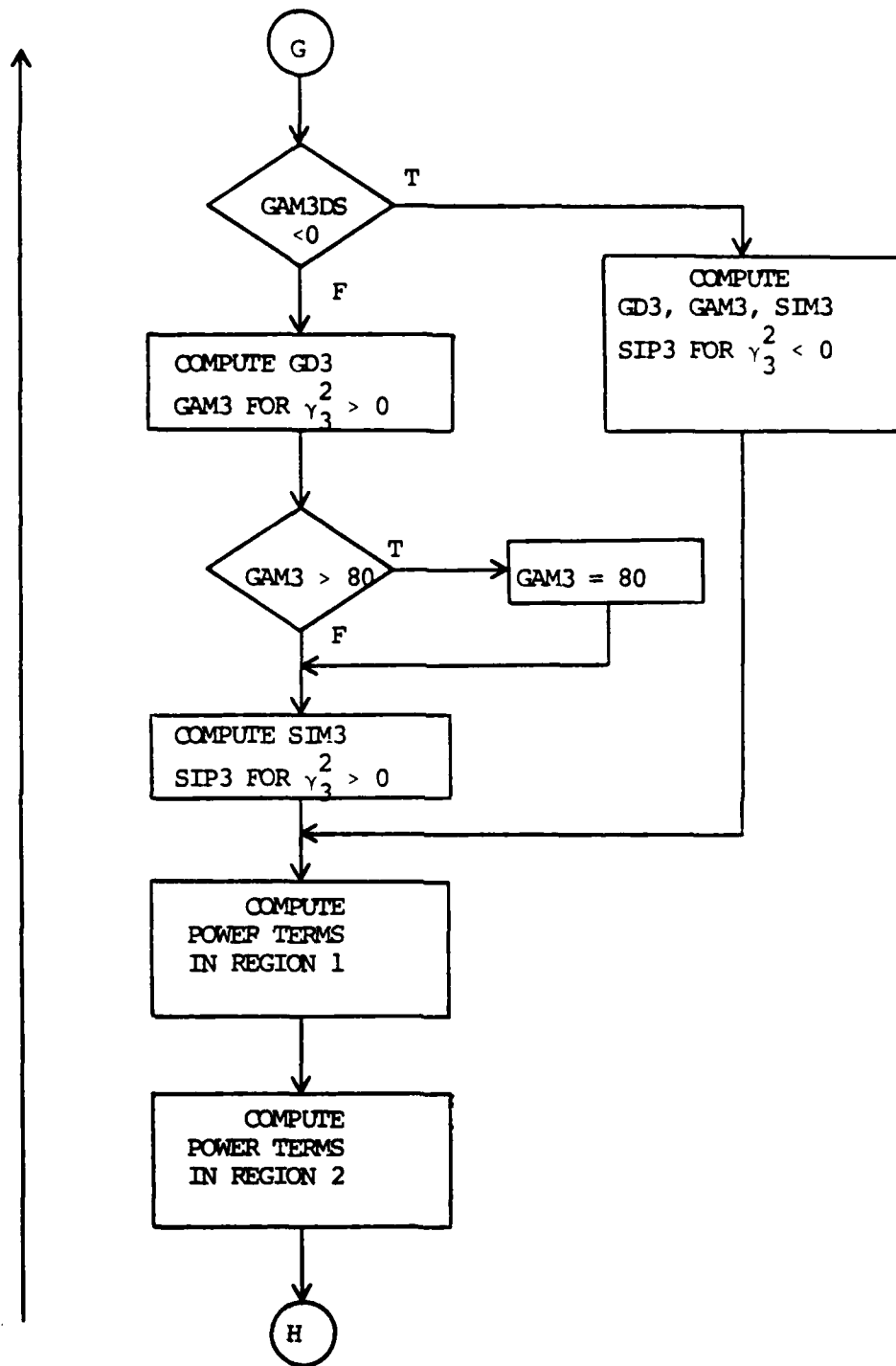
Figure 5h. Flow Diagram of Subroutine 'CALC'
(Continued)
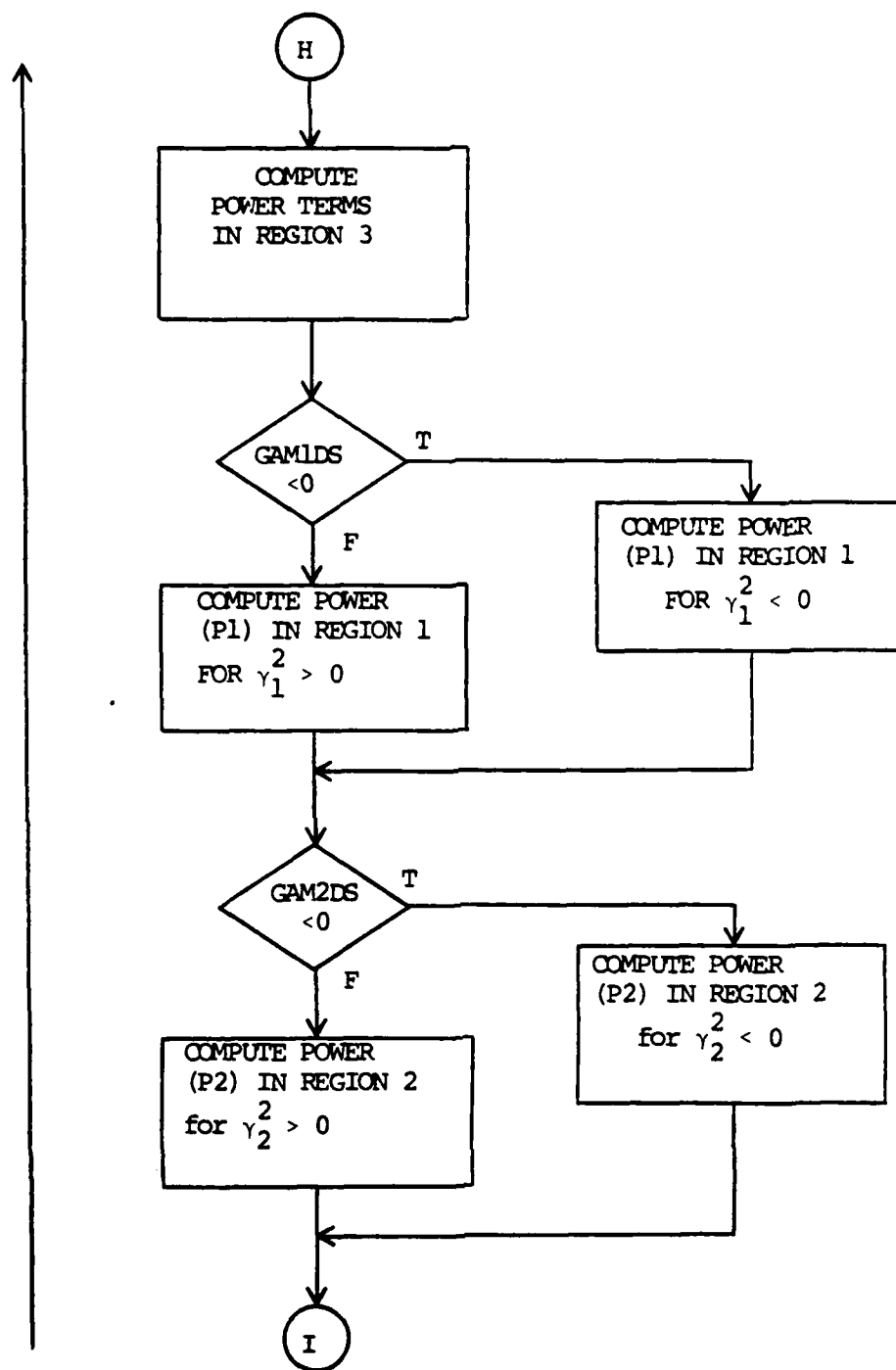
Figure 5i.   Flow Diagram of Subroutine 'CALC'
(Continued)
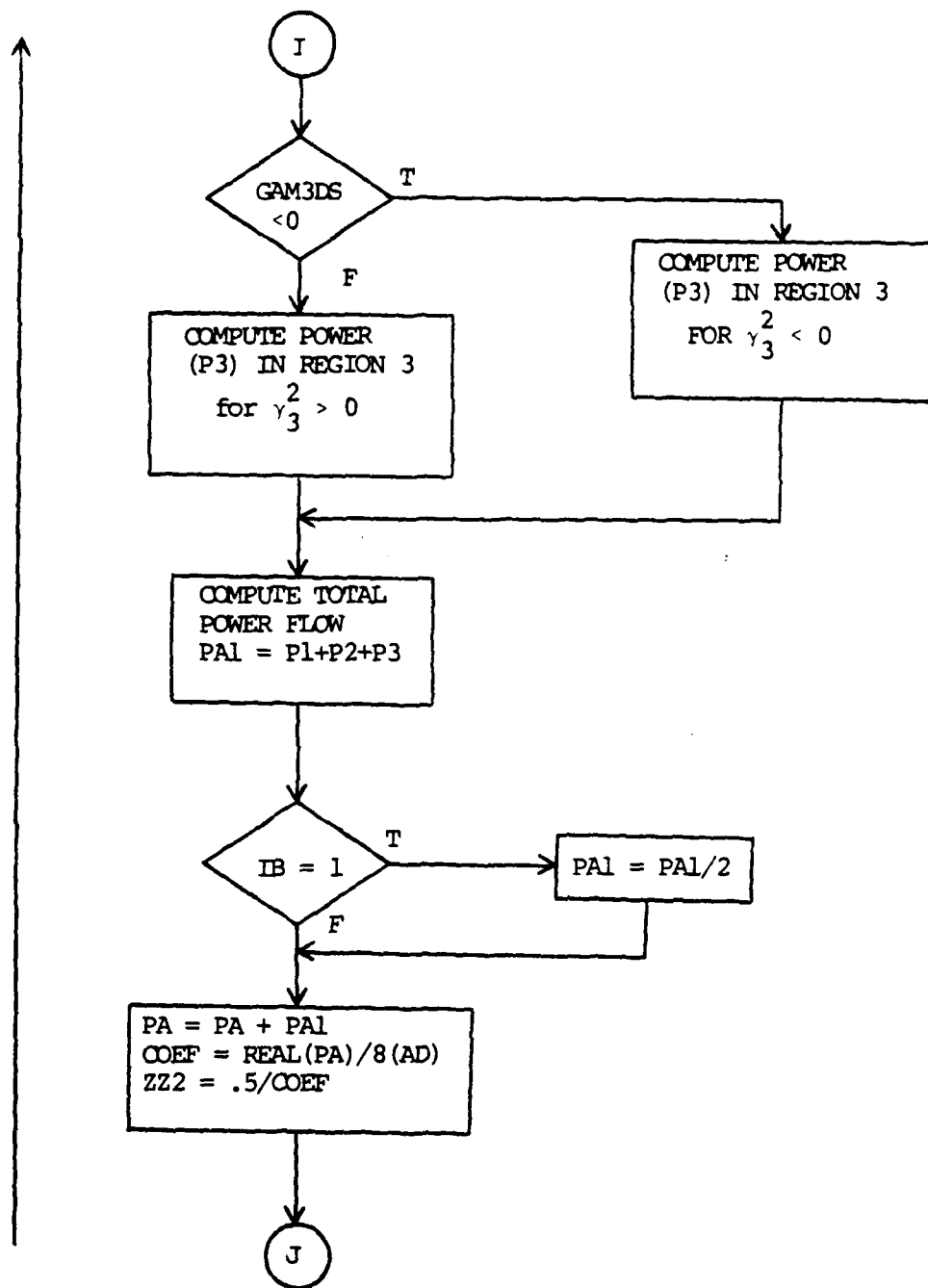
Figure 5j. Flow Diagram of Subroutine 'CALC'
(Continued)

53
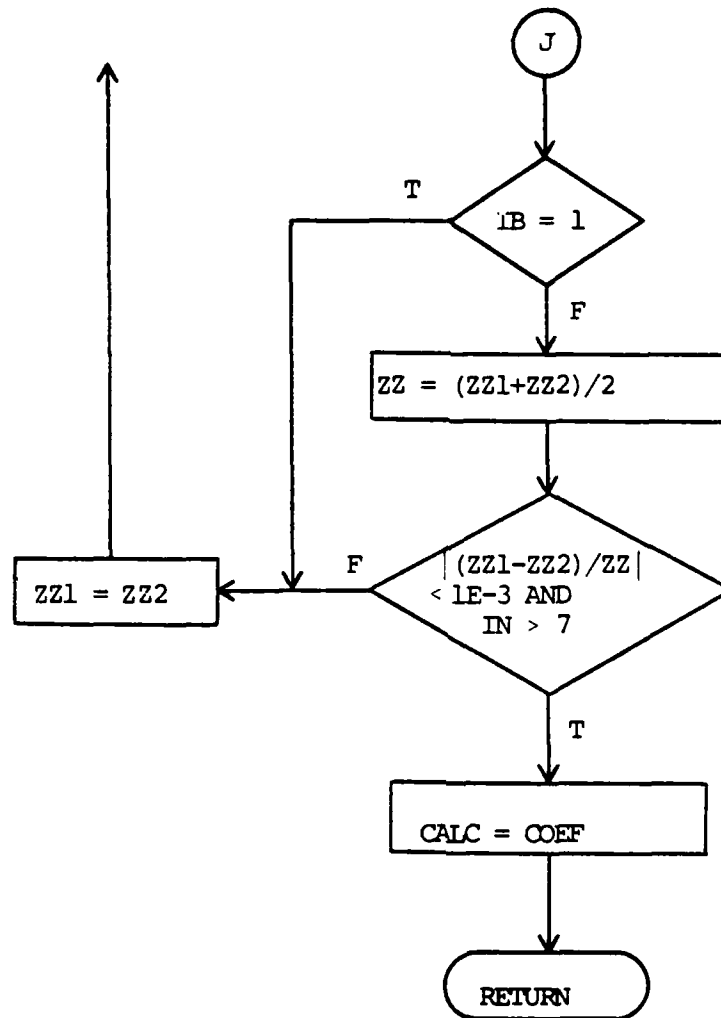
Figure 5k.   Flow Diagram of Subroutine 'CALC'
(Continued)

Once the subroutine is entered from the main program, variables used throughout are computed. Following the initial computations, a decision is made as to whether hyperbolic or trigonometric functions are to be used in the formation of the matrix elements shown in Appendix A. This decision, of course, is made by determining whether γ_i^2 is less than or greater than zero. If $\gamma_i^2 > 0$, hyperbolic functions apply and if $\gamma_i^2 < 0$, trigonometric replace the hyperbolic functions. After the decision making and the formation of the [ME] and [MJ] matrices, the [ME] matrix is inverted and the matrix elements of concern in the [MJ] and $[ME]^{-1}$ matrices are multiplied together for the formation of element G11 of the dyadic Green's functions.

The transform of the assumed slot electric field distribution is determined. At this point the decision, as to whether the dispersion or the impedance is being determined, is made. If the dispersion computation is in process, the subroutine computes the terms of equation (36) and returns to the main program for a new selection of λ'/λ.

If the characteristic impedance computation is being performed, the program continues with the determination of the coefficient matrix elements A^e through D^h. Once again the decision for the use of trigonometric or hyperbolic function is made followed by additional variable computations needed in determination of power.

The power flow in each region is determined for γ_i^2 greater or less than zero, depending on the conditions, and totaled. This procedure is followed until the difference between two consecutive values of the impedance is less than 0.1% at which time return to the main program occurs.

The subroutine 'CMTRIN' takes the complex [ME] matrix and inverts it into the $[ME]^{-1}$ matrix destroying [ME] in the process. The Gaussian Elimination Method with column pivoting is used in determination of the inverse of the matrix. Since this subroutine is small and performs only the one function, it has not been flow charted but is listed in Appendix C.

C. PROGRAM LIMITATIONS

Infinite summations such as those which appear in equations (36) and (41), can not be performed on a digital computer which deals only with finite numbers. Therefore infinity must be replaced by a finite approximation. In the case of equation (36), an analysis of $G_1|E_x(\alpha_n)|^2$ versus n was conducted with results shown in Figure 6. As shown in this figure, when n reaches a value of about 10 the expression is down by at least a factor of 10^{-3} relative to its largest value close to the origin. The value n = 20 is sufficiently large to be considered infinite for all practical purposes. Therefore equation (36) becomes

$$\sum_{n=0}^{\infty} G_1|E|^2 = \frac{G_1(0)}{2} + \sum_{n=1}^{20} G_1(\alpha_n,\beta)|E_x(\alpha_n)|^2. \qquad (45)$$
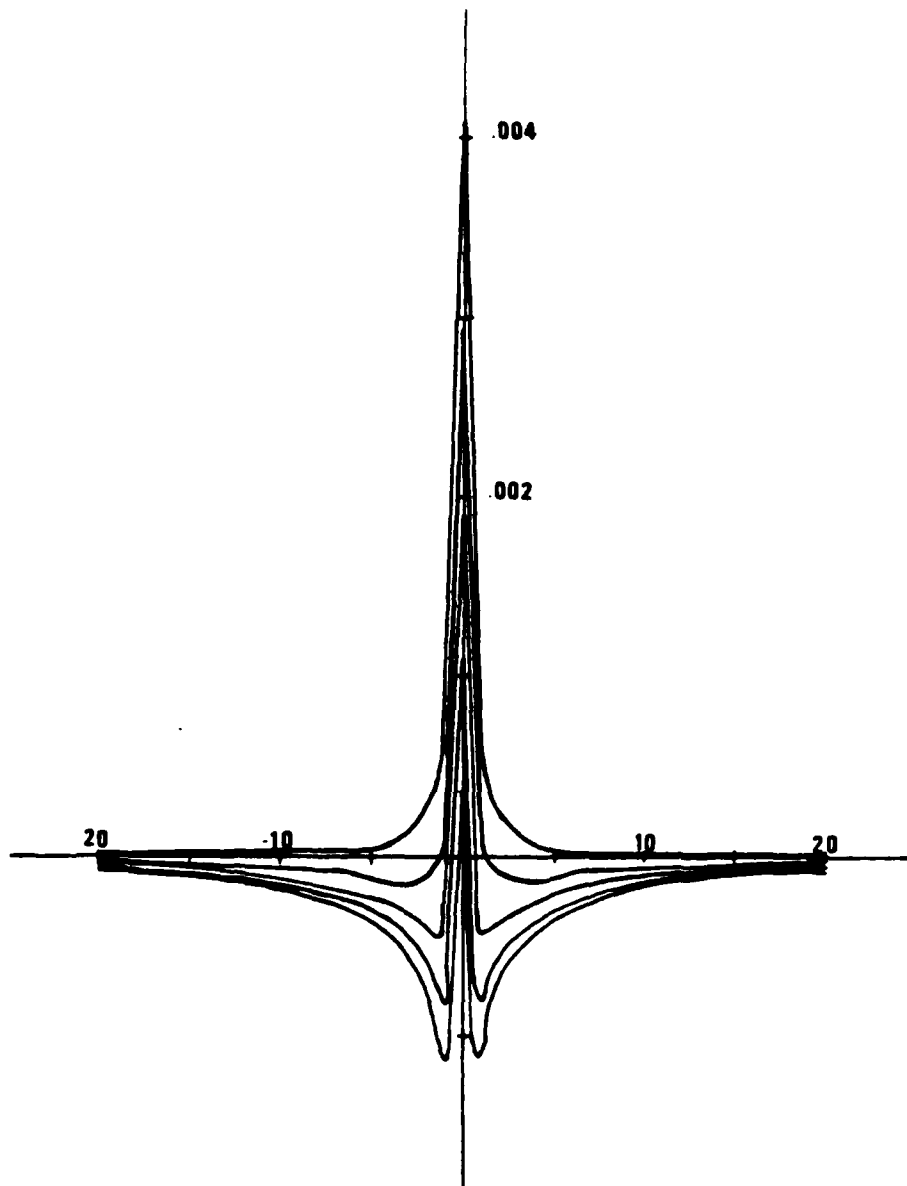
Figure 6. $G_1 |E_x(\alpha_n)|^2$ vs n with $\varepsilon_r = 2.2$ and
$D/\lambda = 0.02$ for Five Arbitrary Values
of λ'/λ

After establishing this limit on the summation, computer errors (overflows) occurred at various points in the summation. An investigation revealed that the problem originated in the dyadic Green's function component when $\gamma_i h_j$ became too large. Varying the size of h_j produced overflows only when h was increased beyond a certain point; a situation where the walls around the central slotline-like structure became far removed from the field. Limits were able to be placed on $\gamma_i h_j$ such that if its value became greater than some value X in this case X = 80, then $\gamma_i h_j$ was set equal to X because of the limited interaction between the walls and the field. When the field-wall interaction becomes a factor, the overflow problem no longer exists. Limitations of this kind are found in the computations of the wavelength as well as the impedance.

The high valued arguments of the hyperbolic functions just discussed cause additional problems when determining the coefficients A^e through D^h in the power flow computations. In the inversion of the matrix [ME], these large values become small ones and when squared produce underflows in the computer system since the magnitude of the elements were less than 10^{-78}. Limitations were placed only on the coefficients A^e, D^e and D^h which caused the underflow problem. The coefficients were limited to magnitudes of $5 \cdot 10^{-38}$. This problem was compounded by the fact that the coefficients are complex and they may also take on either plus or minus signs.

During the investigation of the overflow problem, it was noted that when $W/b = 1$, $E_x = 0$ for $n > 0$ and so $G_1(0)$ was the only important term in the computation. Therefore whenever $W/b = 1$ only the $n = 0$ term is computed in both the wavelength and impedance computations.

In the characteristic impedance equation (41), the coefficients in this infinite series were found to decay rapidly so that a finite approximation yields good results. Figure 7 shows the characteristic impedance as a function of N, the number of terms in the truncated series, for various slot widths. Termination of the impedance computation occurs when the difference between two consecutive values of Z_0 in the iteration loop falls below 0.1% or when the upper limit of $N = 50$ is reached. A minimum of seven iterations is set for the larger values of W/b except for the situation when $W/b = 1$. In this case, only the $N = 0$ term is non-zero.

D. INPUT/OUTPUT DATA

Proper input data formatting is essential for any successful computer program. Input data, similar to that shown in Tables I and II are required with the program 'FIN-LINE'. A minimum of three data cards is necessary to make up the input data deck. The first card specifies the dimensions of the shielding and the permittivity of the dielectric material (b/D, h_1/D, h_2/D and ε_r). This information is entered in a floating point format with the column requirements specified in the program listing in Appendix C. Note that for a ridged
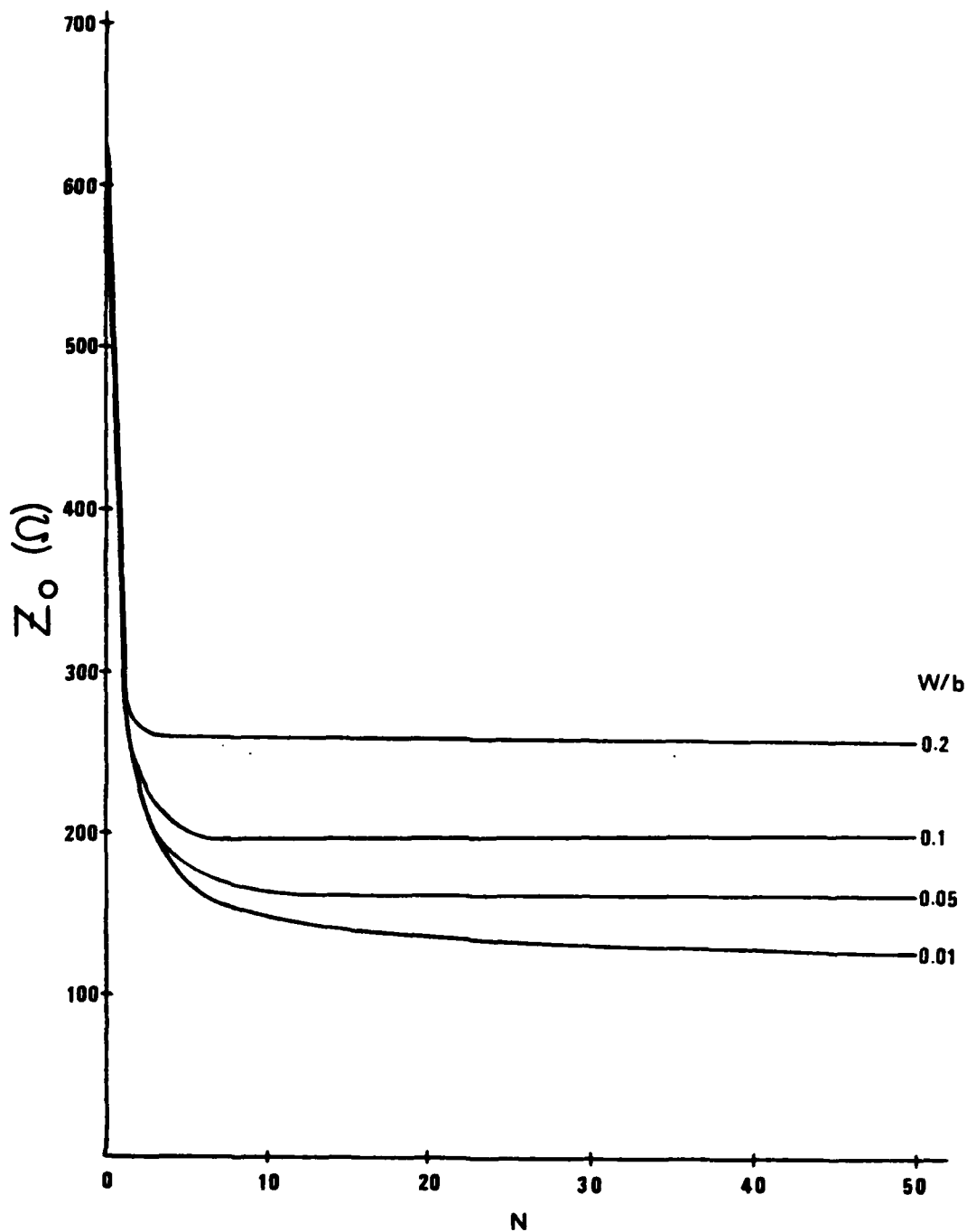
Figure 7. Characteristic Impedance, Z_o, vs. N, the number of terms in the truncated series, with ε_r = 2.2 and D/λ = 0.0212 for a WR(19) shield

60

```
18.8      18.8      17.8      1.0
2
0.1       0.0170    15        0.0       0.0021
0.5       0.0212    24        0.5       0.0021


000G00000 0 00000000000000000 000J00JJ0 0   000000
```

Table I. Sample Input Data for a Ridged Waveguide
Structure with WR(19) Shield

```
18.8      18.8      17.8      2.2
3
0.02      0.0170    15        0.0       0.0021
0.5       0.0170    15        0.0       0.04
1.0       0.01      15        0.0       0.01


00 0G00000 0 00000000000030000 0 0000000 0 0000G00
```

Table II. Sample Input Data for Fin-line Structure
with WR(19) Shield

waveguide, the dielectric substrate thickness is zero. This would result in infinite values for the first three values of the input data (b/D, h_1/D and h_2/D). To eliminate this problem select any thickness greater than zero, but let its dielectric constant equal one.

The second card specifies the number of initial value data cards that follow with nine being the maximum allowed. Sample input of Table I indicates that two cards will follow the second card and sample input of Table II shows three data cards follow.

The third card needed for the input contains initial values for the computations that follow. Six pieces of information are supplied by this card. The first two pieces of information contain the initial values of W/b and D/λ. Next a two digit number specifies the number of different values of W/b (first digit) and D/λ (second digit) that will be computed. On the last card of Table I, the number 24 indicates that the wavelength and impedance will be determined for two different values of W/b and for four different values of D/λ for each W/b. The last two values are the incremental values of W/b and D/λ, respectively. The value of 0.5 will be used to increment the initial value of W/b so that the second value will be W/b = 1. The value 0.0021 will be used to increment the initial value of D/λ so that the four values of D/λ are 0.0212, 0.0233, 0.0254 and 0.0275.

The data shown in Tables III and IV is the computer output from execution of the program listed in Appendix C with the input data of Table I and Table II, respectively.

62

SLOT-TRANSMISSION LINE ON A DIELECTRIC SUBSTRATE
WITH SHIELDED WALLS
(FIN-LINE)

DIMENSIONS: B/D=18.80   H1/D=18.80   H2/D=17.80   EPSR= 1.0

RIDGED WAVEGUIDE STRUCTURE EXISTS
FOR THE FOLLOWING VALUES OF W/B

W/B= 0.100	D/L= 0.0170	LP/L= 1.1559	ZO= 215.7 OHMS
W/B= 0.100	D/L= 0.0191	LP/L= 1.1176	ZO= 208.5 OHMS
W/B= 0.100	C/L= 0.0212	LP/L= 1.0918	ZO= 203.8 OHMS
W/B= 0.100	D/L= 0.0233	LP/L= 1.0738	ZO= 200.5 OHMS
W/B= 0.100	D/L= 0.0254	LP/L= 1.0613	ZO= 198.1 OHMS
W/B= 0.500	C/L= 0.0212	LP/L= 1.1988	ZO= 382.6 OHMS
W/B= 0.500	D/L= 0.0233	LP/L= 1.1559	ZO= 369.1 OHMS
W/B= 0.500	C/L= 0.0254	LP/L= 1.1262	ZO= 359.6 OHMS

TE-20 EMPTY GUIDE MODE PROPAGATES FOR
VALUES OF D/L GREATER THAN 0.027

| W/B= 0.500 | D/L= 0.0275 | LP/L= 1.1051 | ZO= 352.5 OHMS |

RECTANGULAR WAVEGUIDE STRUCTURE
EXISTS FOR W/B= 1.0

W/B= 1.000	D/L= 0.0212	LP/L= 1.2840	ZO= 484.1 OHMS
W/B= 1.000	D/L= 0.0233	LP/L= 1.2176	ZO= 459.2 OHMS
W/B= 1.000	D/L= 0.0254	LP/L= 1.1738	ZO= 442.4 OHMS
W/B= 1.000	D/L= 0.0275	LP/L= 1.1426	ZO= 430.6 OHMS

Table III.   Output Data Obtained Using Sample
Input Data from Table I

63

SLOT-TRANSMISSION LINE ON A DIELECTRIC SUBSTRATE
WITH SHIELDED WALLS
(FIN-LINE)

DIMENSIONS: B/D=18.80   H1/D=18.80   H2/D=17.80   EPSR= 2.2

W/B= 0.020	D/L= 0.0170	LP/L= 0.9183	ZO= 138.6 OHMS
W/B= 0.020	D/L= 0.0191	LP/L= 0.9035	ZO= 138.1 OHMS
W/B= 0.020	D/L= 0.0212	LP/L= 0.8933	ZO= 138.2 OHMS
W/B= 0.020	D/L= 0.0233	LP/L= 0.8855	ZO= 138.9 OHMS
W/B= 0.020	D/L= 0.0254	LP/L= 0.8793	ZO= 139.8 OHMS
W/B= 0.500	D/L= 0.0170	LP/L= 1.2457	ZO= 421.2 OHMS

TE-20 EMPTY GUIDE MODE PROPAGATES FOR
VALUES OF D/L GREATER THAN 0.027

W/B= 0.500	D/L= 0.0570	LP/L= 0.9465	ZO= 501.2 OHMS
W/B= 0.500	D/L= 0.0970	LP/L= 0.9043	ZO= 700.0 OHMS
W/B= 0.500	D/L= 0.1370	LP/L= 0.8683	ZO= 776.9 OHMS

SURFACE WAVES PROPAGATE FOR VALUES OF D/L
GREATER THAN 0.169; RUN TERMINATED

DIELECTRIC SLAB-LOADED WAVEGUIDE
STRUCTURE EXISTS FOR W/B= 1.0

CUTOFF FREQUENCY OF THE DOMINANT MODE
OF EMPTY GUIDE IS D/L= 0.013

W/B= 1.000	D/L= 0.0100	LP/L= *****	ZO= *****
W/B= 1.000	D/L= 0.0200	LP/L= 1.2660	ZO= 508.3 OHMS
W/B= 1.000	D/L= 0.0300	LP/L= 1.0707	ZO= 464.9 OHMS
W/B= 1.000	D/L= 0.0400	LP/L= 1.0191	ZO= 493.8 OHMS
W/B= 1.000	D/L= 0.0500	LP/L= 0.9957	ZO= 553.6 OHMS

Table IV.   Output Data Obtained Using Sample
Sample Input Data from Table II

64

In addition to the tabulated results of the computations for the wavelength and impedance, message statements are also printed under certain conditions. All the messages that can be generated by the program are found in the output of Tables III and IV.

Since various structures may take form by varying the input parameters, description of the type of structure that exists will be printed. For ridged waveguide, the permittivity, ε_r, must be one and $W/b < 1$ whereas the structure becomes empty rectangular waveguide when $W/b = 1$ (shown in Table III). With $\varepsilon_r > 1$ and $W/b < 1$, a fin-line structure is formed. Since this analysis is of fin-line structure, no output statement is printed. When $W/b = 1$ and $\varepsilon_r > 1$, a dielectric slab loaded waveguide structure exists (Table IV).

The analysis of the fin-line structure presented here concerns itself mainly with operation in the dominant TE_{10} limit mode. At the lower end of the dominant mode frequency range when $D/\lambda < D/\lambda_c$, the cutoff frequency of the empty waveguide, an output statement with this information is printed. The cutoff wavelength of the empty waveguide, λ_c, is equal to 2a where $a = h_1 + h_2 + D$. Since the structure takes other forms than just an empty waveguide, operation can exist below D/λ_c. With the presence of a dielectric slab in the fin-line and slab loaded waveguide operation exists below D/λ_c. Therefore analysis below the cutoff frequency of empty waveguide is possible but a lower limit is set. When the value of λ'/λ

exceeds 6, indicating the approach of cutoff, computations terminate without printing values of λ'/λ and Z_o for the values of D/λ for which $\lambda'/\lambda > 6$.

At the high end of the dominant mode frequency range when $\lambda = a$, the TE_{20} of the empty guide can propagate. Therefore a statement is printed when $D/\lambda \geq D/a$. For a value of $D/\lambda \geq 1/(4\sqrt{\varepsilon_r})$, surface waves propagate on the metal-backed dielectric slab and normal operation is no longer possible so the run is terminated for that value of D/λ.

The total program length including all subroutines is 48 K bytes of storage. The sample computer runs presented here with outputs shown in Tables III and IV took 4 and 5 minutes, respectively which includes compilation time of about 20 to 30 seconds.

IV. NUMERICAL RESULTS AND COMPARISONS

To check the accuracy of the numerical results generated by the computer program, comparisons were made with data available in the literature for various fin-line sub-structures. These structures vary from ridged waveguide at one end to dielectric slab loaded waveguide at the other.

A. RIDGED WAVEGUIDE

As mentioned earlier, the fin-line structure shown in Figure 1 becomes ridged waveguide with zero thickness ridges when $\varepsilon_r = 1$ and $W/b < 1$ or when the dielectric substrate thickness D is reduced to zero.

The design of ridged waveguide was first treated by Cohn [Ref. 20] and later by Hopfer [Ref. 21] and Lagerlöf [Ref. 22]. The wavelength and impedance of the ridged waveguide structure can be given by the following expressions

$$\frac{\lambda'}{\lambda} = \frac{1}{[1 - (\frac{\lambda}{\lambda_c})^2]^{1/2}} \tag{46a}$$

$$Z_o = \frac{Z_{o\infty}}{[1 - (\frac{\lambda}{\lambda_c})^2]^{1/2}} \tag{46b}$$

The cutoff wavelength λ_c was obtained from the curves presented in [Ref. 21] for several values of W/b. Using this information and equation (46a), the wavelength ratio λ'/λ was

67

determined. These calculated values were then compared with the results using the spectral domain method of the computer program discussed in Section III. Figure 8 shows the two results with agreement to within 0.5% where the discrete points are from equation (46a).

A similar comparison of the impedance was performed using equation (46b) where Z_o was obtained from curves found in [Ref. 22] and the numerical results of the program 'FIN-LINE.' The results appear in Figure 9 where again very good agreement exists with a difference of only 2%.

B. DIELECTRIC SLAB-LOADED WAVEGUIDE

A variation of the fin-line structure of Figure 1 where $W/b = 1$ and $\varepsilon_r > 1$ results in a dielectric slab loaded rectangular waveguide. This structure has been studied in considerable detail by Vartanian, et al., [Ref. 23]. In their work, the dielectric slab was centered in the waveguide and they presented an analytical expression for the (voltage) impedance, Z_{pv} (using the notation of [23]) at the center of the slab. The impedance computed in this analysis was specified at the edge of the dielectric slab. Therefore a relationship between the two impedances must be defined before any comparison can be made. The impedance at the edge of the slab can be easily defined by the expression

$$Z_o = Z_{pv}\left(\frac{E_x^{edge}}{E_x^{cntr}}\right)^2 \tag{47a}$$
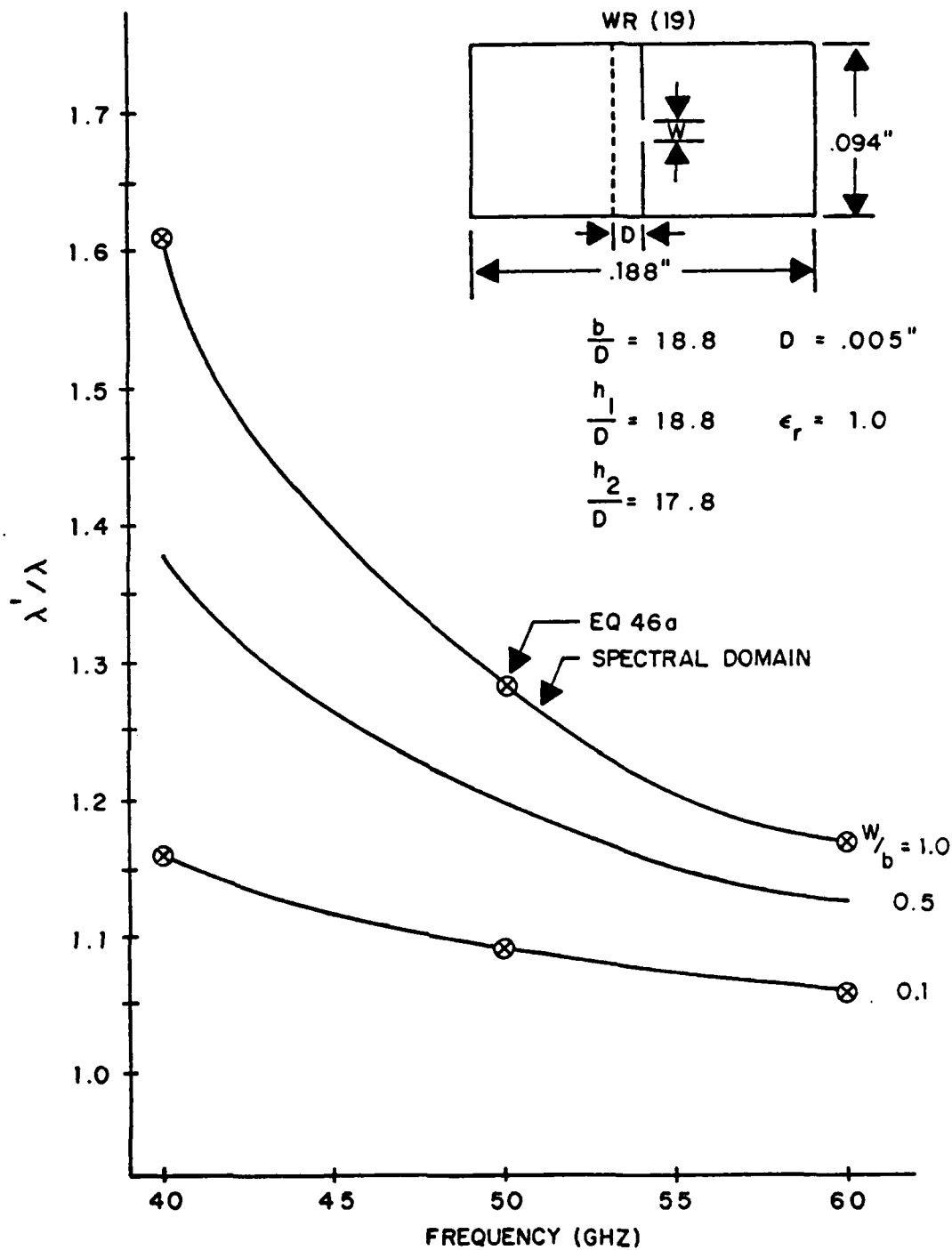
Figure 8. Wavelength ratio, λ'/λ, vs. Frequency for a Ridged Waveguide. Ridges are Centered and Have Zero Thickness
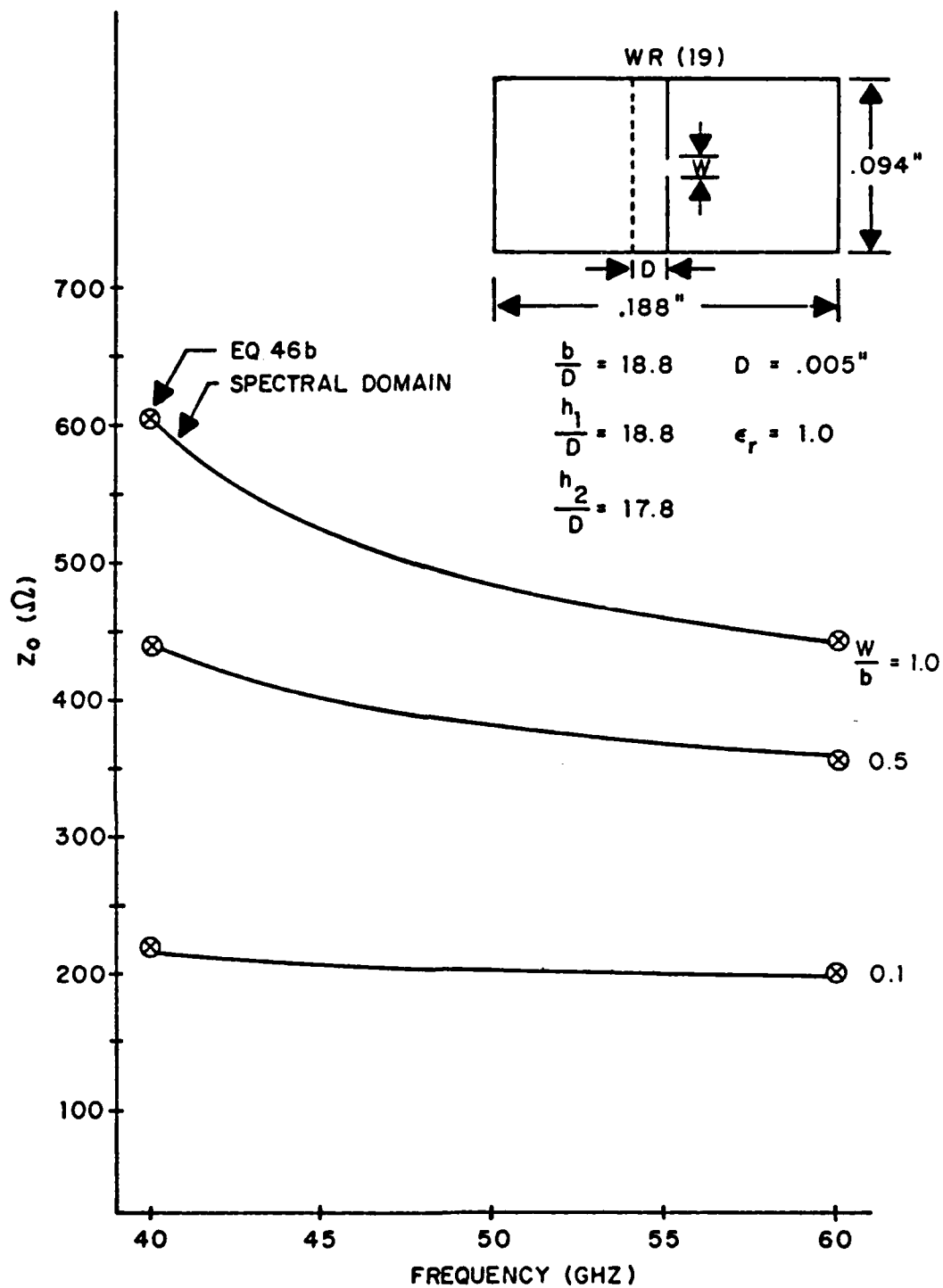
Figure 9. Voltage Impedance Z_o vs. Frequency for a Ridged Waveguide. Ridges are Centered and Have Zero Thickness

70

where E_x^{edge} is the field at the edge of the slab and E_x^{cntr} is the field at the center of the slab. Thus,

$$Z_o = Z_{pv} \cos^2(\frac{qc}{2s}) \qquad (47b)$$

where the various quantities are defined in [22] as

$$q^2 = (2\pi)^2 (\frac{s}{\lambda})^2 [\varepsilon_r - (\lambda/\lambda')^2]$$

$$s = c/2$$

and $C = D$ is the dielectric slab thickness. The characteristic impedance of a slab loaded waveguide was computed using equation (47b) (where Z_{pv} was obtained from Vartanian's curves) and the spectral domain method. The results of the computations are compared in Figure 10 where the discrete points are calculated from equation (47b). It can be seen that the results agree very closely. The difference is less than 1%.

The wavelength of the slab loaded waveguide may be determined analytically by the transverse resonance procedure [Ref. 16] which is found by writing the field expressions for an exact solution of the problem, applying boundary conditions at the air-dielectric interfaces and thereby obtaining the determinantal equation for the structure. The wavelength ratio is found by determining the value of λ'/λ which satisfies
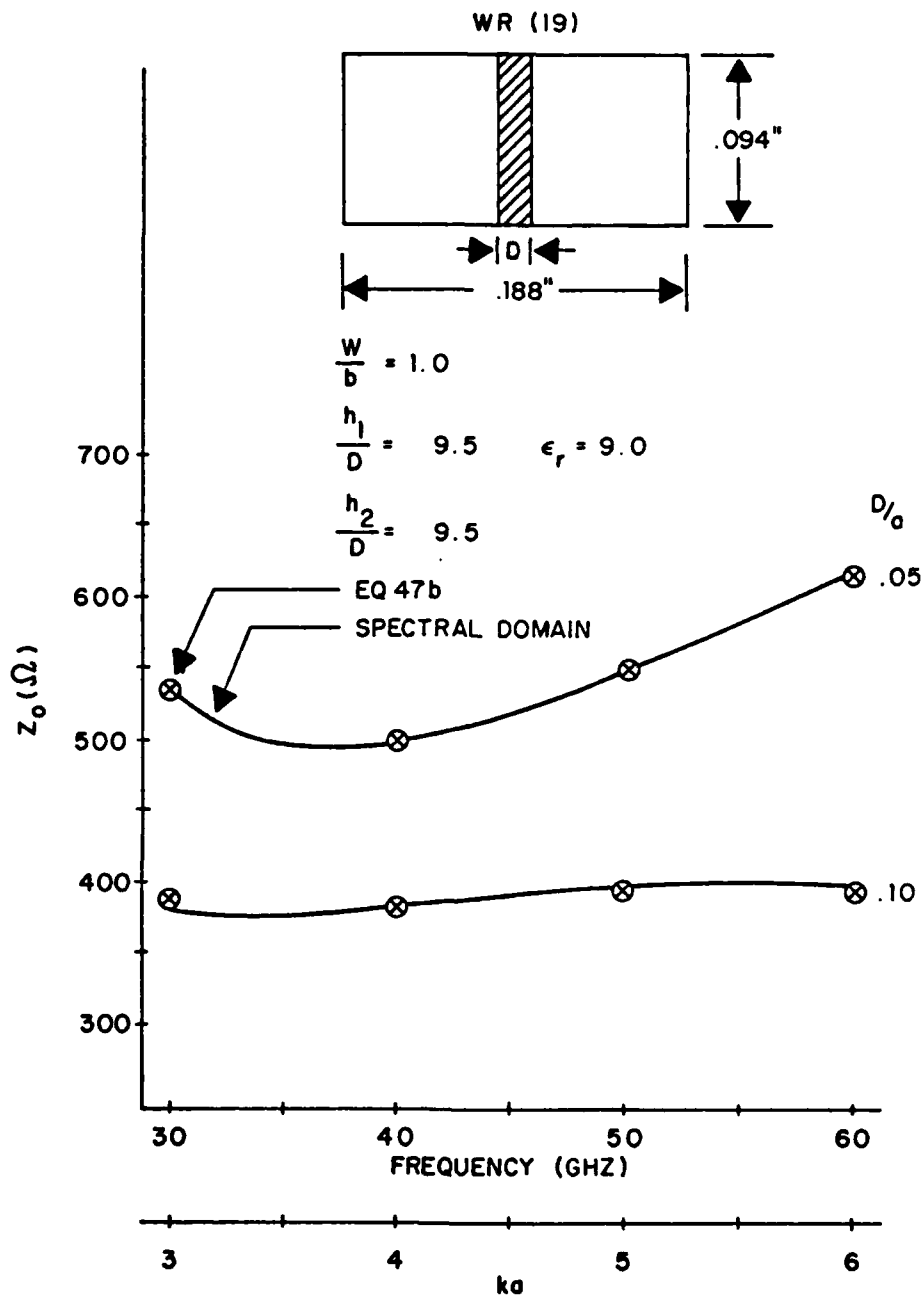
Figure 10. Voltage Impedance Z_o vs. Frequency for a Slab Loaded WR(19) Waveguide. Slab is Centered

the determinantal equation. Figure 11 shows the variation
of the wavelength ratio with dielectric thickness, D, for
several values of ϵ_r obtained by the spectral domain method.
The edge of the slab was placed at the mid-point of the broad
wall of a WR(19) waveguide operating at 40 GHz. The dis-
crete points are those values determined by the transverse
resonance approach. Excellent agreement was obtained between
the results of the two methods. The greatest difference between
the different approaches was only 0.6%.

C. SLOTLINE

If $W/D \leq 2$ and ϵ_r is sufficiently high for the fin-line
structure of Figure 1, the presence of the shield will have
little effect if the walls are sufficiently far removed from
the slot. In this case the structure will behave like a slot-
line. This behavior of fin-line is illustrated in Figure 12
where the wavelength and characteristic impedance is plotted
for $\epsilon_r = 20$ and a slot width normalized to the dielectric
thickness, $W/D = 1$. The discrete points represent the wave-
length (▣) and the impedance (⊗) of a slotline obtained
from [Ref. 24] for the same parameters ϵ_r and W/D as the fin-
line. Agreement between the fin-line and the slotline is
within 1% for the wavelength and 5% for the impedance. The
impedance curve for a ridged waveguide structure with the
same fin separation is plotted for reference.
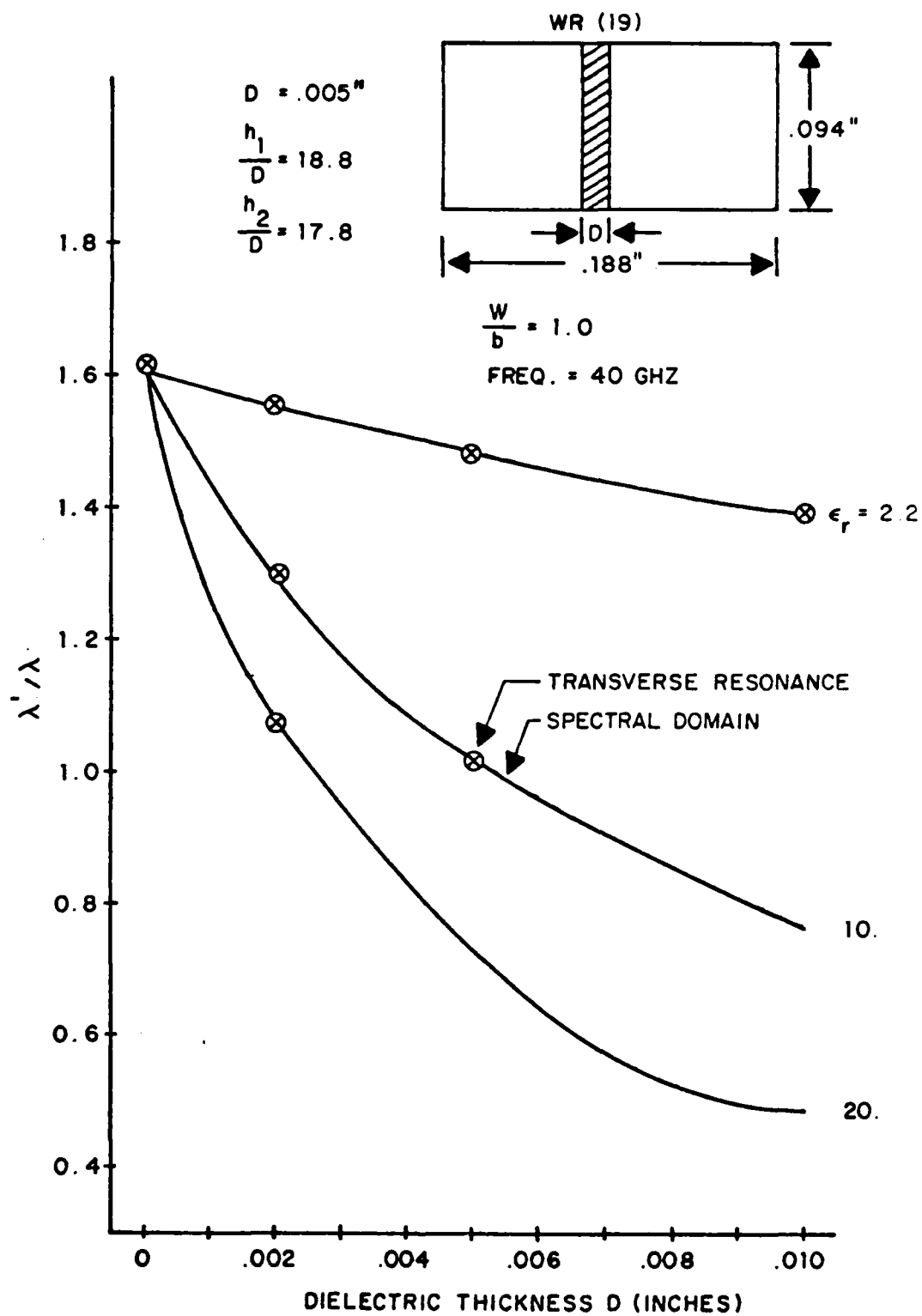
Figure 11. Wavelength ratio, λ'/λ vs. Dielectric Thickness, D_1 for a Slab Loaded WR(19) Guide. Edge of Slab is Centered
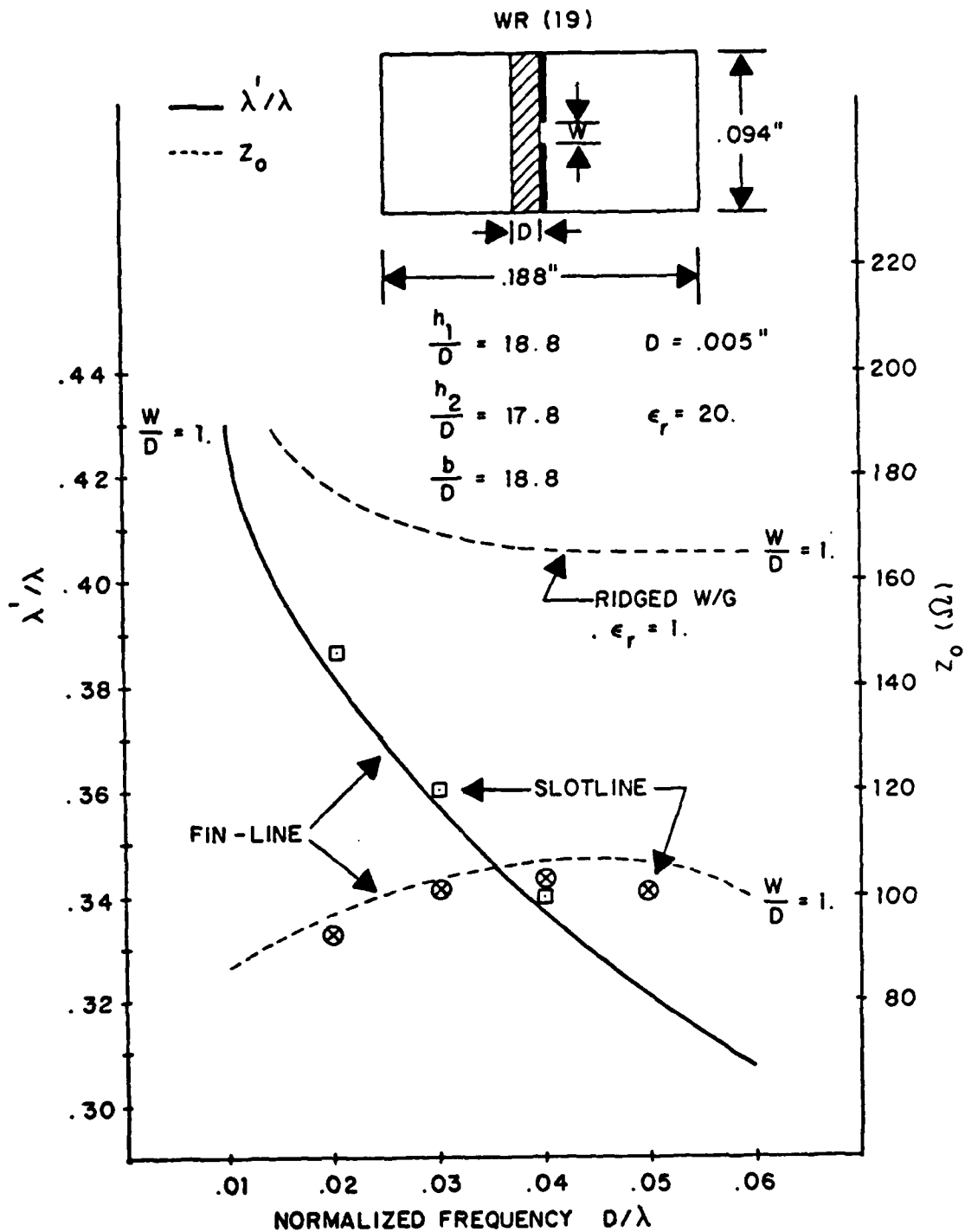
Figure 12. Wavelength Ratio, λ'/λ, and Characteristic Impedance, Z_o vs. Normalized Frequency D/λ for Fin-line and Slotline. Fin-line Has WR(19) Shield and Fins Centered

D. MEASUREMENTS

Very little experimental data is available in the literature for any significant comparison. However, fin-line wavelength measurements have been presented by Meier [Ref. 1]. The guide wavelength in the millimeter fin-line structure was measured across the band of 26.5 - 40 GHz by a sliding short-circuit technique. The fin-line used a D = 10 mil substrate with ϵ_r = 2.2. A WR(28) shield (a = .280", b = .140") was used along with a fin separation W/b = .128 (W = .018"). The results of this experimental work are plotted in Figure 13. A computer run was made for a structure with the parameters reported by Meier and the results were compared with Meier's measured values. This comparison is illustrated in Figure 13 where an agreement to within 1% can be seen.

76
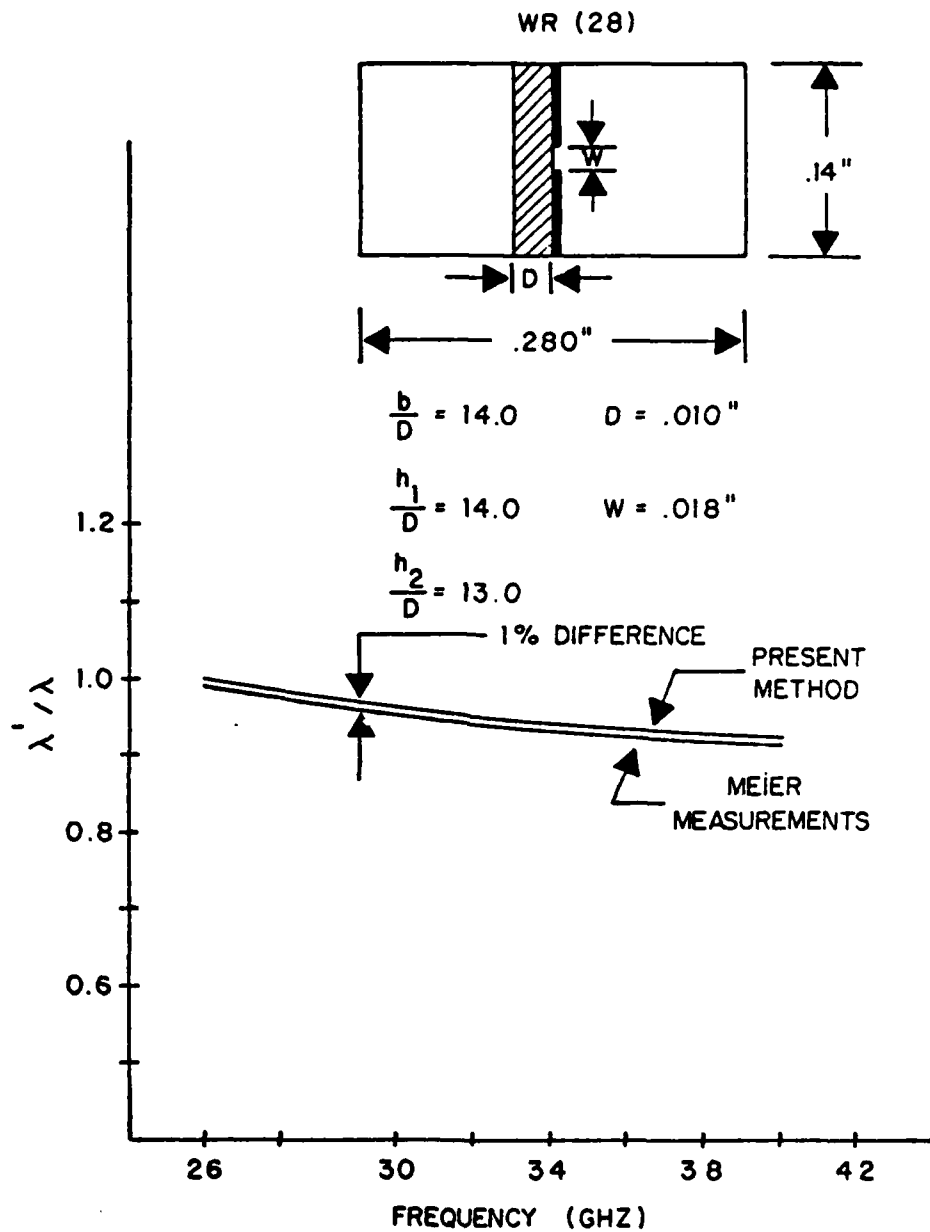
Figure 13. Computed and Measured Values of Wavelength
Ratio λ'/λ vs. Frequency for Fin-line
with WR(28) Shield. Fins are Centered

V. FIN-LINE DESIGN CURVES

A problem exists with the preparation of design curves
for structures like fin-line because of the number of inde-
pendently variable parameters which describe the structure.
This difficulty can be alleviated to some degree by practi-
cal considerations. First, fin-lines are constructed with
a shield that is compatible with the dimensions of standard
rectangular waveguide for the millimeter wavebands. Above
22 GHz, all the standard waveguide structures have aspect
ratios, b/a = 0.5. Furthermore, the fins are normally
printed on 5 mil thick Rogers Duroid 5880 dielectric substrates
with ε_r = 2.2. Design curves have been provided, which
appear in Figures 14-17, for structures with parameters dis-
cussed above for the 26.5 - 40 GHz, 40 - 60 GHz, 60 - 90 GHz
and the 90 - 140 GHz waveguide bands.

It can be seen from Figures 14-17 that even with fin
separations of a few mils, low values of impedance are diffi-
cult to achieve. In some applications lower impedances than
those obtained here which are on the order of 125 - 150 ohms,
are desirable. One method of accomplishing this objective
would be to increase the dielectric constant. This can be
seen by comparing Figure 12 for a W/D = 1 and Figure 15
for W/b = .053. For this W = 5 mil slot, it is found that
the impedance decreases from about 165 ohms to 90 ohms when
the dielectric constant is increased from ε_r = 2.2 to ε_r = 20.

78
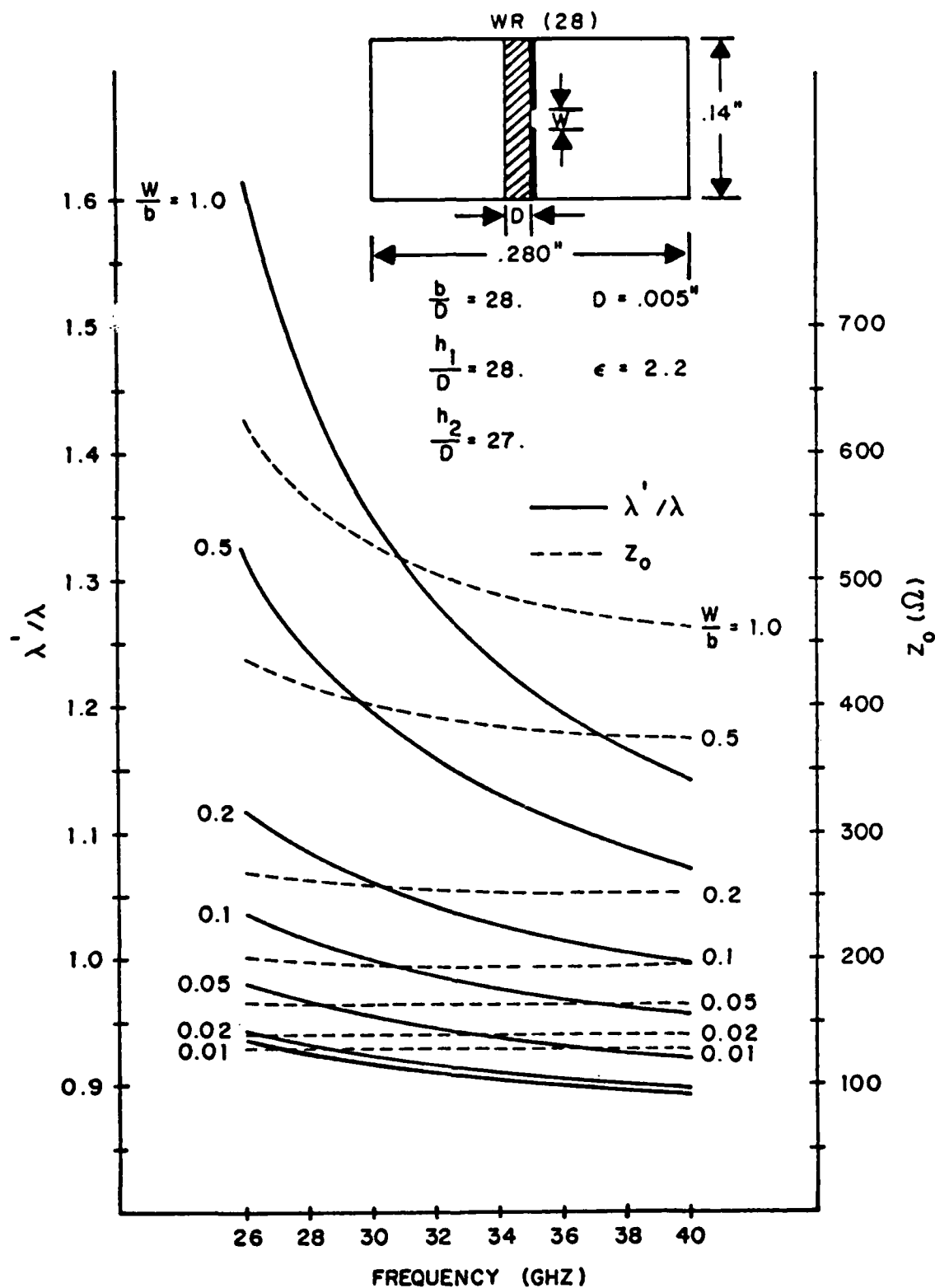
Figure 14. Wavelength Ratio λ'/λ and Characteristic
Impedance Z_o vs. Frequency for Fin-line with
WR(28) Shield. Fins are Centered
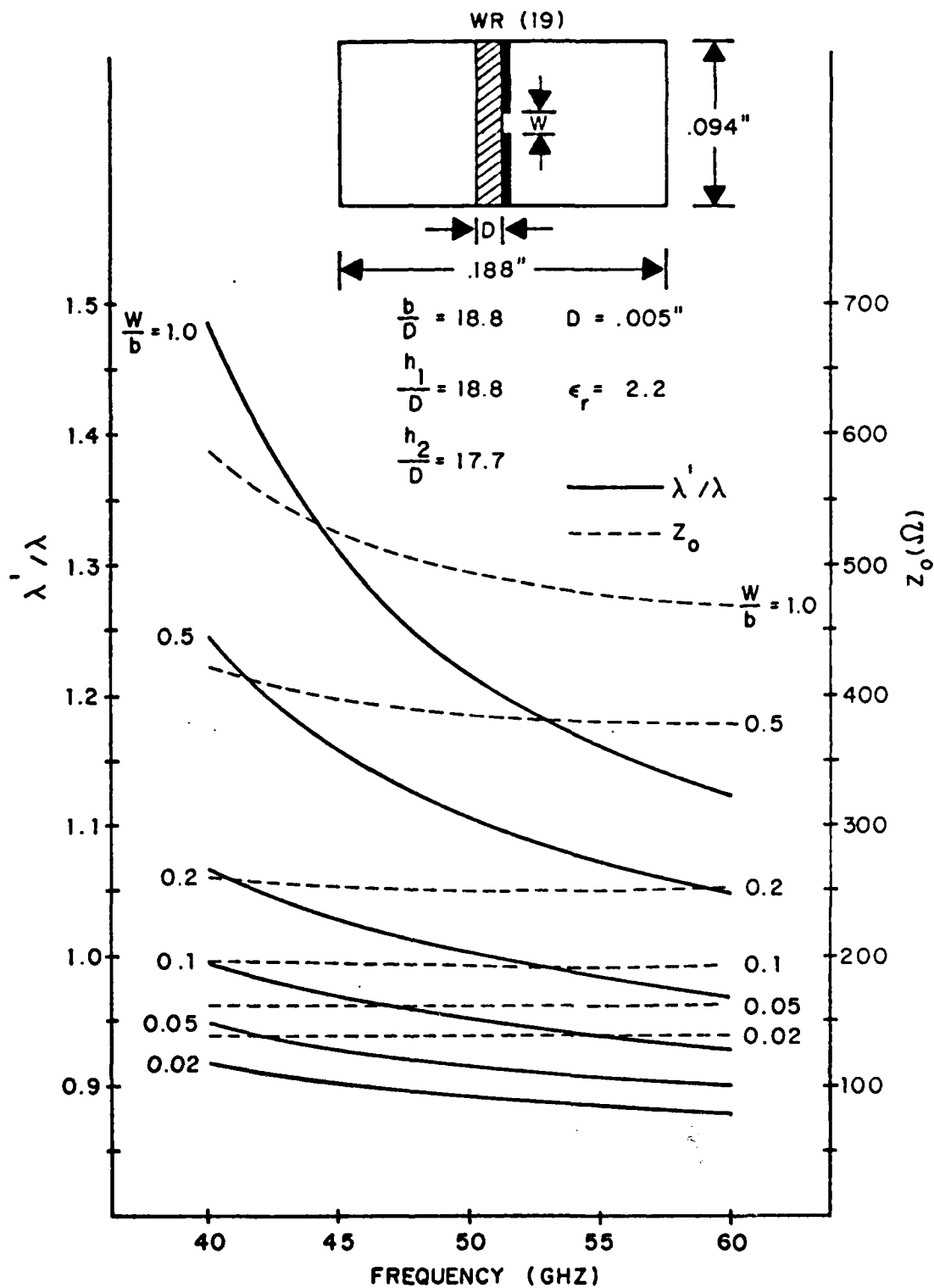
Figure 15.   Wavelength Ratio λ'/λ and Characteristic
Impedance Z_o vs. Frequency for Fin-line with
WR(19) Shield. Fins are Centered
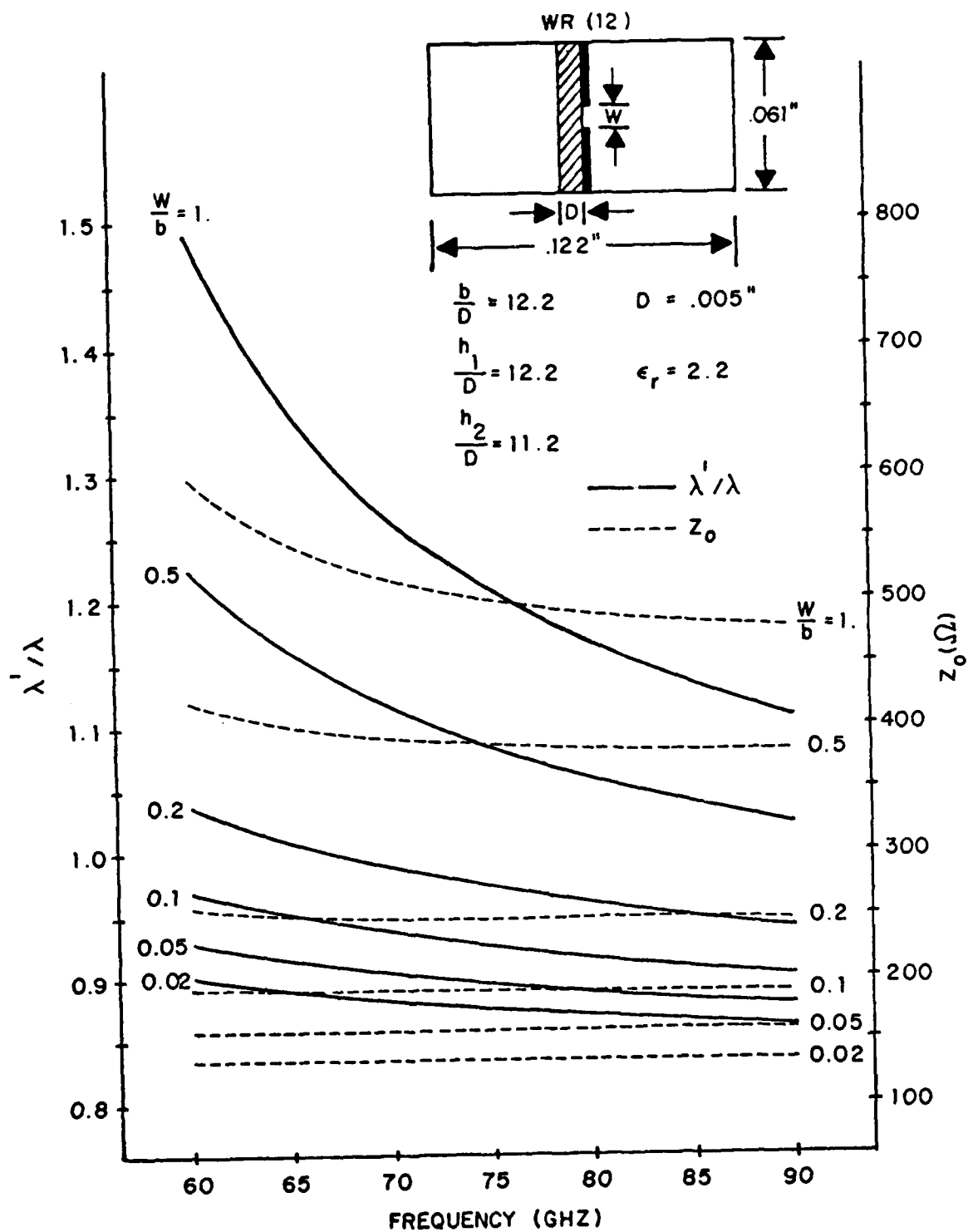
Figure 16. Wavelength Ratio λ'/λ and Characteristic
Impedance Z_o vs. Frequency for Fin-line with
WR(12) Shield. Fins are Centered
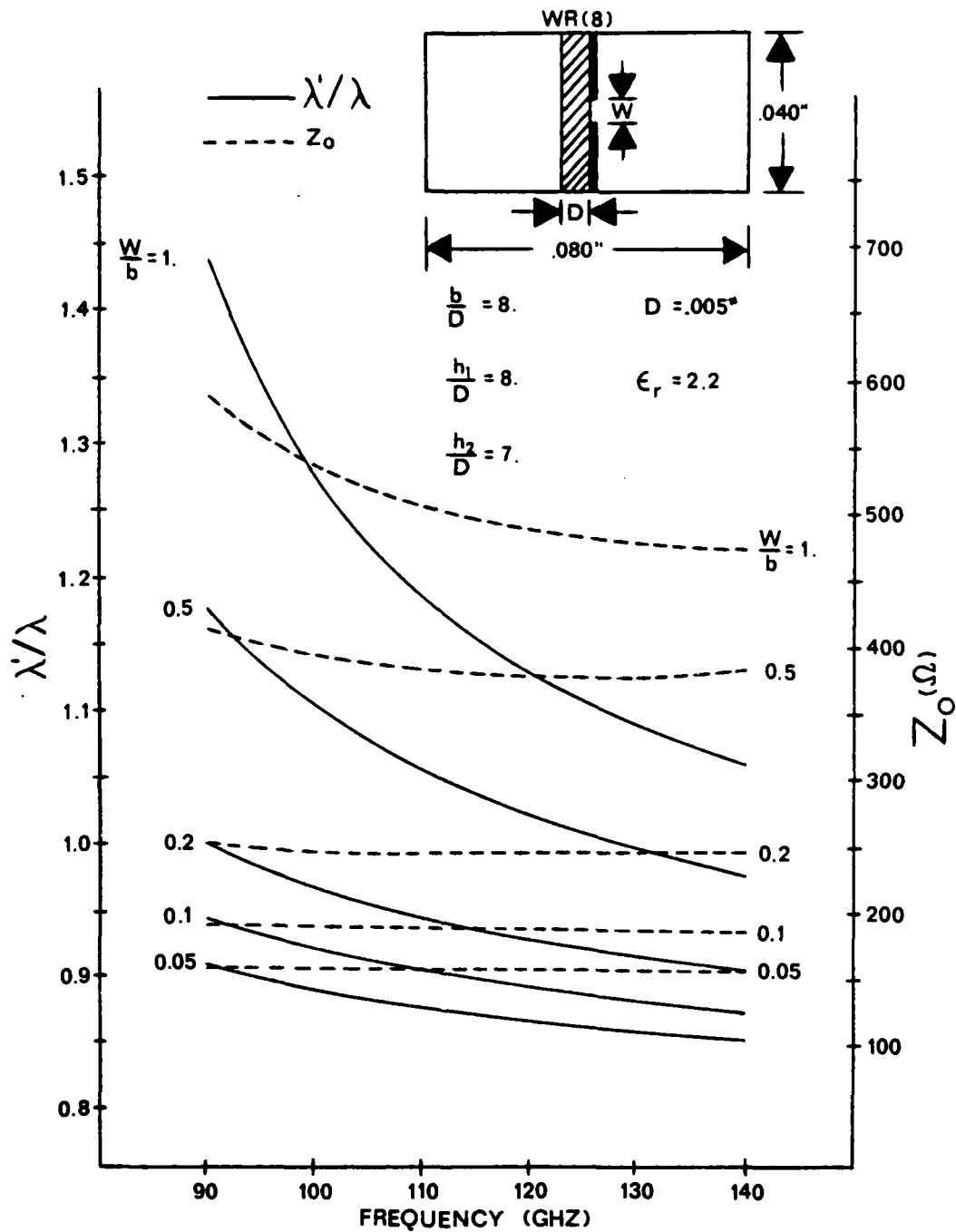
Figure 17.   Wavelength Ratio λ'/λ and Characteristic
Impedance Z_o vs. Frequency for Fin-line
with WR(8) Shield.   Fins are Centered

82

The disadvantage of this method is, of course, a reduction
in the wavelength by a factor of 2.5 causing the already
small circuit dimension to become even smaller.

Another possible way of achieving a lower value of impe-
dance may be in the relocation of the fins toward the side-
walls of the guide. Figure 18 illustrates the wavelength
and the characteristic impedance of a fin-line with the fins
shifted midway between the center and the sidewall of a WR(19)
waveguide. A comparison of Figures 18 and 15 indicates a
2-4% change in the wavelength of the guide for W/b = 1 and
less for smaller values of W/b.

The values of the characteristic impedance for small
values of W/b are relatively unchanged since the fin-line
structure behaves like slotline and the presence of the shield
has little affect. For values of W/b > 0.5, noticeable
decreases in the impedance have taken place. The most signi-
ficant decrease occurs for W/b = 1 where the impedance
decreases from 500 ohms for the centered dielectric slab to
about 275 ohms for the off-centered configuration. In this
condition the structure is a slab loaded waveguide and since
the low dielectric constant results in little change in the
empty guide fields, the results are as expected based on the
voltage impedance definition for the empty rectangular wave-
guide. A point of interest is the impedance for W/b = 1
falling below that for W/b = 0.5. This indicates that for
the off-centered configuration, the impedance increases with
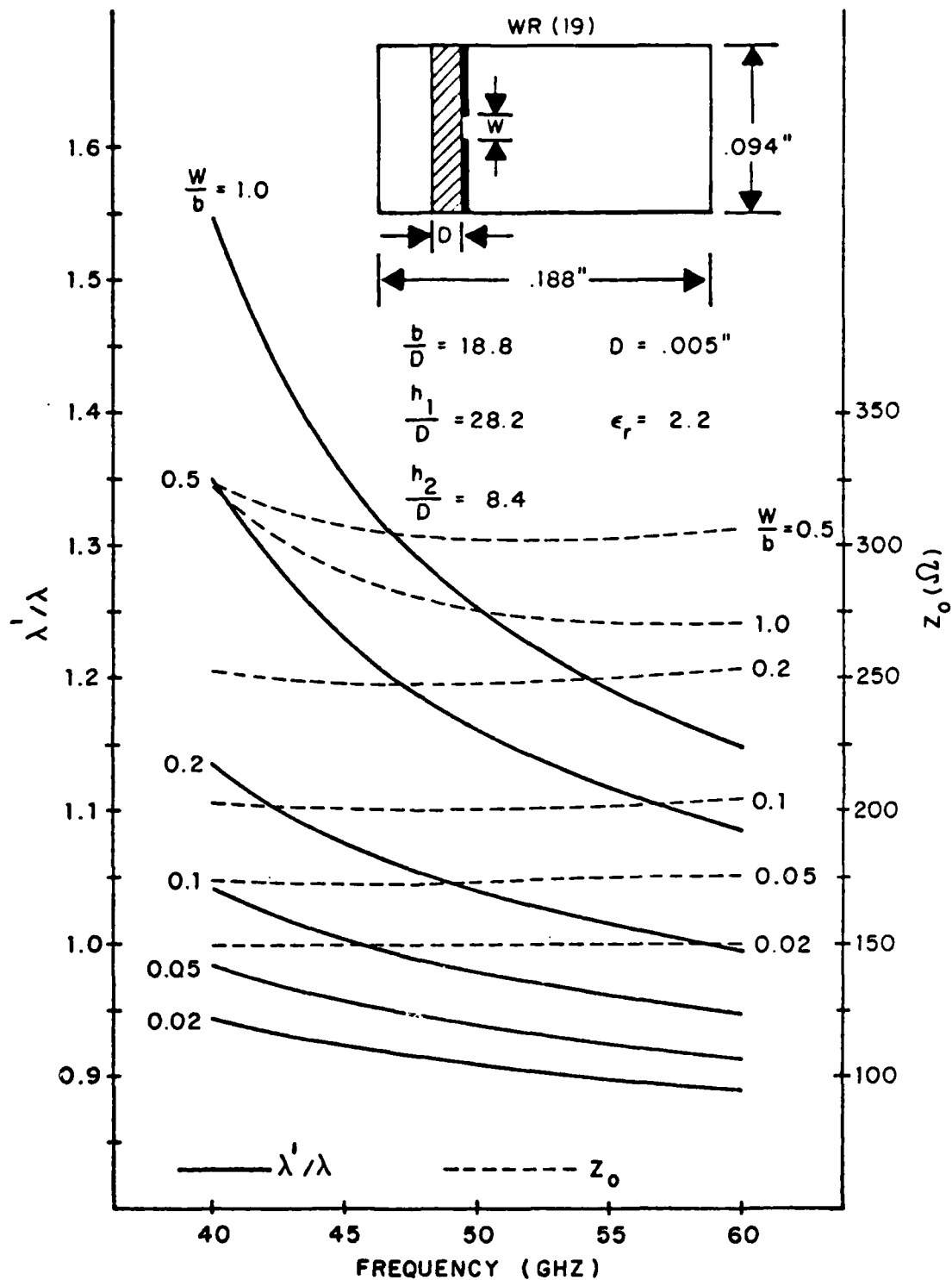
Figure 18. Wavelength Ratio λ'/λ and Characteristic Impedance Z_o vs. Frequency for Fin-line with WR(19) Shield. Fins are Located Half Way between Side Wall and a Guide Center

W/b until a maximum is reached and then decreases until
W/b = 1. Overall, the relocation of the fins toward one side
of the waveguide appears not to have achieved the lowering
of the impedance for small values of W/b as anticipated.
Therefore, of the two methods discussed, increasing the
dielectric constant accomplishes the lowering of the char-
acteristic impedance desired; but as mentioned before, the
circuit dimension shrinkage is unavoidably linked to this
action.

VI. CONCLUSIONS

A spectral domain technique for analysis of the dominant mode of fin-line has been presented. It has been shown that this efficient numerical method can be implemented computationally to accurately calculate the dispersion characteristic and characteristic impedance as a function of frequency. A matrix formulation of the problem permitted the elements of the dyadic Green's function to be computed and circumvented the extensive algebraic manipulations associated with the formulation of the resulting equations. Numerical results obtained by using this method have been presented and compared with existing data for various structures. Excellent agreement was obtained in all cases thus establishing accuracy of the method and the versatility of the computer program.

Design curves for millimeter-wave fin-lines of practical interest were also included here. Both the centered and off-centered fin configurations were discussed and the off-centered fin location was shown to result in no significant impedance change for small values of W/b.

In this thesis, particular interest was devoted to the analysis of fin-line. The method employed, however, is completely versatile since it is a general formulation of an inhomogeneous transmission media problem. Therefore, it can be clearly seen that by varying the parameters of the fin-line structure, it may exhibit the characteristics of ridged

waveguide, dielectric slab loaded waveguide, slotline, and conventional rectangular waveguide. All of these structures are fin-line substructures and as such are included in the approach presented.

APPENDIX A

Derivation of Spectral Domain Matrices
$[M_E]$ and $[M_J]$

The continuity conditions given in equations (9) through (18) are transformed via (24) into the two dimensional Fourier domain which yields

<u>at y = D</u>

$$k_{c1}^2 \, \phi_1^e(\alpha_n, D) = k_{c2}^2 \, \phi_2^e(\alpha_n, D)$$

$$-j\alpha_n \Gamma \phi_1^e(\alpha_n, D) - j\omega\mu\frac{\partial \phi_1^h}{\partial y}(\alpha_n, D) = -j\alpha_n \Gamma \phi_2^e(\alpha_n, D) - j\omega\mu\frac{\partial \phi_2^h}{\partial y}(\alpha_n, D)$$

$$k_{c1}^2 \, \phi_1^e(\alpha_n, D) = E_z(\alpha_n)$$

$$-j\alpha_n \Gamma \phi_1^e(\alpha_n, D) - j\omega\mu\frac{\partial \phi_1^h}{\partial y}(\alpha_n, D) = E_x(\alpha_n) \qquad\qquad (A-1)$$

$$k_{c1}^2\phi_1^h(\alpha_n, D) - k_{c2}^2\phi_2^h(\alpha_n, D) = J_x(\alpha_n)$$

$$-j\alpha_n \Gamma \phi_1^h(\alpha_n, D) + j\omega\varepsilon_1\frac{\partial \phi_1^e}{\partial y}(\alpha_n, D) + j\alpha_n \Gamma \phi_2^h(\alpha_n, D)$$

$$-j\omega\varepsilon_2\frac{\partial \phi_2^e}{\partial y}(\alpha_n, D) = J_z(\alpha_n)$$

<u>at y = 0</u>

$$k_{c2}^2 \, \phi_2^e(\alpha_n, 0) = k_{c3}^2 \, \phi_3^e(\alpha_n, 0)$$

$$-j\alpha_n \Gamma \phi_2^e(\alpha_n,0) - j\omega\mu\frac{\partial \phi_2^h}{\partial y}(\alpha_n \cdot 0) = -j\alpha_n \Gamma \phi_3^e(\alpha_n,0) - j\omega\mu\frac{\partial \phi_3^h}{\partial y}(\alpha_n,0)$$

$$k_{c2}^2\, \phi_2^h(\alpha_n,0) = k_{c3}^2\, \phi_3^h(\alpha_n,0) \qquad (A-2)$$

$$-j\alpha_n \Gamma \phi_2^h(\alpha_n,0) + j\omega\varepsilon_2\frac{\partial \phi_2^e}{\partial y}(\alpha_n,0) = -j\alpha_n \Gamma \phi_3^h(\alpha_n,0) + j\omega\varepsilon_3\frac{\partial \phi_3^e}{\partial y}(\alpha_n,0)$$

where $\mu = \mu_1 = \mu_2 = \mu_3$.

The solutions to the two Helmholtz equations given by equations (26a)-(26f) are now substituted; the dependence of the coefficients A^e through D^h on α_n is understood and from here on is not shown explicitly.

$$(k_{c1}^2\sinh\gamma_1 h_1)A^e - (k_{c2}^2\sinh\gamma_2 D)B^e - (k_{c2}^2\cosh\gamma_2 D)C^e = 0 \qquad (A-3)$$

$$-(j\alpha_n\Gamma\sinh\gamma_1 h_1)A^e + (j\alpha_n\Gamma\sinh\gamma_2 D)B^e + (j\alpha_n\Gamma\cosh\gamma_2 D)C^e + (j\omega\mu\gamma_1\sinh\gamma_1 h_1)A^h$$

$$+ (j\omega\mu\gamma_2\cosh\gamma_2 D)B^h + (j\omega\mu\gamma_2\sinh\gamma_2 D)C^h = 0 \qquad (A-4)$$

$$(k_{c2}^2)C^e - (k_{c3}^2\,\sinh\gamma_3 h_2)D^e = 0 \qquad (A-5)$$

$$-(j\alpha_n\Gamma)C^e + (j\alpha_n\Gamma\sinh\gamma_3 h_2)D^e - (j\omega\mu\gamma_2)B^h \qquad (A-6)$$

$$+ (j\omega\mu\gamma_3\sinh\gamma_3 h_2)D^h = 0$$

$$(k_{c2}^2)C^h - (k_{c3}^2\cosh\gamma_3 h_2)D^h = 0 \qquad (A-7)$$

$$(j\omega\epsilon_2\gamma_2)B^e - (j\omega\epsilon_3\gamma_3\cosh\gamma_3 h_2)D^e - (j\alpha_n\Gamma)C^h \qquad \text{(A-8)}$$

$$+ (j\alpha_n\Gamma\cosh\gamma_3 h_2)D^h = 0$$

$$-(j\alpha_n\Gamma\sinh\gamma_1 h_1)A^e + (j\omega\mu\gamma_1\sinh\gamma_1 h_1)A^h = E_x(\alpha_n) \qquad \text{(A-9)}$$

$$(k_{c1}^2\sinh\gamma_1 h_1)A^e = E_z(\alpha_n) \qquad \text{(A-10)}$$

$$(k_{c1}^2\cosh\gamma_1 h_1)A^h - (k_{c2}^2\sinh\gamma_2 D)B^h - (k_{c2}^2\cosh\gamma_2 D)C^h = J_x(\alpha_n) \qquad \text{(A-11)}$$

$$-(j\omega\epsilon_1\gamma_1\cosh\gamma_1 h_1)A^e - (j\omega\epsilon_2\gamma_2\cosh\gamma_2 D)B^e - (j\omega\epsilon_2\gamma_2\sinh\gamma_2 D)C^e$$

$$\text{(A-12)}$$

$$-(j\alpha_n\Gamma\cosh\gamma_1 h_1)A^h + (j\alpha_n\Gamma\sinh\gamma_2 D)B^h + (j\alpha_n\Gamma\cosh\gamma_2 D)C^h = J_z(\alpha_n).$$

This set of linear equations (A-3) through (A-12) may be written in matrix form, such that

$$\begin{bmatrix} m_{11} & m_{12} & m_{13} & 0 & 0 & 0 & 0 & 0 \\ m_{21} & m_{22} & m_{23} & 0 & m_{25} & m_{26} & m_{27} & 0 \\ 0 & 0 & m_{33} & m_{34} & 0 & 0 & 0 & 0 \\ 0 & 0 & m_{43} & m_{44} & 0 & m_{46} & 0 & m_{48} \\ 0 & 0 & 0 & 0 & 0 & 0 & m_{57} & m_{58} \\ 0 & m_{62} & 0 & m_{64} & 0 & 0 & m_{67} & m_{68} \\ m_{71}^E & 0 & 0 & 0 & m_{75}^E & 0 & 0 & 0 \\ m_{81}^E & 0 & 0 & 0 & 0 & 0 & 0 & 0 \end{bmatrix} \begin{bmatrix} A^e \\ B^e \\ C^e \\ D^e \\ A^h \\ B^h \\ C^h \\ D^h \end{bmatrix} = \begin{bmatrix} 0 \\ 0 \\ 0 \\ 0 \\ 0 \\ 0 \\ E_x \\ E_z \end{bmatrix} \qquad \text{(A-13)}$$

90

where the 8×8 matrix is $[M_E]$ of equation (29a), obtained by combining (A-3) through (A-10).

The combination of equations (A-3) through (A-8), (A-11) and (A-12) form the matrix equation (29b) repeated below in expanded form.

$$\begin{bmatrix} m_{11} & m_{12} & m_{13} & 0 & 0 & 0 & 0 & 0 \\ m_{21} & m_{22} & m_{23} & 0 & m_{25} & m_{26} & m_{27} & 0 \\ 0 & 0 & m_{33} & m_{34} & 0 & 0 & 0 & 0 \\ 0 & 0 & m_{43} & m_{44} & 0 & m_{46} & 0 & m_{48} \\ 0 & 0 & 0 & 0 & 0 & 0 & m_{57} & m_{58} \\ 0 & m_{62} & 0 & m_{64} & 0 & 0 & m_{67} & m_{68} \\ 0 & 0 & 0 & 0 & m_{75}^J & m_{76}^J & m_{77}^J & 0 \\ m_{81}^J & m_{82}^J & m_{83}^J & 0 & m_{85}^J & m_{86}^J & m_{87}^J & 0 \end{bmatrix} \begin{bmatrix} A^e \\ B^e \\ C^e \\ D^e \\ A^h \\ B^h \\ C^h \\ D^h \end{bmatrix} = \begin{bmatrix} 0 \\ 0 \\ 0 \\ 0 \\ 0 \\ 0 \\ J_x \\ J_z \end{bmatrix} \qquad \text{(A-14)}$$

The matrix elements of $[M_E]$ and $[M_J]$ are normalized at this point with respect to D, the dielectric substrate thickness; but before describing them, the normalized constants used in these elements are presented.

$$(\gamma_1 D)^2 = (\gamma_3 D)^2 = (\alpha_n D)^2 + (2\pi)^2 [(\lambda/\lambda')^2 - 1] (D/\lambda)^2$$

$$(\gamma_2 D)^2 = (\alpha_n D)^2 + (2\pi)^2 [(\lambda/\lambda')^2 - \varepsilon_r] (D/\lambda)^2$$

If $(\gamma_i D)^2 < 0$ then the following is defined

91

$$(\gamma_1"D)^2 = -(\gamma_1 D)^2 = -(\gamma_3 D)^2$$

$$(\gamma_2"D)^2 = -(\gamma_2 D)^2$$

Other normalized constants are

$$(k_{c1}D)^2 = (k_{c3}D)^2 = (2\pi)^2[1-(\lambda/\lambda')^2](D/\lambda)^2$$

$$(k_{c2}D)^2 = (2\pi)^2[\epsilon_r-(\lambda/\lambda')^2](D/\lambda)^2$$

$$\omega\mu D = 240\,\pi^2\,(D/\lambda)$$

$$\omega\epsilon_1 D = \omega\epsilon_3 D = 1/60(D/\lambda)$$

$$\omega\epsilon_2 D = \epsilon_r/60(D/\lambda)$$

$$\beta D = 2\pi(D/\lambda)(\lambda/\lambda')$$

$$\alpha_n D = \begin{cases} n2\pi(D/b) & \phi^h \text{ even} \\ \\ (2n-1)\pi(D/b) & \phi^h \text{ odd.} \end{cases}$$

The normalized matrix elements are now presented in two forms. The first of the element equations is for $(\gamma_i D)^2 > 0$ and the second is for $(\gamma_i D)^2 < 0$. For the matrices $[M_E]$ and $[M_J]$, the elements m_{11} through m_{68} are the same.

$$m_{11} = \begin{cases} (k_{c1}D)^2 \sinh[(\gamma_1 D)(h_1/D)] & (\gamma_1 D)^2 \geq 0 \\[2em] j(k_{c1}D)^2 \sin[(\gamma_1''D)(h_1/D)] & (\gamma_1 D)^2 < 0 \end{cases}$$

$$m_{12} = \begin{cases} -(k_{c2}D)^2 \sinh\gamma_2 D & (\gamma_2 D)^2 \geq 0 \\[2em] -j(k_{c2}D)^2 \sin\gamma_2''D & (\gamma_2 D)^2 < 0 \end{cases}$$

$$m_{13} = \begin{cases} -(k_{c2}D)^2 \cosh\gamma_2 D \\[2em] -(k_{c2}D)^2 \cos\gamma_2''D \end{cases}$$

$$m_{14} = m_{15} = m_{16} = m_{17} = m_{18} = 0$$

$$m_{21} = \begin{cases} (\alpha_n D)(\beta D)\sinh[(\gamma_1 D)(h_1/D)] \\[2em] j(\alpha_n D)(\beta D)\sin[(\gamma_1''D)(h_1/D)] \end{cases}$$

$$m_{22} = \begin{cases} -(\alpha_n D)(\beta D)\sinh\gamma_2 D \\[2em] -j(\alpha_n D)(\beta D)\sin\gamma_2''D \end{cases}$$

$$m_{23} = \begin{cases} -(\alpha_n D)(\beta D)\cosh\gamma_2 D \\[2em] -(\alpha_n D)(\beta D)\cos\gamma_2''D \end{cases}$$

$$m_{24} = 0$$

$$m_{25} = \begin{cases} j(\omega\mu D)(\gamma_1 D)\sinh[(\gamma_1 D)(h_1/D)] \\ \\ -j(\omega\mu D)(\gamma_1{''}D)\sin[(\gamma_1{''}D)(h_1/D)] \end{cases}$$

$$m_{26} = \begin{cases} j(\omega\mu D)(\gamma_2 D)\cosh\gamma_2 D \\ \\ -(\omega\mu D)(\gamma_2{''}D)\cos\gamma_2{''}D \end{cases}$$

$$m_{27} = \begin{cases} j(\omega\mu D)(\gamma_2 D)\sinh\gamma_2 D \\ \\ -j(\omega\mu D)(\gamma_2{''}D)\sin\gamma_2{''}D \end{cases}$$

$$m_{28} = 0$$

$$m_{31} = m_{32} = 0$$

$$m_{33} = \begin{cases} (k_{c2}D)^2 \\ \\ (k_{c2}D)^2 \end{cases}$$

$$m_{34} = \begin{cases} -(k_{c3}D)^2\sinh[(\gamma_3 D)(h_2/D)] & (\gamma_3 D)^2 \geq 0 \\ \\ -j(k_{c3}D)^2\sin[(\gamma_3{''}D)(h_2/D) & (\gamma_3 D)^2 < 0 \end{cases}$$

$$m_{35} = m_{36} = m_{37} = m_{38} = 0$$

$$m_{41} = m_{42} = 0$$

$$m_{43} = \begin{cases} (\alpha_n D)(\beta D) \\[2em] (\alpha_n D)(\beta D) \end{cases}$$

$$m_{44} = \begin{cases} -(\alpha_n D)(\beta D)\sinh[(\gamma_3 D)(h_2/D)] \\[2em] -j(\alpha_n D)(\beta D)\sin[(\gamma_3"D)(h_2/D)] \end{cases}$$

$$m_{45} = 0$$

$$m_{46} = \begin{cases} -j(\omega\mu D)(\gamma_2 D) \\[2em] (\omega\mu D)(\gamma_2"D) \end{cases}$$

$$m_{47} = 0$$

$$m_{48} = \begin{cases} j(\omega\mu D)(\gamma_3 D)\sinh[(\gamma_3 D)(h_2/D)] \\[2em] -j(\omega\mu D)(\gamma_3"D)\sin[(\gamma_3"D)(h_2/D)] \end{cases}$$

$$m_{51} = m_{52} = m_{53} = m_{54} = m_{55} = m_{56} = 0$$

$$m_{57} = \begin{cases} (k_{c2}D)^2 \\[2em] (k_{c2}D)^2 \end{cases}$$

$$m_{58} = \begin{cases} -(k_{c3}D)^2 \cosh[(\gamma_3 D)(h_2/D)] \\ \\ -(k_{c3}D)^2 \cos[(\gamma_3"D)(h_2/D)] \end{cases}$$

$$m_{61} = 0$$

$$m_{62} = \begin{cases} j(\omega\epsilon_2 D)(\gamma_2 D) \\ \\ -(\omega\epsilon_2 D)(\gamma_2"D) \end{cases}$$

$$m_{63} = 0$$

$$m_{64} = \begin{cases} -j(\omega\epsilon_3 D)(\gamma_3 D)\cosh[(\gamma_3 D)(h_2/D)] \\ \\ (\omega\epsilon_3 D)(\gamma_3"D)\cos[(\gamma_3"D)(h_2/D)] \end{cases}$$

$$m_{65} = m_{66} = 0$$

$$m_{67} = \begin{cases} (\alpha_n D)(\beta D) \\ \\ (\alpha_n D)(\beta D) \end{cases}$$

$$m_{68} = \begin{cases} -(\alpha_n D)(\beta D)\cosh[(\gamma_3 D)(h_2/D)] \\ \\ -(\alpha_n D)(\beta D)\cos[(\gamma_3"D)(h_2/D)] \end{cases}$$

96

$$m_{71}^{E} = \begin{cases} (\alpha_n D)(\beta D)\sinh[(\gamma_1 D)(h_1/D)] \\ \\ j(\alpha_n D)(\beta D)\sin[(\gamma_1''D)(h_1/D)] \end{cases}$$

$$m_{72}^{E} = m_{73}^{E} = m_{74}^{E} = 0$$

$$m_{75}^{E} = \begin{cases} j(\omega\mu D)(\gamma_1 D)\sinh[(\gamma_1 D)(h_1/D)] \\ \\ -j(\omega\mu D)(\gamma_1''D)\sin[(\gamma_1''D)(h_1/D)] \end{cases}$$

$$m_{76}^{E} = m_{77}^{E} = m_{78}^{E} = 0$$

$$m_{81}^{E} = \begin{cases} (k_{c1}D)^2\sinh[(\gamma_1 D)(h_1/D)] \\ \\ j(k_{c1}D)^2\sin[(\gamma_1''D)(h_1/D)] \end{cases}$$

$$m_{82}^{E} = m_{83}^{E} = m_{84}^{E} = m_{85}^{E} = m_{86}^{E} = m_{87}^{E} = m_{88}^{E} = 0$$

$$m_{71}^{J} = m_{72}^{J} = m_{73}^{J} = m_{74}^{J} = 0$$

$$m_{75}^{J} = \begin{cases} (k_{c1}D)^2\cosh[(\gamma_1 D)(h_1/D)] \\ \\ (k_{c1}D)^2\cos[(\gamma_1''D)(h_1/D)] \end{cases}$$

$$m_{76}^{J} = \begin{cases} -(k_{c2}D)^2 \sinh\gamma_2 D \\ \\ -j(k_{c2}D)^2 \sin\gamma_2"D \end{cases}$$

$$m_{77}^{J} = \begin{cases} -(k_{c2}D)^2 \cosh\gamma_2 D \\ \\ -(k_{c2}D)^2 \cos\gamma_2"D \end{cases}$$

$$m_{78}^{J} = 0$$

$$m_{81}^{J} = \begin{cases} -j(\omega\varepsilon_1 D)(\gamma_1 D)\cosh[(\gamma_1 D)(h_1/D)] \\ \\ (\omega\varepsilon_1 D)(\gamma_1"D)\cos[(\gamma_1"D)(h_1/D)] \end{cases}$$

$$m_{82}^{J} = \begin{cases} -j(\omega\varepsilon_2 D)(\gamma_2 D)\cosh\gamma_2 D \\ \\ (\omega\varepsilon_2 D)(\gamma_2"D)\cos\gamma_2"D \end{cases}$$

$$m_{83}^{J} = \begin{cases} -j(\omega\varepsilon_2 D)(\gamma_2 D)\sinh\gamma_2 D \\ \\ j(\omega\varepsilon_2 D)(\gamma_2"D)\sin\gamma_2"D \end{cases}$$

$$m_{84}^{J} = 0$$

$$m_{85}^{J} = \begin{cases} (\alpha_n D)(\beta D)\cosh[(\gamma_1 D)(h_1/D)] \\ \\ (\alpha_n D)(\beta D)\cos[(\gamma_1"D)(h_1/D)] \end{cases}$$

$$m_{86}^{J} = \begin{cases} (\alpha_n D)(\beta D)\cosh[(\gamma_1 D)(h_1/D)] \\ \quad . \\ (\alpha_n D)(\beta D)\cos[(\gamma_1"D)(h_1/D)] \end{cases}$$

$$m_{87}^{J} = \begin{cases} -(\alpha_n D)(\beta D)\sinh\gamma_2 D \\ \\ -j(\alpha_n D)(\beta D)\sin\gamma_2"D \end{cases}$$

$$m_{88}^{J} = 0$$

Once the matirx elements are determined for the existing condition $(\gamma_1^2 \gtrless 0)$, the $[M_E]^{-1}$ is created for the purpose of eliminating the unknown coefficients A^e through D^h in (31).

APPENDIX B

Time Average Power Flow in the Spectral
Domain of Fin-line

The following expressions for the time average power flow in the three spatial regions are derived from equation (40). The solutions to Helmholtz's equations given in (26a) through (26f) are substituted in the transformed scalar potentials of (41). In the following derivations the dependence of the coefficients A^e through D^h on the variable α_n is understood. Also to be noted is that $\gamma_1 = \gamma_3$ since regions 1 and 3 are assumed air filled.

Region 1

Case la: $(\gamma_1 D)^2 \geq 0$, γ_1 real

$$\phi_1^e = A^e \sinh \gamma_1 (D+h_1-y)$$

$$\phi_1^h = A^h \cosh \gamma_1 (D+h_1-y)$$

$$\frac{\partial \phi_1^e}{\partial y} = -\gamma_1 A^e \cosh \gamma_1 (D+h_1-y)$$

$$\frac{\partial \phi_1^h}{\partial y} = -\gamma_1 A^h \sinh \gamma_1 (D+h_1-y)$$

The term P_{1a} will be used for the power flow in region 1 for the case $(\gamma_1 D)^2 > 0$. Substituting the Helmholtz equation solutions for region 1, (40) becomes

$$P_{1a} = \frac{1}{2b} \text{ Re} \sum_{n=-\infty}^{\infty} \int_{D}^{D+h_1} \{ [-\beta\omega\epsilon_1\alpha_n^2|A^e|^2 - \beta\omega\mu_1\gamma_1^2|A^h|^2 + j\beta^2\alpha_n\gamma_1 A^e(A^h)^*$$

$$-jk_1^2\alpha_n\gamma_1(A^e)^*A^h][\sinh^2\gamma_1(D+h_1-y)]$$

$$+ [-\beta\omega\mu_1\alpha_n^2|A^h|^2 - \beta\omega\epsilon_1\gamma_1^2|A^e|^2 + j\beta^2\alpha_n\gamma_1 A^e(A^h)^*$$

$$-jk_1^2\alpha_n\gamma_1 A^h(A^e)^*][\cosh^2\gamma_1(D+h_1-y)]\}dy \ . \qquad (B-1)$$

Carrying out the integration

$$\int_{D}^{D+h_1} \sinh^2\gamma_1(D+h_1-y)dy = \frac{1}{4\gamma_1}[\sinh(2\gamma_1h_1) - 2\gamma_1h_1]$$

$$\int_{D}^{D+h_1} \cosh^2\gamma_1(D+h_1-y)dy = \frac{1}{4\gamma_1}[\sinh(2\gamma_1h_1) + 2\gamma_1h_1]$$

Equation (B-1) becomes

$$P_{1a} = \frac{1}{8b} \text{ Re} \sum_{n=-\infty}^{\infty} \{ [-\frac{\beta\omega\epsilon_1\alpha_n^2}{\gamma_1}|A^e|^2 - \beta\omega\mu_1\gamma_1|A^h|^2 + j\beta^2\alpha_n A^e(A^h)^*$$

$$- jk_1^2\alpha_n(A^e)^*A^h][\sinh(2\gamma_1h_1) - 2\gamma_1h_1]$$

$$+ [-\frac{\beta\omega\mu_1\alpha_n^2}{\gamma_1}|A^h|^2 - \beta\omega\epsilon_1\gamma_1|A^e|^2 + j\beta^2\alpha_n A^e(A^h)^*$$

$$-jk_1^2\alpha_n A^h(A^e)^*][\sinh(2\gamma_1h_1) + 2\gamma_1h_1]\} \ . \qquad (B-2)$$

101

Equation (B-2) is the final result for the power flow in region 1 when $(\gamma_1 D)^2 \geq 0$. Putting (B-2) in normalized forms produces the following result.

$$P_{1a} = -\frac{1}{8}\left(\frac{D}{b}\right) \text{Re} \sum_{n=-\infty}^{\infty} \left\{ \left[\frac{(\beta D)(\omega\epsilon_1 D)(\alpha_n D)^2}{(\gamma_1 D)} \left|\frac{A^e}{D^2}\right|^2 + (\beta D)(\omega\mu_1 D)(\gamma_1 D)\left|\frac{A^h}{D^2}\right|^2 \right. \right.$$

$$\left. -j(\beta D)^2(\alpha_n D)\frac{A^e}{D^2}\frac{(A^h)^*}{D^2} + j(k_1 D)^2(\alpha_n D)\frac{(A^e)^*}{D^2}\frac{A^h}{D^2} \right]$$

$$\left[\sinh 2(\gamma_1 D)\left(\frac{h_1}{D}\right) - 2(\gamma_1 D)\left(\frac{h_1}{D}\right) \right] + \left[\frac{(\beta D)(\omega\mu_1 D)(\alpha_n D)^2}{(\gamma_1 D)}\left|\frac{A^h}{D^2}\right|^2 \right.$$

$$\left. + (\beta D)(\omega\epsilon_1 D)(\gamma_1 D)\left|\frac{A^e}{D^2}\right|^2 - j(\beta D)^2(\alpha_n D)\frac{A^e}{D^2}\frac{(A^h)^*}{D^2} \right.$$

$$\left. \left. + j(k_1 D)^2(\alpha_n D)\frac{A^h}{D^2}\frac{(A^e)^*}{D^2}\right] \left[\sinh 2(\gamma_1 D)\left(\frac{h_1}{D}\right) + 2(\gamma_1 D)\left(\frac{h_1}{D}\right)\right] \right\} \qquad \text{(B-3)}$$

Case 1b: $(\gamma_1 D)^2 < 0$, γ_1 is imaginary in which case

$$(\gamma_1'' D)^2 = -(\gamma_1 D)^2$$

$$\phi_1^e = jA^e \sin \gamma_1''(D+h_1-y)$$

$$\phi_1^h = A^h \cos \gamma_1''(D+h_1-y)$$

$$\frac{\partial \phi_1^e}{\partial y} = -j\gamma_1'' A^e \cos \gamma_1''(D+h_1-y)$$

$$\frac{\partial \phi_1^h}{\partial y} = \gamma_1"A^h \sin \gamma_1"(D+h_1-y)$$

Substituting the values into equation (41), integrating and normalizing with respect to D results in

$$P_{1b} = -\frac{1}{8}(\frac{D}{b}) \text{ Re} \sum_{n=-\infty}^{\infty} \{ [\frac{(\beta D)(\omega\epsilon_1 D)(\alpha_n D)^2}{(\gamma_1"D)}|\frac{A^e}{D^2}|^2 + (\beta D)(\omega\mu_1 D)(\gamma_1"D)|\frac{A^h}{D^2}|^2$$

$$-(\beta D)^2(\alpha_n D)\frac{A^e}{D^2}\frac{(A^h)^*}{D^2} - (k_1 D)^2(\alpha_n D)\frac{(A^e)^*}{D^2}\frac{A^h}{D^2}]$$

$$\cdot [2(\gamma_1"D)(\frac{h_1}{D}) - \sin 2(\gamma_1"D)(\frac{h_1}{D})] + [\frac{(\beta D)(\omega\mu_1 D)(\alpha_n D)^2}{(\gamma_1"D)}|\frac{A^h}{D^2}|^2$$

$$+(\beta D)(\omega\epsilon_1 D)(\gamma_1"D)|\frac{A^e}{D^2}|^2 + (\beta D)^2(\alpha_n D)\frac{A^e}{D^2}\frac{(A^h)^*}{D^2}$$

$$+(k_1 D)^2(\alpha_n D)\frac{(A^e)^*}{D^2}\frac{A^h}{D^2}][2(\gamma_1"D)(\frac{h_1}{D}) + \sin 2(\gamma_1"D)(\frac{h_1}{D})]\} \qquad (B-4)$$

This is the final result for the power flow in region 1 when $(\gamma_1 D)^2 < 0$.

A shorter version of the derivation will be used for the remaining cases wherein the regional cases will be described and the final normalized result will be shown. This will be similar to that done for case 1b.

103

Region 2

For region 2, the power flow expressions are the same as for unshielded slowline except that the Fourier integral is replaced by a summation and the interval 2π is replaced by the interval b.

Case 2a: $(\gamma_2 D)^2 \geq 0$, γ_2 is real

$$\phi_2^e = B^e \sinh \gamma_2 y + C^e \cosh \gamma_2 y$$

$$\phi_2^h = B^h \sinh \gamma_2 y + C^h \cosh \gamma_2 y$$

$$\frac{\partial \phi_2^e}{\partial y} = \gamma_2 [B^e \cosh \gamma_2 y + C^e \sinh \gamma_2 y]$$

$$\frac{\partial \phi_2^h}{\partial y} = \gamma_2 [B^h \cosh \gamma_2 y + C^h \sinh \gamma_2 y]$$

Substituting into equation (41) and integrating followed by normalizing with respect to D produces the following.

$$P_{2a} = -\frac{1}{8}\left(\frac{D}{b}\right) \text{Re} \sum_{n=-\infty}^{\infty} \left\{ \left[\frac{(\beta D)(\omega\epsilon_2 D)(\alpha_n D)^2}{(\gamma_2 D)} \left|\frac{B^e}{D^2}\right|^2 + \frac{(\beta D)(\omega\mu_2 D)(\alpha_n D)^2}{(\gamma_2 D)} \left|\frac{B^h}{D^2}\right|^2 \right. \right.$$

$$+ (\beta D)(\omega\epsilon_2 D)(\gamma_2 D)\left|\frac{C^e}{D^2}\right|^2 + (\beta D)(\omega\mu_2 D)(\gamma_2 D)\left|\frac{C^h}{D^2}\right|^2$$

$$+ j(\beta D)^2 (\alpha_n D)\left(\frac{B^e}{D^2}\frac{(C^h)^*}{D^2} + \frac{(B^h)^*}{D^2}\frac{C^e}{D^2}\right) - j(k_2 D)^2(\alpha_n D)$$

$$\left. \cdot \left(\frac{(B^e)^*}{D^2}\frac{C^h}{D^2} + \frac{B^h}{D^2}\frac{(C^e)^*}{D^2}\right)\right]$$

$$\cdot [\sinh(2\gamma_2 D) - 2\gamma_2 D)] + \left[\frac{(\beta D)(\omega\epsilon_2 D)(\alpha_n D)^2}{(\gamma_2 D)}\left|\frac{C^e}{D^2}\right|^2\right.$$

$$+ \frac{(\beta D)(\omega\mu_2 D)(\alpha_n D)^2}{(\gamma_2 D)}\left|\frac{C^h}{D^2}\right|^2 + (\beta D)(\omega\epsilon_2 D)(\gamma_2 D)\left|\frac{B^e}{D^2}\right|^2$$

$$+ (\beta D)(\omega\mu_2 D)(\gamma_2 D)\left|\frac{B^h}{D^2}\right|^2 + j(\beta D)^2(\alpha_n D)\left(\frac{(B^h)^*}{D^2}\frac{C^e}{D^2} + \frac{B^e}{D^2}\frac{(C^h)^*}{D^2}\right)$$

$$\left. -j(k_2 D)^2(\alpha_n D)\left(\frac{B^h}{D^2}\frac{(C^e)^*}{D^2} + \frac{(B^e)^*}{D^2}\frac{C^h}{D^2}\right]\right[\sinh(2\gamma_2 D) + 2\gamma_2 D]$$

$$+ \left[(\beta D)(\omega\epsilon_2 D)\left(\frac{(\alpha_n D)^2 + (\gamma_2 D)^2}{(\gamma_2 D)}\right)\left(\frac{B^e}{D^2}\frac{(C^e)^*}{D^2} + \frac{(B^e)^*}{D^2}\frac{C^e}{D^2}\right]\right.$$

$$+ (\beta D)(\omega\mu_2 D)\left(\frac{(\alpha_n D)^2 + (\gamma_2 D)^2}{(\gamma_2 D)}\right)\left(\frac{B^h}{D^2}\frac{(C^h)^*}{D^2} + \frac{(B^h)^*}{D^2}\frac{C^h}{D^2}\right)$$

$$+ j2(\beta D)^2(\alpha_n D)\left(\frac{B^e}{D^2}\frac{(B^h)^*}{D^2} + \frac{C^e}{D^2}\frac{(C^h)^*}{D^2}\right) - j2(k_2 D)^2(\alpha_n D)$$

$$\left.\left. \cdot \left(\frac{(C^e)^*}{D^2}\frac{C^h}{D^2} + \frac{(B^e)^*}{D^2}\frac{B^h}{D^2}\right][\cosh(2\gamma_2 D) - 1]\right\} \right. \qquad (B-5)$$

This is the final result for the power flow in region 2 when $(\gamma_2 D)^2 \geq 0$.

Case 2b: $(\gamma_2 D)^2 < 0$, γ_2 is imaginary in which case

$$(\gamma_2"D)^2 = -(\gamma_2 D)^2$$

$$\phi_2^e = jB^e \sin(\gamma_2"y) + C^e \cos(\gamma_2"y)$$

$$\phi_2^h = jB^h \sin(\gamma_2"y) + C^h \cos(\gamma_2"y)$$

$$\frac{\partial \phi_2^e}{\partial y} = j\gamma_2"B^e \cos \gamma_2"y - \gamma_2" C^e \sin \gamma_2"y$$

$$\frac{\partial \phi_2^h}{\partial y} = j\gamma_2"B^h \cos \gamma_2"y - \gamma_2"C^h \sin\gamma_2"y$$

The final result for region 2 when $(\gamma_2 D)^2 < 0$ after integration and normalization follows.

$$P_{2b} = -\frac{1}{8}(\frac{D}{b}) \ \text{Re} \sum_{n=-\infty}^{\infty} \{ [\frac{(\beta D)(\omega\varepsilon_2 D)(\alpha_n D)^2}{(\gamma_2''D)}|\frac{B^e}{D^2}|^2 + \frac{(\beta D)(\omega\mu_2 D)(\alpha_n D)^2}{(\gamma_2''D)}|\frac{B^h}{D^2}|^2$$

$$+ (\beta D)(\omega\varepsilon_2 D)(\gamma_2''D)|\frac{C^e}{D^2}|^2 + (\beta D)(\omega\mu_2 D)(\gamma_2''D)|\frac{C^h}{D^2}|^2$$

$$+ (\beta D)^2(\alpha_n D)(\frac{B^e}{D^2} \frac{(C^h)^*}{D^2} - \frac{(B^h)^*}{D^2} \frac{C^e}{D^2})$$

$$+ (k_2 D)^2(\alpha_n D)(\frac{(B^e)^*}{D^2} \frac{C^h}{D^2} - \frac{B^h}{D^2} \frac{(C^e)^*}{D^2})][2\gamma_2''D - \sin(2\gamma_2''D)]$$

$$+ [\frac{(\beta D)(\omega\varepsilon_2 D)(\alpha_n D)^2}{(\gamma_2''D)}|\frac{C^e}{D^2}|^2 + \frac{(\beta D)(\omega\mu_2 D)(\alpha_n D)^2}{(\gamma_2''D)}|\frac{C^h}{D^2}|^2$$

$$+ (\beta D)(\omega\varepsilon_2 D)(\gamma_2''D)|\frac{B^e}{D^2}|^2 + (\beta D)(\omega\mu_2 D)(\gamma_2''D)|\frac{B^h}{D^2}|^2$$

$$+ (\beta D)^2(\alpha_n D)(\frac{(B^h)^*}{D^2} \frac{C^e}{D^2} - \frac{B^e}{D^2} \frac{(C^h)^*}{D^2}) + (k_2 D)^2(\alpha_n D)(\frac{B^h}{D^2} \frac{(C^e)^*}{D^2} - \frac{(B^e)^*}{D^2} \frac{C^h}{D^2})]$$

$$\cdot [2\gamma_2''D + \sin(2\gamma_2''D)] + j[(\beta D)(\omega\varepsilon_2 D)(\frac{(\alpha_n D)^2 - (\gamma_2''D)^2}{(\gamma_2''D)})$$

$$(\frac{B^e}{D^2} \frac{(C^e)}{D^2} - \frac{(B^e)^*}{D^2} \frac{C^e}{D^2}) + (\beta D)(\omega\mu_2 D)(\frac{(\alpha_n D)^2 - (\gamma_2''D)^2}{(\gamma_2''D)})$$

$$(\frac{B^h}{D^2} \frac{(C^h)^*}{D^2} - \frac{(B^h)^*}{D^2} \frac{C^h}{D^2}) + 2(\beta D)^2(\alpha_n D)(\frac{B^e}{D^2} \frac{(B^h)^*}{D^2} - \frac{C^e}{D^2} \frac{(C^h)^*}{D^2})$$

$$+ 2(k_2 D)^2(\alpha_n D)(\frac{(C^e)^*}{D^2} \frac{C^h}{D^2} - \frac{(B^e)^*}{D^2} \frac{B^h}{D^2})][1 - \cos(2\gamma_2''D)]\} \qquad \text{(B-6)}$$

Region 3

Case 3a: $(\gamma_3 D)^2 \geq 0$, γ_3 is real

$$\phi_3^e = D^e \sinh \gamma_3(h_2+y)$$

$$\phi_3^h = D^h \cosh \gamma_3(h_2+y)$$

$$\frac{\partial \phi_3^e}{\partial y} = \gamma_3 D^e \cosh \gamma_3(h_2+y)$$

$$\frac{\partial \phi_3^h}{\partial y} = \gamma_3 D^h \sinh \gamma_3(h_2+y)$$

Substituting these expressions into (41), integrating and normalizing yields

$$
\begin{aligned}
P_{3a} = &-\frac{1}{8}\left(\frac{D}{b}\right) \ \mathrm{Re} \sum_{n=-\infty}^{\infty} \{ [\frac{(\beta D)(\omega\varepsilon_3 D)(\alpha_n D)^2}{(\gamma_3 D)}|\frac{D^e}{D^2}|^2 + (\beta D)(\omega\mu_3 D)(\gamma_3 D)|\frac{D^h}{D^2}|^2 \\
&+j(\beta D)^2(\alpha_n D)\ \frac{D^e}{D^2}\ \frac{(D^h)^*}{D^2} - j(k_3 D)^2(\alpha_n D)\frac{(D^e)^*}{D^2}\ \frac{D^h}{D^2}] \\
&\cdot[\sinh 2(\gamma_3 D)(\frac{h_2}{D})-2(\gamma_3 D)(\frac{h_2}{D})] + [\frac{(\beta D)(\omega\mu_3 D)(\alpha_n D)^2}{(\gamma_3 D)}|\frac{D^h}{D^2}|^2 \\
&+(\beta D)(\omega\varepsilon_3 D)(\gamma_3 D)|\frac{D^e}{D^2}|^2 + j(\beta D)^2(\alpha_n D)\frac{D^e}{D^2}\ \frac{(D^h)^*}{D^2} \\
&-j(k_3 D)^2(\alpha_n D)\frac{(D^e)^*}{D^2}\ \frac{D^h}{D^2}][\sinh 2(\gamma_3 D)(\frac{h_2}{D})+2(\gamma_3 D)(\frac{h_2}{D})]\}
\end{aligned}
$$

(B-7)

This is the final result for region 3 power flow for
$(\gamma_3 D)^2 \geq 0$.

Case 3b: $(\gamma_3 D)^2 < 0$, γ_3 is imaginary in which case

$$(\gamma_3 "D)^2 = -(\gamma_3 D)^2.$$

$$\phi_3^e = jD^e \sin \gamma_3"(h_2+y)$$

$$\phi_3^h = D^h \cos \gamma_3"(h_2+y)$$

$$\frac{\partial \phi_3^e}{\partial y} = j\gamma_3"D^e \cos \gamma_3"(h_2+y)$$

$$\frac{\partial \phi_3^h}{\partial y} = -\gamma_3"D^h \sin \gamma_3"(h_2+y)$$

Substituting into equation (41), integrating from $y = -h_2$ to $y = 0$ and normalizing the result with respect to D produces the following.

$$P_{3b} = -\frac{1}{8}\left(\frac{D}{b}\right) \text{ Re} \sum_{n=-\infty}^{\infty} \{ [\frac{(\beta D)(\omega\varepsilon_3 D)(\alpha_n D)^2}{(\gamma_3"D)}|\frac{D^e}{D^2}|^2 + (\beta D)(\omega\mu_3 D)(\gamma_3"D)|\frac{D^h}{D^2}|^2$$

$$+ (\beta D)^2(\alpha_n D)\frac{D^e}{D^2}\frac{(D^h)^*}{D^2} + (k_3 D)^2(\alpha_n D)\frac{(D^e)^*}{D^2}\frac{D^h}{D^2}]$$

$$\cdot [2(\gamma_3"D)(\frac{h_2}{D}) - \sin 2(\gamma_3"D)(\frac{h_2}{D})] + [\frac{(\beta D)(\omega\mu_3 D)(\alpha_n D)^2}{(\gamma_3"D)}|\frac{D^h}{D^2}|^2$$

$$+ (\beta D)(\omega\varepsilon_3 D)(\gamma_3"D)|\frac{D^e}{D^2}|^2 - (\beta D)^2(\alpha_n D)\frac{D^e}{D^2}\frac{(D^h)^*}{D^2}$$

$$- (k_3 D)^2(\alpha_n D)\frac{(D^e)^*}{D^2}\frac{D^h}{D^2}] [2(\gamma_3"D)(\frac{h_2}{D} + \sin 2(\gamma_3"D)(\frac{h_2}{D})] \} \qquad (B-8)$$

This is the final normalized expression for the power flow in region 3 under the $(\gamma_3 D)^2 < 0$ condition. It may be noted that a minus sign appears in front of all the equations, this is because a wave traveling in the -z direction was assumed.

APPENDIX C

Computer Program 'FIN-LINE'

```
C  **********
C  ** FINE-LINE **
C  **********
C
C  THIS PROGRAM PROVIDES A FREQUENCY DEPENDENT ANALYSIS OF SLOT
C  CONFIGURATIONS ON A DIELECTRIC SUBSTRATE WITHIN A SHIELDED
C  STRUCTURE. THE COMPUTED DATA CONTAINS THE DISPERSION CHARACTER-
C  ISTIC AND THE CHARACTERISTIC IMPEDANCE FOR VARIOUS SHIELDED
C  STRUCTURES. DEPENDING ON THE INPUT DATA, ANALYSIS OF (1) FIN-
C  LINE, (2) DIELECTRIC SLAB LOADED WAVEGUIDE, (3) RIDGED WAVEGUIDE,
C  OR (4) RECTANGULAR WAVEGUIDE CAN BE OBTAINED.
C  THE METHODS USED ARE BASED UPON AN EXACT NUMERICAL ANALYSIS IN
C  THE FOURIER TRANSFORM DOMAIN.
C  ALL PARAMETERS ARE NORMALIZED WITH RESPECT TO THE THICKNESS D OF
C  THE DIELECTRIC SUBSTRATE EXCEPT FOR W/B WHICH IS NORMALIZED
C  WITH RESPECT TO THE SIDEWALL DIMENSION.
C
C  THE FOLLOWING NOMENCLATURE IS USED FOR INPUT VARIABLES AND
C  OUTPUT DATA:
C  BD     -- NORMALIZED DIMENSION OF SIDEWALL, B/D
C  DL     -- NORMALIZED FREQUENCY (THICKNESS D / WAVELENGTH LAMBDA,D/L)
C  DL1    -- INITIAL VALUE OF DL
C  DLINC  -- INCREMENTAL VALUE OF DL
C  EPSR   -- PERMITTIVITY OF THE DIELECTRIC MATERIAL
C  HD1    -- NORMALIZED DISTANCE OF SIDEWALLS ABOVE METAL SURFACE
C  HD2    -- NORMALIZED DISTANCE OF SIDEWALLS BELOW DIELECTRIC
C  ICAR   -- NO. OF DIFFERENT INITIAL VALUE DATA CARDS BEING RUN
C  IDL    -- NO. OF DIFFERENT VALUES OF DL
C  IWB    -- NO. OF DIFFERENT VALUES OF WB
C  LPL    -- WAVELENGTH RATIO LAMBDA-P/LAMBDA, LP/L
C  WB     -- NORMALIZED WIDTH OF SLOT,W/B
C  WB1    -- INITIAL VALUE OF WB
C  WBINC  -- INCREMENTAL VALUE OF WB
C  ZO     -- CHARACTERISTIC IMPEDANCE
C
C  REQUIRED INPUT DATA:
C
C  FIRST CARD:  SPECIFIES THE DIMENSIONS OF THE SHIELDING WALLS AND
C               THE PERMITTIVITY
C               COL.  1 - 10: BD  (F10.6 FORMAT)
C               COL. 11 - 20: HD1 (F10.6 FORMAT)
C               COL. 21 - 30: HD2 (F10.6 FORMAT)
```

111

COL. 31 - 40: EPSR (F10.6 FORMAT)

SECOND CARD: SPECIFIES THE NUMBER OF INITIAL VALUE DATA CARDS
THAT FOLLOW. MAXIMUM OF 9 CARDS ALLOWED.
COL. 1: ICAR (I1 FORMAT)

THRID CARD: CONTAINS INITIAL VALUES FOR COMPUTATION AND
SPECIFIES THE NUMBER OF POINTS TO BE COMPUTED AND
THE INCREMENTS BETWEEN THESE.
COL. 1 - 10: WB1 (F10.6 FORMAT)
COL. 11 - 20: DL1 (F10.6 FORMAT)
COL. 21: IWB (I1 FORMAT) MAX = 9
COL. 22: IDL (I1 FORMAT) MAX = 9
COL. 23 - 30: BLANK
COL. 31 - 40: WBINC (F10.6 FORMAT)
COL. 41 - 50: DLINC (F10.6 FORMAT)

OUTPUT: THE OUTPUT CONSISTS OF THE DIMENSIONS OF THE SHIELDING
STRUCTURE AND THE PERMITTIVITY. THE COMPUTED VALUE OF
THE DISPERSION CHARACTERISTICS AND THE CHARACTERISTIC
INPEDANCE FOR THE VARIOUS VALUES OF THE NORMALIZED
SLOTWIDTH AND THE NORMALIZED FREQUENCY IS ALSO PRINTED.

REQUIRED SUBROUTINES: A) SUBROUTINE 'CALC', COMPUTES THE VARIOUS
MATRICES USED IN DETERMINATION OF LPL
AND ZO (SUPPLIED WITH THIS PROGRAM)

B) SUBROUTINE 'CMTRIN', COMPUTES THE IN-
VERSE OF THE MATRICES USED IN 'CALC'
(SUPPLIED WITH THIS PROGRAM)

COMPUTER SPACE REQUIRED: 48K

EQUIPMENT CONFIGURATION: IBM/SYSTEM 360

LANGUAGE: FORTRAN

PROGRAMMER: LT P.M. SHAYDA, UNITED STATES NAVY
SUPERVISED BY DR. J.B. KNORR
U.S. NAVAL POSTGRADUATE SCHOOL, MONTEREY, CALIFORNIA
SEPTEMBER 1979

IMPLICIT INTEGER(I-J), REAL(A-H,K-Z)
COMMON DL, WUD, WF1D, WE2D, WE3D, AB, HD1, HD2, EPSR, TWOPI, AD, WD, S1, IX
EXTERNAL CALC

112

```
      PI    = 3.141592654
      TWOPI = 6.283185307
      PIS   = 9.869604404
      JD    = 1
      JG    = 1
      JH    = 1
      WRITE(6,2000)
C
C     READ IN THE DIMENSIONS OF THE SHIELDED STRUCTURE
C
      READ(5,1000) BD,HD1,HD2,EPSR
      WRITE(6,9001) BD,HD1,HD2,EPSR
      READ(5,1002) ICAR
      AD    = BD/2.
      DLL   = C.25/SQRT(EPSR)
      DA    = 1./(HD1 + HD2 + 1.)
      HDA   = CA/2.
C
C     READ IN NUMBERS OF ITERATIONS, STEP SIZE AND INITIAL VALUES
C
      DO 300 JA=1,ICAR
      READ(5,1001) WB1,DL1,IWB,IDL,WBINC,DLINC
      WD1   = WB1*BD
      WDINC = WBINC*BD
      WD    = WD1 - WDINC
      DO 200 IW=1,IWB
      WD    = WD + WDINC
      WB    = WD/BD
      DL    = DL1 - DLINC
      IF(WD.EQ.BD.AND.EPSR.GT.1.) WRITE(6,3001)
      IF(EPSR.EC.1.) GO TO 30
      IF(DL1.LE.HDA.AND.JD.EC.1) GO TO 46
   5  DO 100 ID=1,IDL
      DL    = CL + DLINC
      IF(DL.GE.DA.AND.JH.EC.1) GO TO 45
   6  IF(DL.GT.DLL) GO TO 47
      IX    = 20
      IF(WD.EQ.BD) IX = 1
      WUD   = 24).*DL*PIS
      WE1D  = DL/60.
      WE2D  = EPSR*DL/60.
      WE3D  = WE1D
      AB    = (TWOPI*DL)**2
      LPL   = 1./SQRT(EPSR) + .1
C
C     ITERATION LOOP FOR THE DISPERSION CHARACTERISTIC
C
      DO 11 IA=1,60
```

```
      S1P    = 0.0
      LLP    = 1./LPL
      SUM    = CALC(LLP)
      IF(SUM) 12,50,10
   10 LPL1   = LPL + ./ GO TO 38
   11 IF(IA.EQ.60) GO TO 38
   12 CONTINUE
      LPL1   = 1./LLP
      LPL2   = LPL1 - .1
      DO 20 IC=1,30
      LPL    = (LPL1 + LPL2)/2.
      IF(ABS(LPL - LPL1).LT.5.E-04) GO TO 50
      LLP    = 1./LPL
      SUM    = CALC(LLP)
      IF(SUM) 14,50,13
   13 LPL2   = LPL
      GO TO 2C
   14 LPL1   = LPL
   20 CONTINUE
      GO TO 50
   30 IF(WC.EC.BD) GO TO 42
   35 IF(JG.EC.1) WRITF(6,3002)
      JG     = 0
      GO TO 2
   38 WRITE(6,2015) WB,DL
      GO TO 100
   40 WRITE(6,3000)
      JG     = 1
      GO TO 2
   45 WRITE(6,3010) DLL
      GO TO 200
   46 WRITE(6,3020) HDA
      JD     = 0
      GO TO 5
   47 WRITE(6,3015) DA
      JH     = 0
      GO TO 6
C
C     COMPUTATION OF CHARACTERISTIC IMPEDANCE
C
   50 S1     = 1.0
      IX     = 50
      IF(WD.EQ.BD) IX = 1
      LLP    = 1./LPL
      PAVG   = CALC(LLP)
      VOS    = 1.0
      ZO     = 0.5*VOS/PAVG
      WRITE(6,2010) WB,DL,LPL,ZO
```

114

```fortran
100  CONTINUE
200  CONTINUE
300  CONTINUE
1000 FORMAT(4F10.6)
1001 FORMAT(2F10.6,2I1,8X,2F10.6)
1002 FORMAT(I1)
2000 FORMAT('1',T25,'SLOT-TRANSMISSION LINE ON A DIELECTRIC SUBSTRATE
    1'/,T39,'WITH SHIELDED WALLS',/,' ',T43,'(FIN-LINE)',///)
2010 FORMAT('0',T21,'W/B=',F6.3,T34,'D/L=',F7.4,T48,'LP/L=',F7.4,T63,
    1'ZO=',F6.1,1X,'OHMS')
2015 FORMAT('0',T21,'W/B=',F6.3,T34,'D/L=',F7.4,T48,'LP/L= ******',
    1T63,'ZC= ******')
3000 FORMAT(' ',T32,'RECTANGULAR WAVEGUIDE STRUCTURE',/,' ',T38,
    1'EXISTS FOR W/B= 1.0')
3001 FORMAT('0',T32,'DIELECTRIC SLAB-LOADED WAVEGUIDE',/,' ',T33,
    1'STRUCTURE EXISTS FOR W/B= 1.0')
3002 FORMAT('0',T31,'RIDGED WAVEGUIDE STRUCTURE EXISTS',/,' ',T32,
    1'FOR THE FOLLOWING VALUES OF W/B')
3010 FORMAT('0',T28,'SURFACE WAVES PROPAGATE FOR VALUES OF D/L',/,
    1' ',T32,'GREATER THAN ',F5.3,' RUN TERMINATED')
3015 FORMAT('0',T29,'TE-20 EMPTY GUIDE MODE PROPAGATES FOR',/,
    1' ',T31,'VALUES OF D/L GREATER THAN ',F5.3)
3020 FORMAT('0',T29,'CUTOFF FREQUENCY OF THE DOMINANT MODE',/,' ',
    1T33,'OF EMPTY GUIDE IS D/L= ',F5.3)
9001 FORMAT(' ','DIMENSIONS: B/D=',F5.2,T44,'H1/D=',F5.2,T58,
    1'H2/D=',F5.2,T72,'EPSR=',F4.1,//)
     END
```

```
      FUNCTION CALC(LLP)

C     FUNCTION CALC USED IN DETERMINATION OF DISPERSION CHARACTERISTIC
C     AND THE CHARACTERISTIC IMPEDANCE

      IMPLICIT INTEGER(I-J), REAL(A-H,K-O,Q-Z), COMPLEX(P)
      COMPLEX ME(8,8), MJ(8,8),AE,BE,CE,DE,AH,BH,CH,DH,AEC,BEC,CEC,
     1 DEC,AHC,BHC,CHC,DHC,AES,BES,CES,DES,AHS,BHS,CHS,DHS,X,G
      COMMON DL,WUD,WE1D,WE2D,WE3D,AB,HD1,HD2,EPSR,TWOPI,AD,WD,S1,IX
      PA   = 0.0
      COEF = CMPLX(0.0,0.0,0.0)
      LLPS = LLP*LLP
      BD   = TWOPI*DL*LLP
      KC1DS = AB*( 1.- LLPS)
      KC2DS = AB*(EPSR - LLPS)
      KC3DS = KC1DS
      DO 30 IB=1,IX
      IN   = IB - 1
      AND  = 0.5*FLOAT(IN)*TWOPI/AD
      ANDS = AND*AND
      ANBDS = AND*BD
      GAM1DS = ANDS + AB*(LLPS - 1.)
      GAM2DS = ANDS + AB*(LLPS - EPSR)
      GAM3DS = GAM1DS

C     CLEARS ME AND MJ ARRAYS

      DO 2 I=1,8
      DO 1 J=1,8
      ME(I,J)=(0.0,0.0,0.0)
      MJ(I,J)=(0.0,0.0,0.0)
    1 CONTINUE
    2 CONTINUE

C     IF GAMMA1**2 IS LESS THAN ZERO TRIGONOMETRIC FUNCTIONS APPLY

      IF(GAM1DS.LT.0.0) GO TO 12
      GAM1D = SQRT(GAM1DS)
      GAMHD1 = GAM1D*HD1
      IF(GAMHD1.GT.80.) GAMHD1 = 80.

C     GAMMA1**2 GREATER THAN ZERO

      HSIN1 = SINH(GAMHD1)
      HCOS1 = COSH(GAMHD1)
      ME(1,1)= CMPLX(KC1DS*HSIN1,0.0)
      ME(2,1)= CMPLX(ANBDS*HSIN1,0.0)
```

```
      ME(2,5)= CMPLX(0.0,WUD*GAM1D*HSIN1)
      ME(4,3)= CMPLX(ANBDS,0.0)
      ME(6,7)= ME(4,3)
      ME(7,1)= ME(2,5)
      ME(7,5)= ME(2,5)
      ME(8,1)= ME(1,1)
      MJ(7,5)= CMPLX(KC1DS*HCOS1,0.0)
      MJ(8,1)= CMPLX(0.0,-WE1D*GAM1D*HCOS1)
      MJ(8,5)= CMPLX(ANBDS*HCOS1,0.0)

C     IF GAMMA2**2 IS LESS THAN ZERO TRIGONOMETRIC FUNCTIONS APPLY
C
   10 IF(GAM2DS.LT.0.0) GO TO 13
      GAM2D =SQRT(GAM2DS)
      IF(GAM2D.GT.80.) GAM2D = 80.
C
C     GAMMA2**2 GREATER THAN ZERO
C
      HSIN2  = SINH(GAM2D)
      HCOS2  = COSH(GAM2D)
      ME(1,2)= CMPLX(-KC2DS*HSIN2,0.0)
      ME(1,3)= CMPLX(-KC2DS*HCOS2,0.0)
      ME(2,2)= CMPLX(-ANBDS*HSIN2,0.0)
      ME(2,3)= CMPLX(-ANBDS*HCOS2,0.0)
      ME(2,6)= CMPLX(0.0,WUD*GAM2D*HCOS2)
      ME(2,7)= CMPLX(0.0,WUD*GAM2D*HSIN2)
      ME(3,3)= CMPLX(KC2DS,0.0)
      ME(4,6)= CMPLX(0.0,-WUD*GAM2D)
      ME(5,7)= ME(3,3)
      ME(6,2)= CMPLX(0.0,WE2D*GAM2D)
      ME(7,6)= ME(1,2)
      ME(7,7)= ME(1,3)
      MJ(8,2)= CMPLX(0.0,-WE2D*GAM2D*HCOS2)
      MJ(8,3)= CMPLX(0.0,-WE2D*GAM2D*HSIN2)
      MJ(8,6)= ME(2,2)
      MJ(8,7)= ME(2,3)

C     IF GAMMA3**2 IS LESS THAN ZERO TRIGONOMETRIC FUNCTIONS APPLY
C
   11 IF(GAM3DS.LT.0.0) GO TO 14
      GAM3D = SQRT(GAM3DS)
      GAMHD3 = GAM3D*HD2
      IF(GAMHD3.GT.80.) GAMHD3 = 80.
C
C     GAMMA3**2 GREATER THAN ZERO
C
      HSIN3  = SINH(GAMHD3)
      HCOS3  = COSH(GAMHD3)
```

117

```
      ME(3,4)= CMPLX(-KC3DS*HSIN3,0.0)
      ME(4,4)= CMPLX(-ANBDS*HSIN3,0.0)
      ME(4,8)= CMPLX(0.0,WUD*GAM3D*HSIN3)
      ME(5,8)= CMPLX(-KC3DS*HCOS3,0.0)
      ME(6,4)= CMPLX(0.0,-WE3D*GAM3D*HCOS3)
      ME(6,8)= CMPLX(-ANBDS*HCOS3,0.0)
      GO TO 15
C
C     GAMMA1**2 LESS THAN ZERO
   12 GAMP1D = SQRT(-GAM1DS)
      SIGN1  = SIN(GAMP1D*HD1)
      COSN1  = COS(GAMP1D*HD1)
      ME(1,1)= CMPLX(0.0,KC1DS*SIGN1)
      ME(2,1)= CMPLX(0.0,ANBDS*SIGN1)
      ME(2,5)= CMPLX(0.0,-WUD*GAMP1D*SIGN1)
      ME(4,3)= CMPLX(ANBDS,0.0)
      ME(6,7)= ME(4,3)
      ME(7,1)= ME(2,1)
      ME(8,1)= ME(1,1)
      MJ(7,5)= CMPLX(KC1DS*COSN1,0.0)
      MJ(8,1)= CMPLX(WE1D*GAMP1D*COSN1,0.0)
      MJ(8,5)= CMPLX(ANBDS*COSN1,0.0)
      GO TO 10
C
C     GAMMA2**2 LESS THAN ZERO
   13 GAMP2D = SQRT(-GAM2DS)
      SIGN2  = SIN(GAMP2D)
      COSN2  = COS(GAMP2D)
      ME(1,2)= CMPLX(0.0,-KC2DS*SIGN2)
      ME(1,3)= CMPLX(-KC2DS*COSN2,0.0)
      ME(2,2)= CMPLX(0.0,-ANBDS*SIGN2)
      ME(2,3)= CMPLX(-ANBDS*COSN2,0.0)
      ME(2,6)= CMPLX(-WUD*GAMP2D*COSN2,0.0)
      ME(2,7)= CMPLX(0.0,-WUD*GAMP2D*SIGN2)
      ME(3,3)= CMPLX(KC2DS,0.0)
      ME(4,6)= CMPLX(WUD*GAMP2D,0.0)
      ME(5,7)= ME(3,3)
      ME(6,2)= CMPLX(-WE2D*GAMF2D,0.0)
      MJ(7,6)= ME(1,2)
      MJ(7,7)= ME(1,3)
      MJ(8,2)= CMPLX(WE2D*GAMP2D*COSN2,0.0)
      MJ(8,3)= CMPLX(0.0,WE2D*GAMP2D*SIGN2)
      MJ(8,6)= ME(2,2)
      MJ(8,7)= ME(2,3)
      GO TO 11
```

```
C
C     GAMMA3**2 LESS THAN ZERO
C
   14 GAMP3D = SQRT(-GAM3DS)
      SIGN3  = SIN(GAMP3D*TD2)
      COSN3  = COS(GAMP3D*TD2)
      ME(3,4)= CMPLX(0.0,-KC3DS**SIGN3)
      ME(4,4)= CMPLX(0.0,-ANRDS**SIGN3)
      ME(4,8)= CMPLX(0.0,-WUD*GAMP3D*SIGN3)
      ME(5,8)= CMPLX(0.0,-KC3DS*COSN3,0.0)
      ME(6,8)= CMPLX(WE3D*GAMP3D*,0.0)
      ME(6,8)= CMPLX(-ANBDS*COSN3,0.0)
   15 DO 20 IA=1.6
      DO 20 JA=1.8
      MJ(IA,JA)= ME(IA,JA)
   20 CONTINUE
   21 CONTINUE
C
C     INVERSION OF ME MATRIX
C
      JN = 8
      JDIM = 8
      DETERM=0.0
      CALL CMTRIN(JN,ME,JDIM,DETERM)
      G     = MJ(7,5)*ME(5,7) + MJ(7,6)*ME(6,7)  +  MJ(7,7)*ME(7,7)
      G11   = AIMAG(G)
      ANW   = ANO*WD/2.
      IF(ANW.EQ.0.0) GO TO 31
      EXAND = SIN(ANW)/ANW
   29 IF(S1.EQ.1.) GO TO 100
      COEF1 = G11*EXAND**2
      IF(IB.EQ.1) COEF1 = COEF1/2.
      COEF  = COEF + COEF1
   30 CONTINUE   COEF
      CALC   COEF
      RETURN
   31 EXAND = 1.0
      GO TO 29
C
C     COMPUTATION OF THE CHARACTERISTIC IMPEDANCE
C
  100 AE  = ME(1,7)*EXAND
      BE  = ME(2,7)*EXAND
      CE  = ME(3,7)*EXAND
      DE  = ME(4,7)*EXAND
      AH  = ME(5,7)*EXAND
      BH  = ME(6,7)*EXAND
      CH  = ME(7,7)*EXAND
```

119

```
      DH    = ME(8,7)*EXAND
      IF(IB.EQ.1) GO TO 104
      IF(AIMAG(AH).LT.0.0.AND.CABS(AH).LT.0.5E-37)  AH=CMPLX(0.,-5.E-38)
      IF(AIMAG(AH).GT.0.0.AND.CABS(AH).LT.0.5E-37)  AH=CMPLX(0.,5.E-38)
      IF(REAL(DE).LT.0.0.AND.CABS(DE).LT.0.5E-37)   DE=CMPLX(-5.E-38,0.)
      IF(REAL(DE).GT.0.0.AND.CABS(DE).LT.0.5E-37)   DE=CMPLX(5.E-38,0.0)
      IF(AIMAG(DH).LT.0.0.AND.CABS(DH).LT.0.5E-37)  DH=CMPLX(0.,-5.E-38)
      IF(AIMAG(DH).GT.0.0.AND.CABS(DH).LT.0.5E-37)  DH=CMPLX(0.,5.E-38)
  104 AEC   = CONJG(AE)
      BEC   = CONJG(BE)
      CEC   = CONJG(CE)
      DEC   = CONJG(DE)
      AHC   = CONJG(AH)
      BHC   = CONJG(BH)
      CHC   = CONJG(CH)
      CHC   = CONJG(DH)
      AES   = AE*AEC
      BES   = BE*BEC
      CES   = CE*CEC
      BHS   = BH*BHC
      CHS   = CH*CHC
      X     = CMPLX(0.0,1.0)
      BUWD  = BC*WUD
      BEWD  = BD*WE1D
      BE2WC = BD*WE2D
      BDS   = BD*BD
      K1DS  = WUD*WF1D
      K2DS  = WUD*WE2D
      K3DS  = K1DS
C
C     IF GAMMA1**2 IS LESS THAN ZERO, TRIGONOMETRIC FUNCTIONS APPLY
C
      IF(GAM1DS.LT.0.0) GO TO 200
      GD1   = GAM1D
      GAM1  = 2.*GD1*HD1
      IF(GAM1.GT.80.) GAM1 = 80.
      SIM1  = SINH(GAM1) - GAM1
      SIP1  = SINH(GAM1) + GAM1
C
C     IF GAMMA2**2 IS LESS THAN ZERO, TRIGONOMETRIC FUNCTIONS APPLY
C
  110 IF(GAM2DS.LT.0.0) GC TO 220
      GD2   = GAM2D
      GAM2  = 2.*GD2
      GD2S  = GD2*GD2
      IF(GAM2.GT.80.) GAM2 = 80.
      ANGDS = (ANDS + GD2S)/GD2
      SIM2  = SINH(GAM2) - GAM2
```

```fortran
      SIP2   = SINH(GAM2) + GAM2
      COP2   = COSH(GAM2) - 1.
C
C     IF GAMMA3**2 IS LESS THAN ZERO, TRIGONOMETRIC FUNCTIONS APPLY
C
  120 IF(GAM3CS.LT.0.0) GO TO 240
      GD3  = GAM3D
      GAM3 = 2.*GD3*HD2
      IF(GAM3.GT.80.) GAM3 = 80.
      SIM3 = SINH(GAM3) - GAM3
      SIP3 = SINH(GAM3) + GAM3
C
C     POWER IN REGION 1
C
  130 P1A = BEWD*ANDS*AES/GD1
      P1B = BUWD*GD1*AH
      P1C = BCS*AND*AE*AHC
      P1D = K1DS*AND*AFC*AH
      P1E = BUWD*ANDS*AH/GD1
      P1F = BEWD*GD1*AES
      P1G = P1C
      P1H = P1D
C
C     POWER IN REGION 2
C
      P2A  = BE2WD*ANDS*BES/GD2
      P2B  = BUWD*ANDS*BHS/GD2
      P2C  = BE2WD*GD2*CES
      P2D  = BUWD*GD2*CHS
      P2EA = BDS*AND*BE*CHC
      P2EB = BDS*AND*BHC*CE
      P2FA = K2DS*AND*BEC*CH
      P2FB = K2DS*AND*BH*CEC
      P2G  = BE2WD*ANDS*CES/GD2
      P2H  = BUWD*ANDS*CHS/GC2
      P2I  = BE2WD*GD2*BES
      P2J  = BUWD*GD2*BHS
      P2KA = P2EB
      P2KB = P2EA
      P2LA = P2FB
      P2LB = P2FA
      P2MA = BE2WD*ANGDS*BE*CEC
      P2MB = BE2WD*ANGDS*BEC*CE
      P2NA = BUWD*ANGDS*BH*CHC
      P2NB = BUWD*ANGDS*BHC*CH
      P2OA = 2.*BDS*AND*BE*BHC
      P2OB = 2.*BDS*AND*CE*CHC
      P2PA = 2.*K2DS*AND*CEC*CH
```

121

```
      P2PB    = 2.*K2DS*AND*BEC*BH
C
C     POWER IN REGION 3
      P3A   = BEWD*ANDS*DE/GD3
      P3B   = BUWD*GD3*DH
      P3C   = BDS*AND*DE*CHC
      P3D   = K3DS*AND*DEC*DH
      P3E   = BUWD*ANDS*DH/GD3
      P3F   = BEWD*GD3*DE
      P3G   = P3C
      P3H   = P3D
      IF(GAM1DS.LT.0.0) GO TO 180
      P1    =*AHC + (P1D - P1C)*X)*SIM1 + (P1B*SIM1 + P1E*SIP1)
1           *AHC + (P1F + (P1H - P1G)*X)*SIP1
150 IF(GAM2DS.LT.0.0) GO TO 185
      P2   =(P2A+P2B +P2C + P2D + (P2EA +P2EB - P2FA
1           - P2FB)*X)*SIM2 + (P2G + P2H + P2I + P2J + (P2KA
2           + P2KB - P2LA - P2LB)*X)*SIP2 + (P2MA + P2MB
3           + P2NB + P2NA + (P2OA + P2OB - P2PA - P2PB)*X)*COP2
16C IF(GAM3DS.LT.0.0) GO TO 190
      P3   =(P3A*SIM3 + P3F*SIP3)*DEC + (P3B*SIM3 + P3E*SIP3)
1           *DHC + ((P3C - P3D)*SIM3 + (P3G - P3H)*SIP3)*X
17C PA1   = P1 +P2 + P3
      IF(IB.EQ.1) PA1 = PA1/2.
      PA    = PA +PA1
      COEF  = C.1250*REAL(PA)/AD
      ZZ2   = 0.5/COEF
      IF(IB.EC.1) GO TO 175
      ZZ   =(ZZ1 - ZZ2)/2.
      IF(ABS((ZZ1 - ZZ2)/ZZ).LT.1.E-03.AND.IN.GT.7) GO TO 178
      ZZ1  = ZZ
175 ZZ2  = ZZ2
      GO TO 30
178 CALC = COEF
      RETURN
180 P1   = (P1B*SIM1 + P1E*SIP1)*AHC + (P1A - P1C - P1D)*SIM1
1           + (P1F + P1G + P1H)*SIP1
185 GO TO 15C
      P2   =(P2A + P2B + P2C + P2D + P2EA - P2EB + P2FA
1           - P2FB)*SIM2 + (P2G + P2H + P2I + P2J + P2KA
2           - P2KB + P2LA - P2LB)*SIP2 + (P2MA - P2MB + P2NA
3           - P2NB + P2OA - P2OB + P2PA - P2PB)*X*COP2
19C GO TO 16C
      P3   = (P3A*SIM3 + P3F*SIP3)*DEC + (P3B*SIM3 + P3E*SIP3)
1           *DHC + ((P3C + P3D)*SIM3 - (P3G + P3H)*SIP3
20C GO TO 170
      GD1  = GAMP1D
      GAM1 = 2.*GD1*HD1
```

```
      SIM1  = GAM1 + SIN(GAM1)
      SIP1  = GAM1 + SIN(GAM1)
      GO TO 110
220   GD2   = GAMP2D
      GD2S  = GD2*GD2
      GAM2  = 2.*GD2
      ANGDS = (ANDS - GD2S)/GD2
      SIM2  = GAM2 - SIN(GAM2)
      SIP2  = GAM2 + SIN(GAM2)
      COP2  = 1. - COS(GAM2)
      GO TO 120
240   GD3   = GAMP3D
      GAM3  = 2.*GD3*HD2
      SIM3  = GAM3 - SIN(GAM3)
      SIP3  = GAM3 + SIN(GAM3)
      GO TO 130
      END
```

```
      SUBROUTINE CMTRIN (N,A,NDIM,DETERM)
      COMPLEX A(NDIM,NDIM),PIVOT(100),AMAX,T,SWAP,DETERM,U
      INTEGER*4 IPIVOT(100),INDEX(100,2)
      REAL TEMP,ALPHA(100)
C
C     INITIALIZATION
C
      DETERM=CMPLX(1.0,0.0,0.0)
      DO 20 J=1,N
      ALPHA(J)=0.000
      DO 10 I=1,N
 10   ALPHA(J)=ALPHA(J)+A(J,I)*CONJG(A(J,I))
      ALPHA(J)=SQRT(ALPHA(J))
 20   IPIVOT(J)=0
      DO 600 I=1,N
C
C     SEARCH FOR PIVOT ELEMENT
C
      AMAX=CMPLX(0.0,0.0,0.0)
      DO 105 J=1,N
      IF (IPIVOT(J)-1) 60,105,60
 60   DO 100 K=1,N
      IF (IPIVOT(K)-1) 80,100,740
 80   TEMP=AMAX*CONJG(AMAX)-A(J,K)*CONJG(A(J,K))
      IF(TEMP) 85, 85, 100
 85   IROW=J
      ICOLUM=K
      AMAX=A(J,K)
 100  CONTINUE
 105  CONTINUE
      IPIVOT(ICCLUM)=IPIVOT(ICCLUM)+1
C
C     INTERCHANGE ROWS TO PUT PIVOT ELEMENT ON DIAGONAL
C
 140  IF(IROW-ICOLUM) 140, 260, 140
      DETERM=-DETERM
      DO 200 L=1,N
      SWAP=A(IROW,L)
      A(ICOLUM,L)=A(ICOLUM,L)=SWAP
 200  A(ICOLUM,L)=SWAP
      SWAP=ALPHA(IROW)
      ALPHA(IROW)=ALPHA(ICOLUM)
      ALPHA(ICOLUM)=SWAP
 260  INDEX(I,1)=IROW
      INDEX(I,2)=ICOLUM
      PIVOT(I)=A(ICOLUM,ICOLUM)
      U=PIVOT(I)
      TEMP=PIVOT(I)*CONJG(PIVOT(I))
```

124

```
         IF(TEMP) 330, 720, 330
C     DIVIDE PIVOT ROW BY PIVOT ELEMENT
C
330   A(ICOLUM,ICOLUM)=CMPLX(1.0,0.0)
      DO 350 L=1,N
      U=PIVOT(I)
350   A(ICOLUM,L)=A(ICOLUM,L)/U
C
C     REDUCE NON-PIVOT ROWS
C
380   DO 550 L1=1,N
      IF(L1-ICOLUM) 400, 550, 400
400   T=A(L1,ICOLUM)
      A(L1,ICOLUM)=CMPLX(0.0,0.0)
      DO 450 L=1,N
      U=A(ICOLUM,L)
450   A(L1,L)=A(L1,L)-U*T
550   CONTINUE
600   CONTINUE
C
C     INTERCHANGE COLUMNS
C
620   DO 710 I=1,N
      L=N+1-I
      IF(INDEX(L,1)-INDEX(L,2)) 630, 710, 630
630   JROW=INDEX(L,1)
      JCOLUM=INDEX(L,2)
      DO 705 K=1,N
      SWAP=A(K,JROW)
      A(K,JROW)=A(K,JCOLUM)
      A(K,JCOLUM)=SWAP
705   CONTINUE
710   CONTINUE
      RETURN
720   WRITE(6,750)
      STOP
740   RETURN
750   FORMAT('0',T39,'INPUT DATA ERROR')
      END
```

LIST OF REFERENCES

1. Ticher, F.J., "Transmission Media for Millimeter-Wave Integrated Circuits," 1979 IEEE MTT-S Symposium Digest, p. 203-207, May 1979.

2. Meier, P.J., "Two New Integrated-circuit Media with Special Advantages at Millimeter Wavelengths," IEEE 1972 G-MTT Symposium Digest, p. 221-223, May 1972.

3. Meier, P.J., "Integrated Fin-line Millime-er Components," IEEE Transactions on Microwave Theory and Techniques, vol. MTT-22, p. 1209-1216, December 1974.

4. Meier, P.J., "Millimeter Integrated Circuits Suspended in the E-Plane of Rectangular Waveguide," IEEE Transactions on Microwave Theory and Techniques, vol. mTT-26, p. 726-733, October 1978.

5. Meier, P.J., "Printed Circuit Balanced Mixer for the 4 and 5 mm Bands," 1979 IEEE MTT-S Symposium Digest, p. 84-86, May 1979.

6. Kopdzo, E., Schuenemann, K. and El-Hennawy, H., "A Quadriphase Modulator in Fin-line Techniques," 1979 IEEE MIT-S Symposium Digest, p. 119-121, May 1979.

7. Begermann, G., "An X-Band Balanced Fin-line Mixer," IEEE Transactions on Microwave Theory and Techniques, vol. MTT-26, p. 1007-1011, December 1978.

8. Hofmann, H., "Fin-line Dispersion," Electronic Letters, vol. 12, p. 428-429, August 1976.

9. Hoefer, W.J.R., "Fin-line Parameters Calculated with the TLM-Method," 1979 MTT-S Symposium Digest, p. 341-343, May 1979.

10. Saad, A.M.K. and Schünemann, K., "A Simple Method for Analyzing Fin-line Structures," IEEE Transactions on Microwave Theory and Techniques, vol. MTT-26, p. 1002-1007, December 1978.

11. Chang C. and Itoh, T., "Spectral Domain Analysis of Dominant and Higher Order Modes in Fin-lines," 1979 IEEE MTT-S Symposium Digest, p. 344-346, May 1979.

12. Itoh, T. and Mittra, R., "Dispersion Characteristics of Slot Lines," Electronic Letters, vol. 7, p. 364-365, July 1971.

13. Itoh, T. and Mittra, R., "Spectral-Domain Approach for Calculating the Dispersion Characteristics of Microstrip Lines," _IEEE Transactions on Microwave Theory and Techniques_, (Short Papers), vol. MTT-21, p. 496-499, July 1973.

14. Itoh, T. and Mittra, R., "A Technique for Computing Dispersion Characteristics of Shielded Microstrip Lines," _IEEE Transactions on Microwave Theory and Techniques_, (Short papers), Vol. MTT-22, p. 896-898, October 1974.

15. Knorr, J.B. and Tufekcioglu, A., "Spectral-Domain Calculation of Microstrip Characteristic Impedance," _IEEE Transactions on Microwave Theory and Techniques_, vol. MTT-23, p. 725-728, September 1975.

16. Collin, R.W., _Field Theory of Guided Waves_, McGraw-Hill Book Company, Inc., 1960.

17. Harrington, R.F., _Field Computations by Moment Methods_, the MacMillan Company, 1968.

18. Knorr, J.B. and Kuchler, K.D., "Analysis of Coupled Slot and Coplanar Strips on Dielectric Substrate," _IEEE Transactions on Microwave Theory and Techniques_, vol. MTT-23, p. 541-548, July 1975.

19. Kuchler, K.B., _Hybrid Mode Analysis of Coplanar Transmission Lines_, Ph.D. Thesis, U.S. Naval Postgraduate School, Monterey, CA., June 1975.

20. Cohn, S.B., "Properties of Ridged Wave Guide," _IRE Transactions on Microwave Theory and Techniques_, vol. 35, p. 783-788, August 1947.

21. Hopfer, S., "The Design of Ridged Waveguides," _IRE Transactions on Microwave Theory and Techniques_, vol. MTT-3, p. 20-29, October 1955.

22. Lagerlöf, R.D.E., "Ridged Waveguide for Planar Microwave Circuits," _IEEE Transactions on Microwave Theory and Techniques_ (Short papers), vol. MTT-21, p. 499-501, July 1973.

23. Vartanian, P.H., Ayres, W.P. and Helgessen, A.L., "Propagation in Dielectric Slab Loaded Rectangular Waveguide," _IRE Transactions on Microwave Theory and Techniques_, vol. MTT-6, p. 215-222, April 1958.

24. Mariani, E.A., Heinzman, C.P., Agrios, J.P. and Cohn, S.B., "Slot Line Characteristics," _IEEE Transactions on Microwave Theory and Techniques_, vol. MTT-17, p. 1091-1096, December 1969.

INITIAL DISTRIBUTION LIST

		No. Copies
1.	Defense Technical Information Center Cameron Station Alexandria, Virginia 22314	2
2.	Library, Code 0142 Naval Postgraduate School Monterey, California 93940	2
3.	Department Chairman, Code 62 Department of Electrical Engineering Naval Postgraduate School Monterey, California 93940	1
4.	Professor Jeffrey B. Knorr, Code 62Ko Department of Electrical Engineering Naval Postgraduate School Monterey, California 93940	2
5.	LT Paul Mark Shayda, USN 413 South Macon Street Baltimore, Maryland 21224	2
6.	Professor Kenneth G. Gray, Code 62Gy Department of Electrical Engineering Naval Postgraduate School Monterey, California 93940	1